

Investigation of Intermetallic Communication in Novel Bimetallic Catalysts using Cyclic Voltammetry

A thesis submitted in partial fulfilment of the
requirements for the degree of Masters of Research

By

Raphael Hoikin LAM

Department of Chemistry and Biomolecular Sciences

Macquarie University

Supervisor: Prof. Barbara Messerle

9th October, 2015

Preface

This thesis is a report of original research undertaken by the author and is submitted for admission to the degree of Masters of Research at Macquarie University. This work was performed in the Department of Chemistry and Biomolecular Sciences at Macquarie University and the School of Chemistry at the University of New South Wales during the period of January 2015 to October 2015. The work and results presented in this thesis are those of the author, unless otherwise acknowledged.

Sections of this work have been published in a peer-review journal:

Lam, R. H.; Walker, D. B.; Tucker, M. H.; Gatus, M. R. D.; Bhadbhade, M.; Messerle, B. A., *Organometallics* **2015**, 34, 4312-4317.

Acknowledgements

The MRes year has been formidable yet very rewarding, from the big move to Macquarie, the adjustment to the place to meeting so many new faces, while getting the project going at the same time. I could not have survived without the support of the BAM group, and my friends old and new alike. I would like to thank the following people for their support all the way through.

First and foremost, I would like to thank Prof. Barbara Messerle for her excellent supervision and patience in the past two years. Her understanding and devotion to quality have encouraged me to undertake my research project to the best of my ability.

Thank you to Sam and Mark for their outstanding advice and suggestions on my lab work as well as writing. I would have pulled off all my hair when making my first bimetallic complexes without your assuring words. I would also like to thank Barney for providing plenty of advice. You left the party a bit early but here's more interesting stories!

To the members of BAM group: Ash, Chin, Matt, Sandy and Shelly, thank you for making the lab an enjoyable place to work at with all your help and odd sense of humour.

Thank you to Dr. Louise Brown and A/Prof. Bridget Mabbutt for clearing my questions during the MRes year; to Ryan and Harry for your help with NMR experiments, your quirky company and help of different sorts; and to Mr. Anthony Gurlica and Mr. Joe Ghatt for logistics of chemicals and supply.

I am grateful to Dr. Danny Wong, Dr. Leigh Aldous, Dr. Neeraj Sharma, and A/Prof. Steve Colbran for electrochemistry resources and useful discussions.

I am also grateful to the UNSW NMR Facility for their assistance with instrumentation.

Last but not least, I would like to express my deepest gratitude to all my family and friends, in particular Cecilia, Henry and Ady. I couldn't have found the way out in times of confusion and frustration all these years without your endless love and support.

Raphael Lam

October 2015

List of Abbreviations

Ar	Aryl
atm	Atmosphere
$\text{BAr}_4^{\text{F}^-}$	<i>tetrakis</i> [3,5-bis(trifluoromethyl)phenyl]borate anion
bpm	<i>bis</i> (1-pyrazolyl)methane
br	broad (NMR)
Bu	Butyl
cat.	Catalyst
COD	1,5-cyclooctadiene
Conv.	Conversion
COSY	Correlation Spectroscopy
δ	chemical shift (ppm)
DCM	Dichloromethane
DMA	<i>N,N</i> -dimethylacetamide
dpm	Dipyrinato
D	Deuterium
equiv.	Equivalent
E_{pa}	Peak anodic/oxidation potential
E_{pc}	Peak cathodic/reduction potential
ESI-MS	Electrospray Ionisation Mass Spectrometry
Et	Ethyl
Et_2O	Diethyl Ether
Et_3N	Triethylamine
Fc	Ferrocene
Fc^+	Ferrocenium
FTIR	Fourier Transform Infra Red
h	hour(s)
HMBC	Heteronuclear Multiple Bond Correlation
HSQC	Heteronuclear Single Quantum Coherence
Hz	Hertz
<i>i</i>	ipso (NMR)
<i>i</i> Pr	Isopropyl
IVCT	Intervalence Charge Transfer
<i>J</i>	scalar coupling constant (NMR)
L	Ligand
[M]	metal complex
m	multiplet (NMR)
<i>m</i>	Meta
<i>m/z</i>	mass to charge ratio
Me	Methyl
MeOH	Methanol
mim	(1-methylimidazolyl)imine

mmol	Millimoles
mol	Moles
NIR	Near Infra-red
NMR	Nuclear Magnetic Spectroscopy
nOe	nuclear Overhauser effect (NMR)
NOESY	Nuclear Overhauser Effect Spectroscopy
<i>o</i>	Ortho
o.n.	Overnight
<i>p</i>	Para
Ph	Phenyl
Phdpm	5-phenyldipyrinato
Phmim	(1-methylimidazolyl-methyleneamino)benzene
ppm	parts per million
Pz	Pyrazole or Pyrazolyl
q	quartet (NMR)
Quant.	Quantities
[Rh]	rhodium complex
r.t.	room temperature
s	singlet (NMR) or strong (FTIR)
S	Substrate
t	triplet (NMR)
^t Bu	tert-butyl
THF	Tetrahydrofuran
TLC	Thin Layer Chromatography
TM	Transition metal
ToF	Turnover Frequency
VT	Variable Temperature

Table of Contents

Preface	i
Acknowledgements	ii
List of Abbreviations	iii
Table of Contents.....	v
List of Figures	viii
List of Schemes	x
List of Tables	xi
Abstract.....	xii
1 Introduction	1
1.1 Catalysis	1
1.2 Transition Metal Complexes in Homogeneous Catalysis	1
1.2.1 C-X Bond Forming Reactions	3
1.3 Bimetallic Catalysts and Cooperativity	4
1.3.1 Electronic Interactions in Bimetallic Complexes	5
1.3.2 Spatial Dependence of Intermetallic Interactions in Bimetallic Complexes	5
1.3.3 Tandem Reaction – Dihydroalkoxylation Reaction	7
1.4 Objectives of this Project.....	9
2 Catalysed Intermolecular Hydroalkoxylation Reaction Using a Monometallic Rh(I) Catalyst	11
2.1 Establishing Optimal Conditions.....	13
2.2 Substrate Scope of the Reaction	14
2.3 Electrochemical Studies of Complexes $[\text{Rh}(\text{CO})_2\text{Phdp}^{\text{m}}]$ (18) and $[\text{Rh}(\text{CO})_2\text{bpm}]\text{Bar}^{\text{F}}_4$ (19)	17
2.4 Summary for Chapter 2	19

3	Heteroditopic Ligands and Their Dirhodium Complexes: Synthesis and Catalysis.....	19
3.1	Synthesis of $[\text{Rh}_2(\text{CO})_4(o\text{-bpm/mim})][\text{BAR}^{\text{F}}_4]_2$ (16).....	20
3.1.1	Route A Towards Complex 16	20
3.1.2	Route B Towards Complex 16	21
3.1.3	NMR Characterisation of Complex 16	21
3.2	Synthesis of <i>o</i> -dpmH/mim (32)	23
3.2.1	Route A Towards <i>o</i> -dpmH/mim (32).....	23
3.2.2	Route B Towards <i>o</i> -dpmH/mim (32)	24
3.3	Synthesis of $[\text{Rh}_2(\text{COD})_2(o\text{-dpm/mim})]\text{BAR}^{\text{F}}_4$ (33) and $[\text{Rh}_2(\text{CO})_4(o\text{-dpm/mim})]\text{BAR}^{\text{F}}_4$ (17).....	25
3.4	Catalysed C-O Bond Formation	26
3.4.1	Catalysed Intermolecular Hydroalkoxylation	27
3.4.2	Catalysed Intramolecular Dihydroalkoxylation	28
3.5	Electrochemical Studies.....	30
3.5.1	Comparison of Bimetallic Complex 16 with Monometallic Complexes 19 and 13a	35
3.5.2	Comparison of Bimetallic Complex 17 and Monometallic Complexes 18 and 13a	36
3.5.3	Comparison between Bimetallic Complexes 16 and 17	37
3.5.4	CV Studies on Bimetallic Complex 10	38
3.5.5	Correlation of Electrochemical Studies with Catalysis Results	39
3.6	Summary for Chapter 3	40
4	Conclusions and Future Work.....	41
4.1	Conclusions for This Thesis.....	41
4.2	Future Work.....	43
5	Experimental	44
5.1	General Procedure.....	44
5.2	Experimental Procedures for Chapter 2	46
5.3	Experimental Procedures for Chapter 3	50
6	References.....	R1

Appendix A: Catalysis Data (Chapter 3)	A1
A1 Catalysed Dihydroalkoxylation of 2-(5-(hydroxymethyl)phenyl)pent-4-yn-1-ol (11)	A1
A2 Catalysed Dihydroalkoxylation of 2-(4-hydroxypent-1-ynyl)benzyl alcohol (23).....	A5
Appendix B: Stacked Cyclic Voltammograms of Complexes 13a , 19 and 16 , the Corresponding Free Ligands and $[\text{Rh}(\text{CO})_2\text{Cl}]_2$	A10
Appendix C: List of Numbered Compounds.....	A12

List of Figures

Figure 1a) Metals attached to separate ligands on the same scaffold. b) Different modes of bimetallic cooperativity: i) substrate molecule coordinated to both metals simultaneously; ii) the coordinated metal stabilised by the second metal centre of the same complex. iii) two substrate molecules coordinated to a metal centre each, creating a high local concentration of activated substrates.....	4
Figure 2 A bimetallic Ir(III)/Ru(II) complex prepared by Peris and co-workers (1), and its diiridium and diruthenium analogues 2a and 2b	5
Figure 3 Targeted bimetallic complexes in this project.	10
Figure 4 Possible reaction pathways for Rh vinylidene complex formation.	16
Figure 5 Cyclic voltammogram of complex 18 (red) and complex 19 (blue), both 1 mM in 0.1M [Bu ₄ N][PF ₆]/CH ₂ Cl ₂ supporting electrolyte at 100 mV/s.....	17
Figure 6 Complex 18 and structurally similar Rh(I) complexes containing anionic ligands and CO co-ligand. The CVs of the latter were reported in literature. ³⁷	18
Figure 7 Stacked voltammograms for complex 18 . Measurement was initiated with either an anodic sweep (red) or a cathodic sweep (black) in 0.1 M [Bu ₄ N][PF ₆]/DCM, 100 mV/s.	18
Figure 8a) bpm, mim and dpm ligand motifs bound to Rh(I) centre. b) Dirhodium complexes incorporating the bpm, mim and dpm moieties.	20
Figure 9a) Stacked VT ¹ H NMR spectra of complex 16 taken in CD ₂ Cl ₂ . b) HSQC spectrum of complex 16 at 243 K, in the <i>bis</i> (pyrazolyl)methane methylene region, showing the correlation of between the carbon-13 and proton resonances at position 2' in complex 16 . c) NOESY spectrum of complex 16 at 243 K showing correlation between the H2' resonances of two different conformers of complex 16 (labelled a & b).....	22
Figure 10 2D NOESY spectrum for complex 17 taken at 298 K in CD ₂ Cl ₂ . Both nOe cross peaks (green) and dynamic exchange cross peaks (blue) are present, indicating nOe transfer between closely situated protons as well as conformational exchange of complex 17	26
Figure 11 Intermolecular hydroalkoxylation of methanol and phenylacetylene using catalysts 13a , 18 , 19 , 16 and 17 in DMA (<i>N,N</i> -dimethylacetamide), using 1 mol% rhodium loading, at 25°C over 24 h. Conversion was determined after 24 h by comparing the integral ratio of the alkyne proton resonance (<i>ca.</i> 3 ppm) and the product alkene resonances (5-7 ppm) using ¹ H NMR spectroscopy; <i>E/Z</i> ratios were determined by comparing the intensity of <i>E</i> and <i>Z</i> alkene resonances. *Results from previous studies. ³³	27
Figure 12a) Reaction profiles of dihydroalkoxylation of 2-(5-hydroxypent-1-ynyl)benzyl alcohol (11) to give spiroketals 22a and 22b in C ₂ D ₂ Cl ₄ at 100	

°C using individual catalysts, 0.5 mol% $[\text{Rh}_2(\text{CO})_4(o\text{-bpm/mim})][\text{BAR}^{\text{F}}_4]_2$ (16), 0.5 mol% $[\text{Rh}_2(\text{CO})_4(o\text{-dpm/mim})]\text{BAR}^{\text{F}}_4$ (17), 2 mol% $[\text{Rh}(\text{CO})_2\text{dpm}]$ (18), and 1 mol% $[\text{Rh}(\text{CO})_2\text{bpm}]\text{BAR}^{\text{F}}_4$ (19). b) Reaction profiles of dihydroalkoxylation of 2-(4-hydroxypent-1-ynyl)benzyl alcohol (23) to give spiroketal 24 and enol ether 25 in $\text{C}_2\text{D}_2\text{Cl}_4$ at 100 °C using individual catalysts, 0.5 mol% $[\text{Rh}_2(\text{CO})_4(o\text{-bpm/mim})][\text{BAR}^{\text{F}}_4]_2$ (16), 0.5 mol% $[\text{Rh}_2(\text{CO})_4(o\text{-dpm/mim})]\text{BAR}^{\text{F}}_4$ (17), and 1 mol% $[\text{Rh}(\text{CO})_2\text{bpm}]\text{BAR}^{\text{F}}_4$ (19).....	31
Figure 13 Proposed mechanisms for C-O bond formation by the addition of oxygen nucleophile to $\text{C}\equiv\text{C}$ bond. Mechanism A: direct addition of oxygen nucleophile to the metal-alkyne π -complex. Mechanism B: oxidative C-H insertion, followed by the formation of a vinylidene intermediate and then the attack of oxygen nucleophile.	32
Figure 14 Cyclic voltammograms of complexes 16 , 13a and 19 . at 100 mV/s. Measurements were conducted in 0.1 M $[\text{Bu}_4\text{N}][\text{PF}_6]/\text{CH}_2\text{Cl}_2$ vs. a leakless Ag/AgCl reference electrode at 298 K. Scans were initiated in the positive direction.	34
Figure 15 Cyclic voltammograms of complexes 17 , 13a and 18 at 100 mV/s. Measurements were conducted in 0.1 M $[\text{Bu}_4\text{N}][\text{PF}_6]/\text{CH}_2\text{Cl}_2$ vs. a leakless Ag/AgCl reference electrode at 298 K. Scans were initiated in the positive direction.	35
Figure 16 Cyclic voltammograms of complexes 16 and 17 at 100 mV/s. Measurements were conducted in 0.1 M $[\text{Bu}_4\text{N}][\text{PF}_6]/\text{CH}_2\text{Cl}_2$ vs. a leakless Ag/AgCl reference electrode at 298 K. Scans were initiated in the positive direction.	38
Figure 17 Cyclic voltammograms of complex 10 , ligand 34 and $[\text{Rh}(\text{CO})_2\text{Cl}]_2$ at 100 mV/s. Measurements were conducted in 0.1 M $[\text{Bu}_4\text{N}][\text{PF}_6]/\text{CH}_2\text{Cl}_2$ vs. a leakless Ag/AgCl reference electrode at 298 K. Scans were initiated in the positive direction.	38
Figure 18 Cyclic voltammograms of complex 13a , ligand 36 and $[\text{Rh}(\text{CO})_2\text{Cl}]_2$ at 100 mV/s. Measurements were conducted in 0.1 M $[\text{Bu}_4\text{N}][\text{PF}_6]/\text{CH}_2\text{Cl}_2$ vs. a leakless Ag/AgCl reference electrode at 298 K. Scans were initiated in the positive direction.	10
Figure 19 Cyclic voltammograms of complex 19 , ligand 35 and $[\text{Rh}(\text{CO})_2\text{Cl}]_2$ at 100 mV/s. Measurements were conducted in 0.1 M $[\text{Bu}_4\text{N}][\text{PF}_6]/\text{CH}_2\text{Cl}_2$ vs. a leakless Ag/AgCl reference electrode at 298 K. Scans were initiated in the positive direction.	10
Figure 20 Cyclic voltammograms of complex 16 , ligand 26 and $[\text{Rh}(\text{CO})_2\text{Cl}]_2$ at 100 mV/s. Measurements were conducted in 0.1 M $[\text{Bu}_4\text{N}][\text{PF}_6]/\text{CH}_2\text{Cl}_2$ vs. a leakless Ag/AgCl reference electrode at 298 K. Scans were initiated in the positive direction.	11

List of Schemes

Scheme 1a) Intermolecular hydroalkoxylation of phenylacetylene with methanol to afford enol ethers. b) Dihydroalkoxylation of 2-(5-hydroxypent-1-ynyl)-benzyl alcohol to produce spiroketals.	3
Scheme 3a) Intramolecular dihydroalkoxylation of alkyne diol to furnish spiroketal products. b) Mono- and dirhodium complexes that were used as catalysts for the dihydroalkoxylation reaction.	8
Scheme 4a) Dihydroalkoxylation reaction of 11 . b) (1-methylimidazolyl)- <i>N</i> -phenyl-imine (Phmim) complexes and derivatives that were used as catalysts.	9
Scheme 5 Synthesis of $[\text{Rh}(\text{CO})_2\text{Phdp}m]$ (18).	12
Scheme 6a) Intermolecular hydroalkoxylation of methanol and phenylacetylene using DMA (<i>N,N</i> -dimethylacetamide) as the co-solvent. b) Dihydroalkoxylation of alkyne diol to afford 5,6- or 6,5-spiroketals. c) Dihydroalkoxylation of alkyne diol to afford 5,5-spiroketal and enol ether products.	12
Scheme 7 Synthesis of $[\text{Rh}_2(\text{CO})_4(o\text{-bpm}/\text{mim})][\text{BAR}^F_4]_2$ (16) and $[\text{Rh}_2(\text{COD})_2(o\text{-bpm}/\text{mim})][\text{BAR}^F_4]_2$ (27) from ligand 26	21
Scheme 8 The preparation of pro-ligand 32 from ligand precursor 28 via two synthetic pathways.	24
Scheme 9 Synthesis of complex 17 and complex 33 from pro-ligand 32	25

List of Tables

Table 1 Hydroalkoxylation of phenylacetylene and different alcohols catalysed by complex 18 (<i>ca.</i> 1 mol%).....	13
Table 2 Hydroalkoxylation of methanol and various alkyne substrates catalysed by catalyst 18 (<i>ca.</i> 1 mol%).....	15
Table 3 Conversion of alkyne diols (11 & 23) to regioisomeric spiroketal products (22a , 22b & 24) and the monocyclised product 25 , using catalysts 16 and 17 , at 1 mol% rhodium loading.	29
Table 4 Electrochemical oxidation and reduction data for complexes 16-19 & 13a . Measurements were undertaken in 0.1 M [Bu ₄ N][PF ₆]/CH ₂ Cl ₂ using a leakless Ag/AgCl reference electrode at 298 K (which comes at -0.625 V vs. Fc/Fc ⁺). All potentials were measured at a constant sweep rate of 100 mV/s and are reported relative to the Fc/Fc ⁺ couple.	33
Table 5 Summary of trends observed for mono- and bimetallic complexes as catalysts for C-O bond formation and in electrochemical studies.....	43
Table 6 Quantities of catalyst and phenylacetylene used.....	54
Table 7 Quantities of catalyst and 2-(5-hydroxypent-1-ynyl)benzyl alcohol (11) used.	55
Table 8 Quantities of catalyst and 2-(4-hydroxypent-1-ynyl)benzyl alcohol (23) used.	55

Abstract

The first part of this thesis describes the intermolecular hydroalkoxylation of terminal alkynes catalysed by $[\text{Rh}(\text{CO})_2\text{Phdpm}]$ (**18**), affording enol ethers with high yield and selectivity. The reactions proceed with optimum conversion and selectivity in the absence of moisture and oxygen and tolerate a range of substituted aryl and allyl acetylene substrates, but do not proceed with internal alkynes. The redox behaviour of complexes **18** and $[\text{Rh}(\text{CO})_2\text{bpm}]\text{BAR}^{\text{F}}_4$ (**19**), probed using cyclic voltammetry, indicate the reaction may proceed *via* formation of a vinylidene intermediate.

In the second part, two novel bimetallic complexes with heteroditopic ligands (**16** with bpm/mim motifs; **17** with dpm/mim motifs) were synthesised and characterised. These were tested as catalysts for the intermolecular hydroalkoxylation of phenylacetylene with methanol, and the intramolecular dihydroalkoxylation of alkyne diols **11** and **23**. Compared to analogous monometallic complexes, **17** exhibited cooperative rate enhancement in the intermolecular hydroalkoxylation reaction; and both **16** and **17** displayed rate inhibition in the intramolecular dihydroalkoxylation. The redox potentials of **16** and **17**, and **10** were compared to those of **18**, **19** and $[\text{Rh}(\text{CO})_2\text{Phmim}]\text{BAR}^{\text{F}}_4$ (**13a**). Evidence supports a rate limiting vinylidene formation step for the intermolecular hydroalkoxylation reaction.

1 Introduction

The aim of this project is to discover novel, effective monometallic and bimetallic catalysts for homogeneous C-X bond formation reactions. In the case of bimetallic catalysts, the aim is also to better understand the role of electronic communication between the metal centre pair during catalysis, as bimetallic complexes have been shown to enhance C-X bond formation more effectively than monometallic complexes and the mechanism is not fully understood.

1.1 Catalysis

Catalysis is integral to the industries that support our society,¹ playing a central role in many different processes ranging from fuel processing to the production of bulk and fine chemicals, agrochemicals and pharmaceuticals.¹⁻² According to IUPAC (International Union of Pure and Applied Chemistry), the process of catalysis involves adding a substance that *“increases the rate of a reaction without modifying the overall standard Gibbs energy change in the reaction”*, where the substance (catalyst) is not consumed during the reaction.³ On the addition of a very small quantity of catalyst, the efficiency of chemical reactions can be greatly enhanced. Catalysts provide alternative reaction pathways of lower activation energy to achieve an overall chemical transformation, and/or lower time demand of chemical reactions, thereby decreasing waste generation.^{2a, 4}

The major challenges of catalysis today include the discovery of catalysts that give high levels of product selectivity (enantio-, diastereo-, regio- and chemo-), and the ability to design catalysts to target specific chemical transformations.⁵ Catalysts can promote single-step direct bond formation in addition to tandem catalytic processes, reducing the number of synthetic steps and improving the overall atom economy of reactions.⁶ The benefits of catalysts are especially attractive as resources become scarcer or new feedstocks become available.⁷

1.2 Transition Metal Complexes in Homogeneous Catalysis

The defining feature of homogeneous catalysis is that the catalyst is in the same phase as the reactants, most commonly the solution phase.^{2b, 5} Examples of homogeneous catalysts include metallic complexes, Lewis acids and bases, ionic liquids, organic and inorganic compounds.⁸ This project will focus on homogeneous organometallic complexes, defined as complexes containing metal-carbon bonds.

Homogeneous catalysts generally exhibit higher catalytic activity and product selectivity than heterogeneous catalysts, and require milder reaction conditions.⁹ They are applied in some of the most important processes in the chemical industry.¹ Classic examples include hydroformylation of ethylene to form butyraldehyde, the Monsanto process to produce acetic acid, and the use of Ziegler-Natta type catalysts for terminal alkene polymerisation.^{2, 5, 9} The products of these processes are important bulk chemicals that can be used in further preparation of specialised chemicals.

The role of homogeneous catalysis is of particular importance in pharmaceutical chemistry, as chiral centres are often introduced into the products and homogeneous catalysis can achieve high levels of enantioselectivity.¹⁰ Examples include asymmetric hydrogenation, oxidation (e.g. epoxidation), metathesis, and cross-coupling reactions.¹¹

The many combinations of metals and ligands available render organometallic complexes among the most versatile classes of catalyst.^{2b, 5, 12} The metal centres employed are often d-block metals due to the excellent catalytic abilities and plentiful options of metals, coordination geometries and oxidation states available. The choice of the corresponding oxidation state and coordination geometry dictates the type of reaction that can be efficiently catalysed by a given complex. Late transition metals, such as Rh, have been extensively studied and will be the focus of this project. Complexes containing Group 9 & 10 metals have the ability to undergo two electron redox processes, which is important in catalytic cycles that involve oxidative additions and reductive eliminations.¹² The electronic properties and accessibility of the metal centres can be fine-tuned by varying the ligands.^{5, 10, 13} Depending on the metal-ligand bonding and the ligand substituents, the Lewis acidity or electrophilicity of the metal centre can be tailored to favour the interaction with target substrates.¹⁴ The orientation and the chirality of the ligand may restrict the intermediate conformation and lead to selective product formation.¹⁵

In addition to the range of catalysts available, homogeneous catalysis is also attractive because the reaction intermediates can be characterised by spectroscopic methods. This can facilitate mechanism elucidation, which can in turn lead to the improvement of catalyst design.¹⁶ The structure of reaction intermediates reveals valuable information, about catalyst-substrate interactions and the key steps that determine product selectivity. The chemical and structural dynamics of these intermediate complexes can be monitored using

variable temperature NMR spectroscopy.^{16a} This technique can be coupled with isotopic labelling to observe changes in the conformation of specific ligands about the metal centre(s) even for short lived intermediate species.

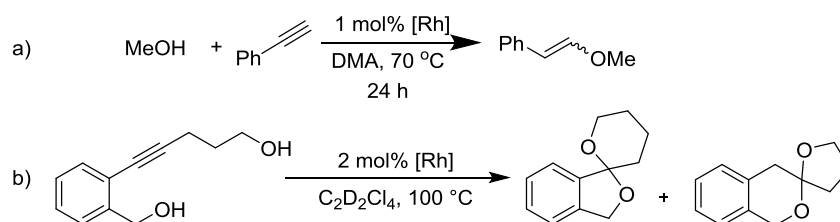
Information about the redox behaviour and the metal-ligand interaction can also be obtained by means of electrochemistry and spectroscopy, providing a better understanding and prediction of metal catalyst reactivity.¹⁷ The use of electrochemical techniques such as cyclic voltammetry is particularly relevant for investigating electronic communication between the metal centres(s) of a bimetallic complex and/or other parts of the complex, as well as elucidating the reaction mechanism.¹⁸ The evidence of electronic coupling of the metals in of bimetallic complexes can be found in a straightforward manner by inspection of the voltammograms.

1.2.1 C-X Bond Forming Reactions

Attention in recent years has been directed at improving the atom economy of chemical processes and circumventing multiple, arduous purification steps.^{6b} Direct bond formation and substrate activation are straightforward strategies to construct complex architecture in the target compounds, and catalysed one-pot, multistep chemical transformations have become an important and popular area of research.¹⁹

The catalysis scope of this project is directed towards C-X bond formation, where X can be a heteroatom such as O, N or S. Developing highly efficient synthetic approaches to C-X bond formation reactions would have a significant impact on reducing the often lengthy synthetic pathways for the synthesis of biologically active molecules.^{6c, 20}

The reactions that will be the focus of this project are the catalysed intermolecular hydroalkoxylation and intramolecular dihydroalkoxylation reactions (Scheme 1). In these cases, new C-O bonds are formed to afford enol ether and spiroketal products respectively.



Scheme 1a) Intermolecular hydroalkoxylation of phenylacetylene with methanol to afford enol ethers. **b)** Dihydroalkoxylation of 2-(5-hydroxypent-1-ynyl)-benzyl alcohol to produce spiroketals.

1.3 Bimetallic Catalysts and Cooperativity

A variety of bimetallic catalysts have been reported to efficiently catalyse chemical transformations, and these bimetallic complexes can exhibit synergistic effects such that they catalyse reactions more efficiently than their analogous monometallic counterparts.^{13b,}

²¹ The two metal centres of bimetallic complexes can be attached to separated binding sites tethered to the same scaffold (also known as bridging scaffold, Figure 1a), or connected by bridging atoms, or directly bonded to each other.

This project focuses on bimetallic complexes built on a bridging scaffold (Figure 1a). Their catalytic properties can be fine-tuned by varying the steric demand or the rigidity of the ligand system, including the scaffold. Connecting the metal centres with a bridging scaffold greatly reduces the likelihood of the bimetallic complex fragmenting into monometallic species during catalysis, unlike bimetallic complexes with bridging atoms or direct metal-metal bonds. Fragmentation of the complex removes the advantages of the bimetallic catalysts.^{21e}

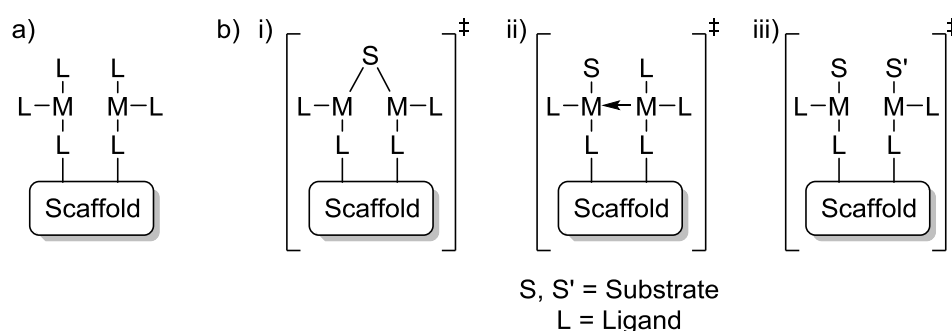


Figure 1a) Metals attached to separate ligands on the same scaffold. **b)** Different modes of bimetallic cooperativity: **i)** substrate molecule coordinated to both metals simultaneously; **ii)** the coordinated metal stabilised by the second metal centre of the same complex. **iii)** two substrate molecules coordinated to a metal centre each, creating a high local concentration of activated substrates.

In comparison with their monometallic analogues, bimetallic catalysts can exhibit enhanced catalytic activity^{21b, 22} and/or product selectivity.^{21d-g} This phenomenon has generally become known as “bimetallic cooperativity”,²³ as the two metals are believed to participate in the catalysis event in a synergistic manner. The transition state of catalysed chemical reactions using bimetallic catalysts (Figure 1b) may involve the substrate bound to both metals, one substrate molecule bound to a metal and the structure stabilised by the second metal, or two separate substrate molecules bound to a metal each.^{8e} The key in the enhancement of catalysis using these modes of bimetallic cooperativity is believed to be the close proximity

of the two metal centres. The optimum metal-metal separation is proposed to be 3.5-6 Å for a pronounced bimetallic cooperativity of single-step reactions.²⁴

1.3.1 Electronic Interactions in Bimetallic Complexes

It is thought that by tethering two metal centres to a highly conjugated ligand scaffold, or by allowing two metal centres to interact through space, the electronic structure and the redox properties of the metals could be altered to favour specific catalysed chemical reactions. While the role of intermetallic electronic communication in bimetallic cooperativity is not well understood, examples of changes in the redox behaviour of one metal in the presence of a second metal have been reported.^{18, 23}

In the preparation of bimetallic complexes, Peris and co-workers²⁵ showed that the heterobimetallic Ir(III)/Ru(II) complex **1** (Figure 2) exhibits different redox potentials than the diiridium and diruthenium analogues **2a** and **2b**. These different redox potentials were attributed to electronic communication between the two metals in the bimetallic complex, mediated by the 1,2,4-triazole-diylidene ligand.

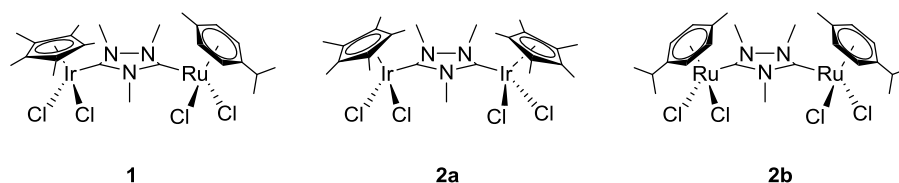


Figure 2 A bimetallic Ir(III)/Ru(II) complex prepared by Peris and co-workers (**1**), and its diiridium and diruthenium analogues **2a** and **2b**.

Complex **1** displayed reversible redox processes at 1.29 and 1.35 V, which were intermediate between those exhibited by complexes **2a** (1.34 and 1.46 V) and the irreversible oxidation of **2b** at 1.15 V. The shifted oxidation potentials in **1** compared to **2a** and **2b** indicate the Ir metal and the ruthenium metal in complex **1** are coupled electronically.

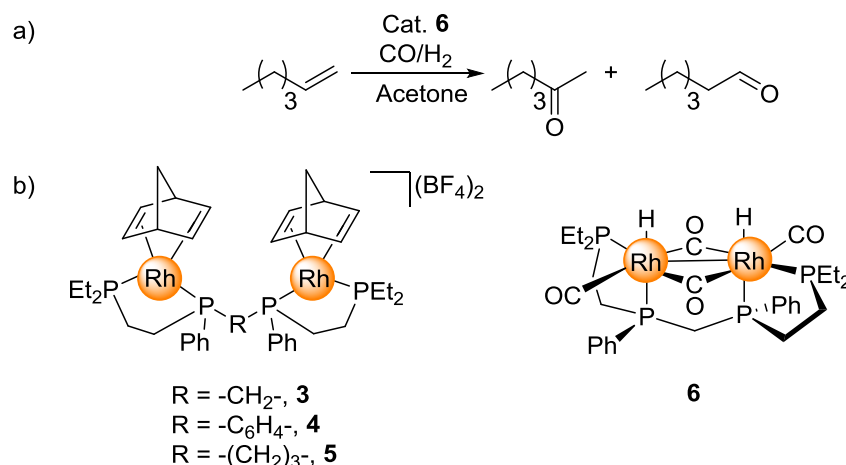
Complexes **1**, **2a** and **2b** were used to catalyse the Oppenauer oxidation of 1-phenylethanol. The Ir(III)/Ru(II) complex **1** was found to achieve a product yield in between those of the analogous bimetallic complexes **2a** and **2b**. This trend correlates to their oxidation potentials recorded in electrochemical studies.

1.3.2 Spatial Dependence of Intermetallic Interactions in Bimetallic Complexes

While the direct correlation of electronic coupling and observed bimetallic cooperativity has not been well investigated to date, the superior catalytic activity and product selectivity of

bimetallic catalysts over analogous monometallic species have been found to be closely related to the spatial proximity of the metal centres.^{8e, 13b, 21a, 21d, 21f}

Stanley *et al.* were able to catalyse the hydroformylation of 1-hexene (Scheme 2a) with excellent product selectivity and conversion using the dirhodium catalyst **3**, which was 600 times more efficient than the monometallic “half unit”, and 9 – 14 times more selective to the linear product.^{21a}



Scheme 2a) Hydroformylation of 1-hexene in the presence of carbon monoxide, hydrogen and catalyst. **b)** Dirhodium catalysts for hydroformylation (**3-5**) and a proposed reaction intermediate (**6**) for the hydroformylation reaction.

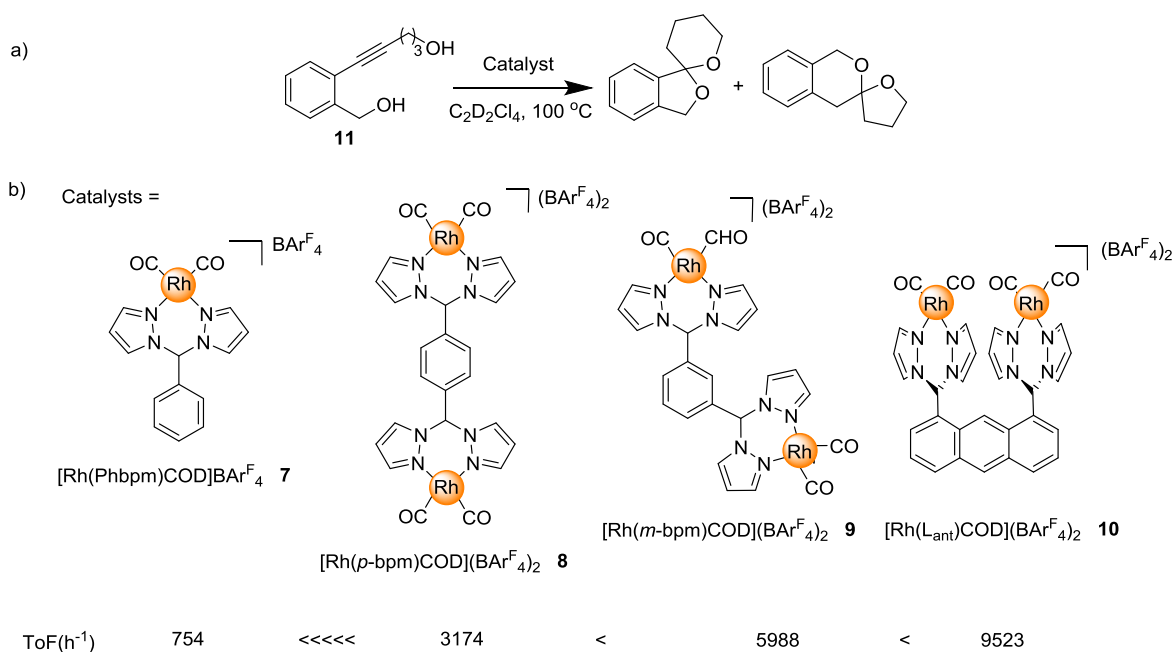
To illustrate the importance of the short Rh...Rh distance, Stanley and co-workers repeated the experiment using complexes with longer linking spacers (**4** and **5**). The Rh...Rh separation and structural flexibility were greater in complexes **4** and **5** than those in **3**, and the substrate conversion dramatically decreased when using catalyst **4** or **5**. Based on *in situ* spectroscopic studies, a catalytic cycle was proposed that involves the formation of a dicationic Rh(II) dimer **6** as the catalytically active species (Scheme 2b). The Rh(II) oxidation state of dimer **6** and the dicationic character reduce the degree of π -backbonding to the CO co-ligand, thereby increasing its lability and creating a vacant site for incoming substrates. This was not observed for complexes **4** and **5** which have well separated rhodium centres that disfavour the formation of the Rh(II) dimer. The CO co-ligand remain bound to the rhodium metals in complexes **4** and **5** due to the strongly donating phosphorus ligand and the relatively electron rich Rh(I) centre, and reduces the efficiency of the catalyst.

1.3.3 Tandem Reaction – Dihydroalkoxylation Reaction

Bimetallic complexes are being investigated as useful catalysts for tandem, one-pot reactions which can generate more complicated structures in one step, leading to a more atom economical reaction.²⁶

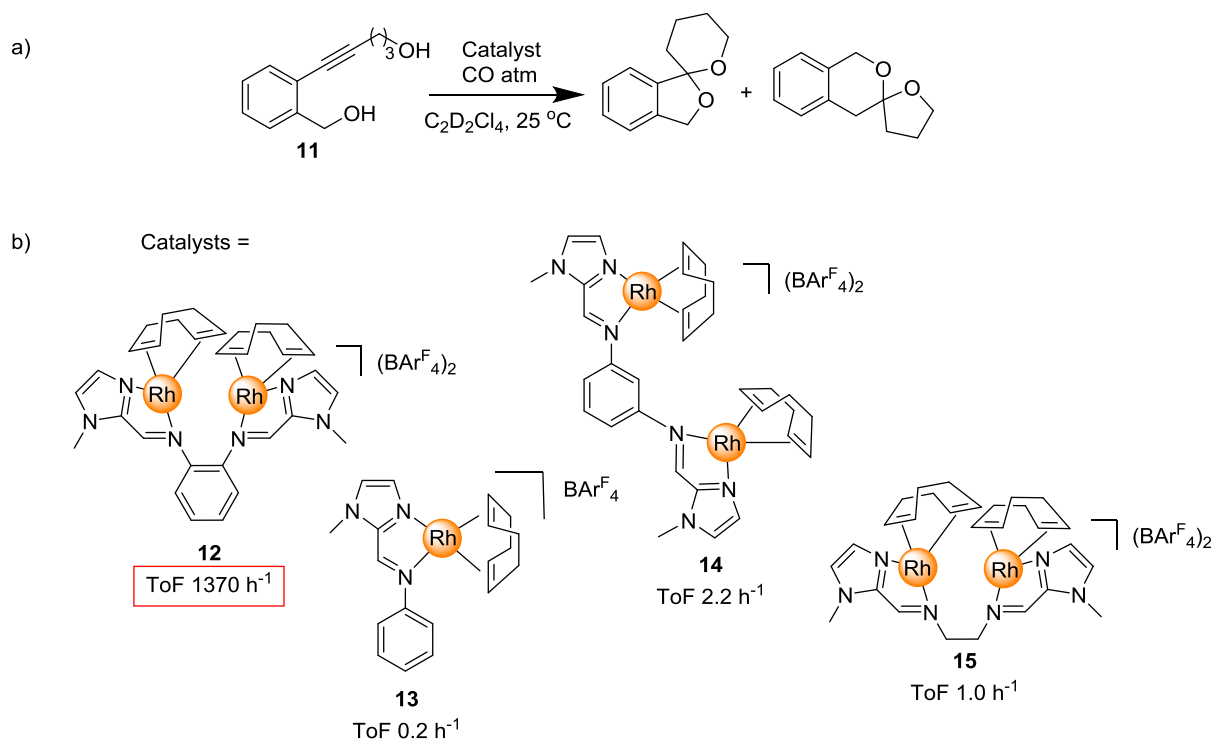
Messerle *et al.* have investigated a range of mono- and bimetallic Rh(I) and Ir(I) complexes containing bidentate *N*-donor ligands as catalysts for C-O bond forming reactions, in particular the dihydroalkoxylation reaction of alkyne diols.^{21b, 22, 27} Rh(I) complexes containing the *bis*(1-pyrazolyl)methane (bpm) moiety (Scheme 3b) were found to be excellent catalysts for the intramolecular dihydroalkoxylation of alkyne diols to form spiroketals. On comparing the activities of catalysts **7**, **8**, **9**, and **10** for the dihydroalkoxylation reaction of **11** (Scheme 3a), it was apparent that the bimetallic catalysts **8**, **9**, and **10** are more efficient at catalysing the dihydroalkoxylation reaction than the monometallic analogue **7**. The catalytic efficiency was found to increase as the Rh centres come closer in space.^{22, 27b}

In an attempt to better understand the structure-activity relationship of the bimetallic catalysts **8**, **9**, and **10**, their structural conformations were modelled using DFT calculations.^{21c} These studies revealed a large degree of variability in the metal-metal distances due to the rotation of the substituent complexes about the bpm-arene bonds and also conformational changes within the six-membered metallacycles. Owing to this structural flexibility in these bimetallic complexes, the intermetallic distances are poorly defined and a direct correlation between the reactivity and metal-metal separation could not be drawn.



Scheme 3a) Intramolecular dihydroalkoxylation of alkyne diol to furnish spiroketal products. **b)** Mono- and dirhodium complexes that were used as catalysts for the dihydroalkoxylation reaction.

To reduce this fluxionality and bring the metal centres closer together, complexes containing the (1-methylimidazolyl)imine (mim) motifs were synthesised (**12-15**, Scheme 4b) and tested as catalysts for the dihydroalkoxylation reaction of **11**.^{21b} The structure of the imine-imidazole ligand when bound to a metal is a flat 5-membered metallacycle with a rigid geometry, with less conformational freedom than present in the bpm ligand system, as well as better alignment of the Rh metals with shorter intermetallic distances. Catalyst **12** displayed the greatest bimetallic enhancement compared to other bimetallic catalysts, **8-10**, and **14-15**, and the turnover frequency (ToF) was observed to be 6800 times greater for the dihydroalkoxylation of alkyne diol **11** than that using the monometallic analogue **13**. Increasing the intermetallic distance (**14**) or the flexibility of the ligand backbone (**15**) resulted in significantly reduced catalytic activity.



Scheme 4a) Dihydroalkoxylation reaction of **11**. **b)** (1-methylimidazolyl)-*N*-phenyl-imine (Phmim) complexes and derivatives that were used as catalysts.

The investigation of the bimetallic complexes **12**, **14**, and **15** led to the conclusion that the enhancement in catalytic efficiency is very sensitive to the intermetallic distances. It is possible that the second metal centre stabilises the reaction intermediate better on using complexes **12**, **14**, and **15** than is achieved for complexes **8-10**, where the Rh...Rh distances are poorly defined. However, the ligand scaffold linking the two metals in complex **12** is conjugated from one metal to the other, thus it is possible that electronic influence through bond coupling plays a role here.

1.4 Objectives of this Project

In recent work developing new highly efficient catalysts for C-X bond formation, a novel Rh(I) complex containing the dipyrinato motif (dpm) with bidentate *N* donors was found to catalyse the intermolecular hydroalkoxylation of alcohols and terminal alkynes.²⁸ Here, the reaction conditions for the application of this catalyst to C-O bond formation will be further optimised and the substrate scope expanded. A preliminary mechanistic study using cyclic voltammetry will also be undertaken.

Given the high levels of catalytic efficiency achieved using bimetallic complexes with pairs of identical metal complexes attached to suitable scaffolds, and the extremely high levels of efficiency of Rh(I)-bpm and Rh(I)-mim complexes in catalysing intramolecular

dihydroalkoxylation reactions, heteroditopic dirhodium species with two different motifs (bpm, mim, and dpm) attached to scaffolds will be synthesised and explored as catalysts in the intermolecular hydroalkoxylation and intramolecular dihydroalkoxylation reactions.

Building upon previous work that has demonstrated electronic communication between metal centres in multimetallic systems, it is of particular interest to investigate whether electronic communication could be playing a role in the bimetallic cooperativity exhibited by bimetallic catalysts **8-10**, **12**, **14**, and **15** and related complexes.^{21b, 22} This project aims to elucidate the role of electron transfer in the bimetallic cooperativity of catalysts with conjugated ligand scaffolds. This project will involve:

- i) Optimising the intermolecular hydroalkoxylation reaction between methanol and phenylacetylene to form anti-Markovnikov enol ether products, using complex **18** as catalyst (Figure 3), and probing the reaction mechanism using cyclic voltammetry.
- ii) The synthesis of novel bimetallic catalysts **16** and **17** containing bpm, mim and dpm coordinating groups.

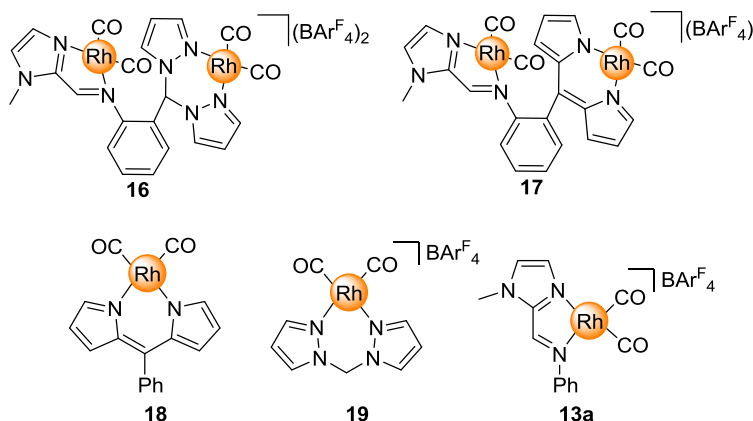


Figure 3 Targeted bimetallic complexes in this project.

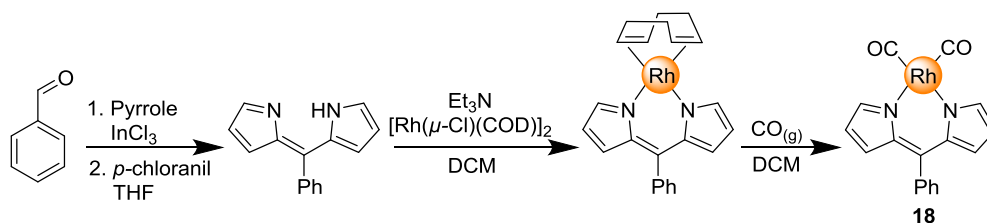
- iii) Testing **16** and **17** as catalysts for the dihydroalkoxylation reaction of the alkyne diol substrate **11** as well as the hydroalkoxylation of phenylacetylene with methanol. The catalytic performance of complexes **16** and **17** will be compared to that of the monometallic analogues **18**, **19** and **13a** to determine if there are any cooperative effects observed on using the bimetallic species.

iv) Examining the redox behaviour of related bimetallic catalysts, including **10**, **12**, **16**, and **17** using cyclic voltammetry and attempting to correlate the catalytic data with the electrochemical results obtained.

2 Catalysed Intermolecular Hydroalkoxylation Reaction Using a Monometallic Rh(I) Catalyst

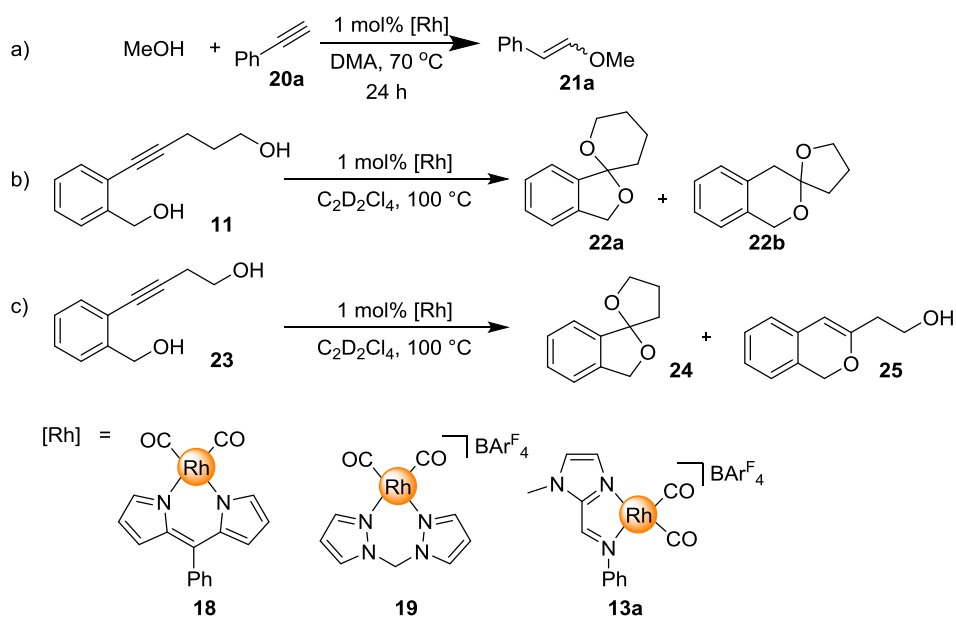
Rh(I) and Ir(I) complexes with bidentate *N* donor ligands are highly efficient catalysts for C-X (X = S, N, O) bond formation using substrates with unsaturated C-C bonds.²⁹ When exploring Rh(I) complexes with a planar and rigid rhodacycle as potential catalysts for C-X bond formation reactions, the (5-phenyldipyrrinato)rhodium dicarbonyl complex **18** was found to efficiently catalyse the intermolecular hydroalkoxylation of alcohols and terminal alkynes,²⁸ yielding enol ethers which can be employed as useful building blocks for cycloaddition, cross-coupling, and ring-closing metathesis reactions.³⁰ Similar to the recent progress made by Kakiuchi and co-workers on the same reaction using a neutral Rh(I) complex containing *N*, *O*-donors, complex **18** was found to promote the formation of exclusively the anti-Markovnikov enol ethers, but with an opposite *E:Z* ratio.³¹ This interesting finding prompted the further investigation of optimal reaction conditions, substrate scope expansion and initial reaction mechanism elucidation presented in this chapter.

The 5-phenyldipyrrinato ligand (Phdpm) is a bidentate *N*-donor ligand that may form effective organometallic catalysts for a variety of C-X bond forming reactions upon complexation with Rh(I) metal. On comparing the structure of complexes formed using the Phdpm ligand with those formed using other *N,N* donor ligands, the rigid, conjugated backbone of dpm results in a rhodacycle with a planar geometry, while the *bis*(pyrazole-1-yl)methane (bpm) ligand forms flexible, boat-shaped metallacycles.^{21c, 28} Bearing a negative charge, the Phdpm ligand should also be less labile compared to the bpm and (1-methylimidazolyl)-*N*-phenyl-imine (Phmim) ligands, due to increased coulombic attraction to the positively charged metal. The dipyrinato Rh(I) complex [Rh(CO)₂Phdpm] (**18**) was prepared and tested as a catalyst for the intermolecular hydroalkoxylation of alcohols and terminal alkynes. These results provide a benchmark for the comparison to the bimetallic complex containing the Rh-dpm motif investigated later in this work.



Scheme 5 Synthesis of $[\text{Rh}(\text{CO})_2\text{Phdp}]$ (**18**).

Complex **18** was prepared according to reported procedure (Scheme 5).³² Previous studies showed that complex **18** has complementary catalytic activities to $[\text{Rh}(\text{CO})_2\text{bpm}][\text{BAR}^{\text{F}}_4]$ (**19**) and $[\text{Rh}(\text{CO})_2\text{Phmim}][\text{BAR}^{\text{F}}_4]$ (**13a**, Scheme 6).³³ Of the three metal complexes **18**, **19**, and **13a**, only **18** is efficient as a catalyst for the intermolecular hydroalkoxylation of methanol and phenylacetylene to afford anti-Markovnikov enol ether products (Scheme 6a).^{28, 33} Complexes **19** and **13a** meanwhile are highly efficient at catalysing intramolecular dihydroalkoxylation and hydroamination reactions.^{28, 33}



Scheme 6a Intermolecular hydroalkoxylation of methanol and phenylacetylene using DMA (*N,N*-dimethylacetamide) as the co-solvent. **b**) Dihydroalkoxylation of alkyne diol to afford 5,6- or 6,5-spiroketal. **c**) Dihydroalkoxylation of alkyne diol to afford 5,5-spiroketal and enol ether products.

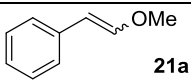
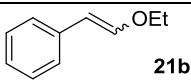
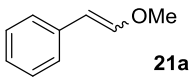
The original work investigating the catalysed intermolecular hydroalkoxylation of phenylacetylene with methanol found that use of *N,N*-dimethylacetamide (DMA) as the co-solvent led to optimal product yield and selectivity.^{28, 33} The reaction conditions were further optimised and the substrate scope was expanded, and these investigations of the reaction scope are included in this work.

2.1 Establishing Optimal Conditions

In the original work optimising co-solvents and conditions,^{28, 33} reactions were carried out under a nitrogen atmosphere. Anhydrous grade alcohols and solvents were sparged with nitrogen gas for 10 min before the reactions; while the alkyne substrates were used as received. In this work, the effects of increasing the dissolved oxygen and the moisture content of the solvent on product yield and selectivity were also investigated (Table 1).

Table 1 Hydroalkoxylation of phenylacetylene and different alcohols catalysed by complex **18** (ca. 1 mol%).

ROH + **20a** $\xrightarrow[\text{DMA, 70 } ^\circ\text{C, 24 h}]{\text{1 mol\% } \mathbf{18}}$ Ph-CH=CH-OR + Ph-CH=CH-OR

Entry	Alcohol	Product	Conv. ^a	E/Z ratio ^b
1 ^c	MeOH	 21a	>98% (95%)	7:1
2 ^c	EtOH	 21b	>98% (75%)	3:1
3 ^d	MeOH	 21a	50%	8:1
4 ^e			57%	2:1

^a Isolated yield in parentheses. ^b E/Z ratio determined by comparing the ratio of the product alkene resonances (5-7 ppm) using ¹H NMR spectroscopy. ^c Results from previous studies.³³ ^d MeOH and DMA were aerated prior to reaction. ^e Reaction mixture was wetted with 10 drops of water.

DMA and methanol were aerated separately by bubbling compressed air for 10 min before mixing with phenylacetylene substrate and catalyst **18**. Conversion to the products using aerated solvents was monitored by ¹H NMR spectroscopy. The hydroalkoxylation using O₂ aerated methanol afforded a substantially lower yield (50%, entry 3) than had been observed for methanol and DMA under N₂, probably due to deactivation of the catalyst or a key reaction intermediate by atmospheric oxygen. A similar selectivity for the *E* product (*E*/*Z* ratio = 8:1) was observed in the aerated reaction compared to previous studies (entry 1). Addition of water to the reaction mixture resulted in decreased substrate conversion (57%, entry 4) and product selectivity (*E*/*Z* ratio = 2:1), as well as the formation of trace amounts of an aldehyde product. While water can compete against methanol in coordinating to the Rh centre, it may also be involved in the reaction mechanism. The reaction intermediate originated from water and catalyst **1** may be able to react with methanol too but with an elevated energy barrier to both the *E* and *Z* enol ether compared to the case without added water. As such, conversion to the final products would be slower in the presence of water

(hence the lower product yield) and accompanied by a different product distribution at the same reaction temperature. These results indicate that the intermolecular hydroalkoxylation reaction is best carried out under an inert atmosphere using dry solvents for optimal yield and selectivity.

2.2 Substrate Scope of the Reaction

A series of readily accessible alkynes were tested as substrates to investigate the effect of electron donating/withdrawing groups on phenylacetylene (Table 2). On the introduction of either electron donating or withdrawing groups in the *para*-position of the aryl acetylene, the reaction retained high (>98%) levels of conversion (Table 2, entries 1-3). While some product selectivity varies amongst these entries, no strong correlation of reaction efficiency was made with the nature of the *p*-substituents. The attachment of inductively electron donating methyl groups to both *o*- and *p*- positions of the aryl acetylene substantially hampered the substrate conversion (Table 2, entry 4). This may be due to the electronic effect of the three electron donating methyl groups, or steric hindrance caused by the *ortho*-substituted methyl groups.

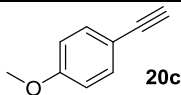
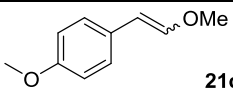
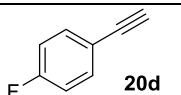
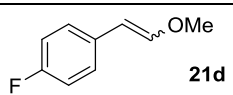
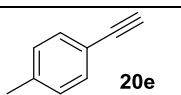
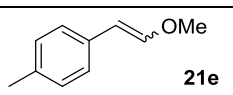
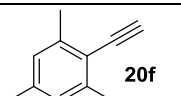
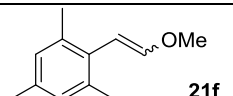
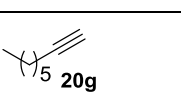
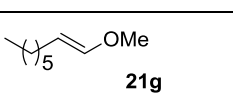
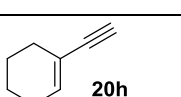
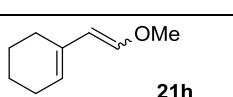
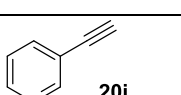
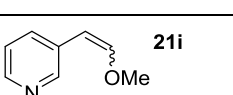
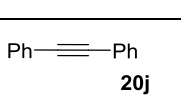
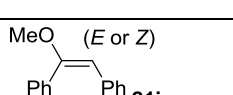
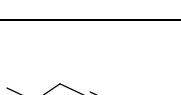
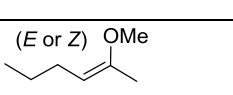
Replacement of the aryl ring of phenylacetylene with an alkyl chain resulted in only 14% conversion (Table 2, entry 5), but with exclusive formation of the *E*-enol ether isomer. Replacing the saturated alkyl chain with cyclohex-1-enyl substituent also led to the formation of only the *E* isomer but with high product yield (Table 2, entry 6). It was speculated that the π systems adjacent to the alkyne in aryl substituted acetylene substrates form more conjugated intermediates, and stabilise the intermediate structure with higher degree of electron delocalisation (the reaction intermediates are speculated to be vinylidene complexes, see Figure 4 and Figure 13). If this holds true, it implies that with a less conjugated substrate, the energy barrier to furnish both the *E* and *Z* isomers would be higher, and the given reaction conditions may not provide enough energy to overcome all energy barriers to either of the two products. The formation of the *E* product alone in the case of the allyl substituted acetylene substrate may involve a more stable transition state, which may be thermodynamically more favourable and provides a greater driving force for the reaction to proceed.

Reversed product selectivity, favouring the *Z*-enol ether isomer, was observed when pyridine was incorporated instead of a phenyl ring on the acetylene substrate (Table 2, entry 5).

While the nitrogen atom is electron withdrawing, it also has a lone pair that can coordinate with the rhodium metal. This suggests the pyridine nitrogen on the substrate may direct the reaction intermediate to a configuration where the formation of the *Z* products is more energetically favourable than the *E* product.

Table 2 Hydroalkoxylation of methanol and various alkyne substrates catalysed by catalyst **18** (*ca.* 1 mol%)

$$\text{MeOH} + \text{R} \text{---} \text{C} \equiv \text{C} \xrightarrow[24 \text{ h}]{\text{1 mol\% } \mathbf{18}, \text{DMA}, 70^\circ \text{C}} \text{R} \text{---} \text{CH} = \text{CH} \text{---} \text{OMe}$$

Entry	Substrate	Product	Conv. ^a	E/Z ratio ^b
1	 20c	 21c	>98% (90%)	4:1
2	 20d	 21d	>98% (84%)	5:1
3	 20e	 21e	>98% (75%)	6:1
4	 20f	 21f	72% (50%)	3:1
5	 20g	 21g	14%	<i>E</i> -isomer only
6	 20h	 21h	>98% (85%)	<i>E</i> -isomer only
7	 20i	 21i	28%	1:3
8	 20j	 21j	0%	n/a
9	 20k	 21k	0%	n/a

^a Isolated yield in parenthesis. ^b *E/Z* ratio determined by comparing the ratio of the alkyne proton resonance (*ca.* 3 ppm) and the product alkene resonances (5-7 ppm) using ¹H NMR spectroscopy.

Utilising internal aromatic and aliphatic alkynes did not yield any hydroalkoxylation products at all (Table 2, entries 8 & 9). The contrasting results when using terminal and internal alkyne

substrates suggests that the reaction catalysed by **18** may proceed through the formation of a vinylidene complex intermediate during the reaction mechanism (Figure 4). This is consistent with the findings suggested by Kakiuchi *et al.*³¹ using a neutral Rh(I) complex with *N*, *O*-donor ligand and supported by DFT calculations by Wang *et al.*³⁴ The formation of the vinylidene complex requires the terminal alkyne proton to undergo a [1,2]-hydride shift, which may in some cases proceed *via* oxidative addition of the alkynyl C-H bond to the metal (Figure 4). The analogous oxidative C-C addition is not likely for internal alkyne substrates.³⁵ The formation of the vinylidene complex, which resembles a Fischer carbene that donates π -electrons to the ligand, as well as the oxidative addition step are favoured by more electron rich metal centres, and these are possible reasons that catalyst **18** outperforms catalyst **19** in the intermolecular hydroalkoxylation of methanol and phenylacetylene.

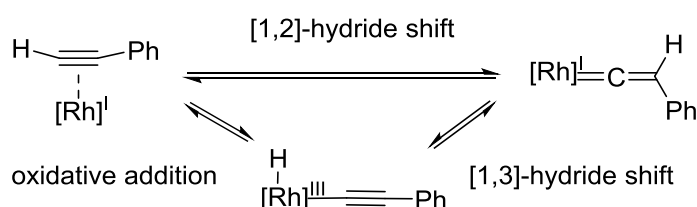


Figure 4 Possible reaction pathways for Rh vinylidene complex formation.

The difference in yield when using alkyne substrates with unsaturated (Table 1, entries 1-4; Table 2, 1-4 & 6) and saturated (Table 2, entry 5) substituents appears to have risen from the ability of the substituents to stabilise the key reaction intermediate at first sight. The aryl ring adjacent to the alkyne $C\equiv C$ can stabilise the formation of a vinylidene intermediate with a high degree of conjugation. The electron delocalisation about the aryl substituent would impart lower orbital energy levels than would be possible with a saturated, non-conjugated substituent, and better stabilise the vinylidene intermediate and the final product.

A study³⁶ on the formation of rhodium vinylidene complexes bearing both alkyl and aryl substituents, however, not only showed that the alkyne complex and the hydrido-alkynyl complex are almost isoenergetic, the substitution of the phenyl ring with an *n*-butyl chain also raised the rate constant of the interconversion between the alkyne complex and the hydrido-alkynyl complex by an order of magnitude; while that of converting the hydrido-alkynyl to the vinylidene complex was lowered by 3-4 times. As a consequence, complex **18** and 1-octyne may exist in a dynamic equilibrium of the alkyne complex and the hydrido-

alkynyl complex, and hinders the conversion to the vinylidene complex in entry 5 (Table 1) with a higher energy barrier.

The low yield and differing selectivity found for the pyridyl substituted alkyne (Table 2, entry 7) does not share this trend. This may be due to the availability of a lone pair on the nitrogen on the pyridine ring, which can coordinate to the rhodium centre, leading to a different reaction mechanism; or the pyridyl nitrogen acting as a base to deprotonate the vinylidene intermediate and results in a species that exists in equilibrium with the vinylidene.

2.3 Electrochemical Studies of Complexes $[\text{Rh}(\text{CO})_2\text{Phdp}m]$ (**18**) and $[\text{Rh}(\text{CO})_2\text{bpm}]\text{Bar}^F_4$ (**19**)

To gain further insight into the reaction mechanism (see Figure 13 for more detailed possible reaction pathways), the redox behaviour of monometallic complexes **18** and **19** was studied using cyclic voltammetry (CV) under an inert atmosphere. Scans were started at 0 V *versus* a leakless Ag/AgCl reference electrode with an anodic sweep. At a sweep rate of 100 mV/s, an irreversible oxidation peak was observed for **18** at +0.96 V and an irreversible reduction peak at -0.88 V; whereas for **19**, an irreversible oxidation event occurred at +1.14 V, and no reduction took place within the scan window (Figure 5).

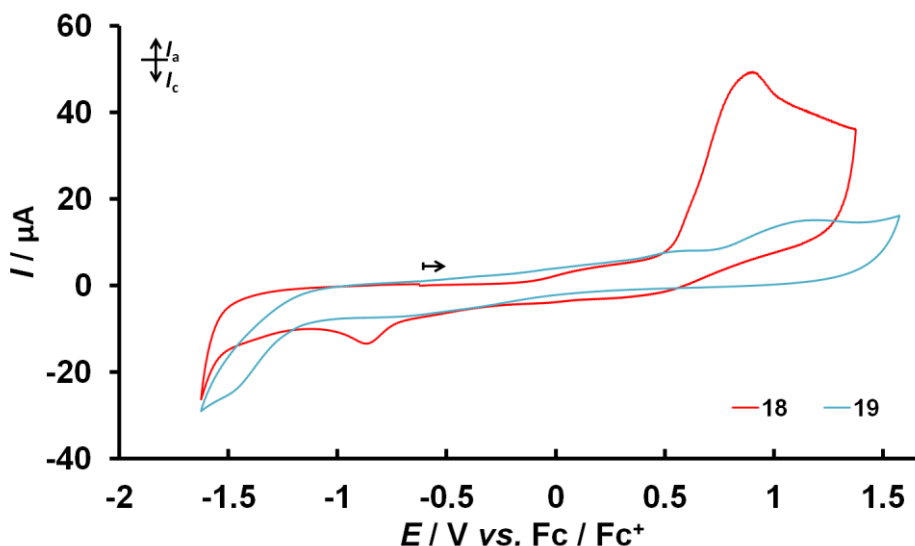


Figure 5 Cyclic voltammogram of complex **18** (red) and complex **19** (blue), both 1 mM in 0.1M $[\text{Bu}_4\text{N}][\text{PF}_6]/\text{CH}_2\text{Cl}_2$ supporting electrolyte at 100 mV/s.

By comparison to the CVs of the structurally similar acetylacetone complexes shown in Figure 6,³⁷ the anodic peak for **18** at +0.96 V was assigned to be a two electron oxidation corresponding to formation of a Rh(III) species. This species undergoes a chemical process, and the cathodic peak at -0.88 V was assigned to be the reduction of the chemically formed

Rh(III) species to a +1 oxidation state of the rhodium centre. This conclusion is supported by initiating the measurement with a cathodic sweep, whereby the reduction peak at -0.88 V was not observable in the first scan (Figure 7).

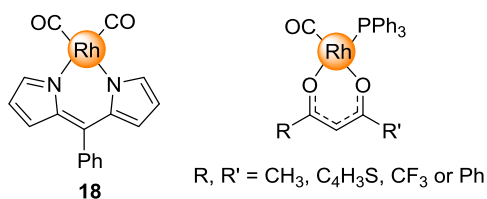


Figure 6 Complex **18** and structurally similar Rh(I) complexes containing anionic ligands and CO co-ligand. The CVs of the latter were reported in literature.³⁷

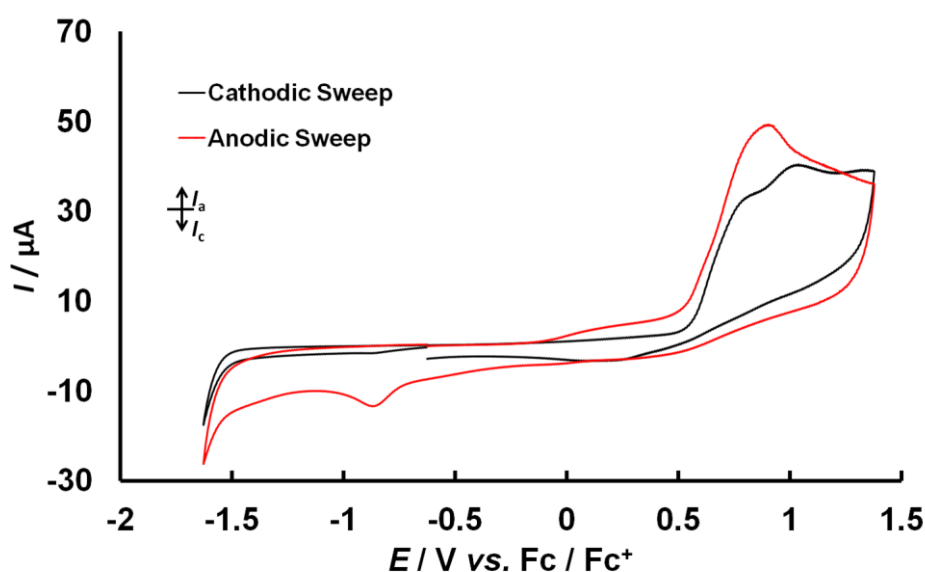


Figure 7 Stacked voltammograms for complex **18**. Measurement was initiated with either an anodic sweep (red) or a cathodic sweep (black) in 0.1 M [Bu₄N][PF₆]/DCM, 100 mV/s.

It can be noted that complex **18** oxidises at a potential that is 180 mV less positive than that of complex **19**. This indicates the electron density at the Rh(I) centre in complex **18** is higher and can be more easily removed, consistent with the use of an anionic dpm ligand compared to a neutral bpm ligand. This could imply the energy required to oxidise the rhodium centre of complex **18** is lower than that of complex **19**, or reflect the more pronounced donor ability of the anionic dpm ligand than the neutral bpm ligand. The formation of a vinylidene complex during the reaction mechanism would be favoured by coupling the electron accepting properties of vinylidene ligands as conjugated systems and the use of a metal centre with higher electron density. Should the intermolecular hydroalkoxylation of alcohols and alkynes involve the formation of a vinylidene complex, and commonly *via* the oxidative

addition route for rhodium complexes where the Rh(III) species could be better stabilised by a stronger donor ligand, the energy requirement for using complex **18** would therefore be lower than that of using complex **19**, consistent with the catalysis results obtained.

2.4 Summary for Chapter 2

In summary, complex **18** was found to efficiently catalyse the intermolecular hydroalkoxylation of a series of alcohols and alkynes. Following on from the co-solvent screening conducted in previous work,^{28, 33} the presence of oxygen and moisture in the co-solvent was found to subdue the product yield for this reaction significantly. The catalytic efficiency of **18** was retained with a range of different alkyne substrates. *E*-substituted enol ethers were selectively formed, in contrast to results reported using a structurally similar Rh(I) catalyst bearing an anionic ligand. The use of an aliphatic terminal alkyne substrate led to poorer yield, which is believed to be a result of a dynamic equilibrium of the alkyne complex and the hydrido-alkynyl complex, but exclusively the *E* product. This may be because the *E* product is thermodynamically more stable than the *Z* product and provides a larger driving force for the reaction, and/or the formation of the *E* product goes through a more accessible transition state and is thus more kinetically favourable in the current system³⁴. Interestingly, no hydroalkoxylation product was formed when internal alkynes were employed as substrates. It is postulated therefore that the reaction mechanism proceeds *via* the formation of a vinylidene complex involving a [1,2]-hydride shift. Cyclic voltammetry experiments reveal that complex **18** can be irreversibly oxidised at less extreme potentials compared to complex **19**, implying that complex **18** could form a more stable intermediate should it go through a change of oxidation state.

3 Heteroditopic Ligands and Their Dirhodium Complexes: Synthesis and Catalysis

Bimetallic complexes where the two metal centres are held in close proximity by the ligand scaffold have been shown to be superior catalysts to their monometallic analogues for selected transformations.^{21a, 21b, 21e, 22} In the Messerle laboratory, a range of dirhodium complexes containing the bpm and mim motifs (Figure 8a) have been found to catalyse the dihydroalkoxylation of alkyne diols more efficiently than either the monometallic analogues or a mixture of the monometallic counterparts.²² The two rhodium centres of the bimetallic complex are thought to work in a cooperative manner during the transformation.^{21b, 21c, 22}

The exact mechanism for this cooperativity, however, is currently not known. A possible mode of cooperativity is the electronic communication between the two rhodium centres *via* the ligand scaffold. A range of bimetallic complexes were developed here by incorporating the bpm, dpm and mim motifs on a phenyl ring scaffold to yield the corresponding ditopic ligands and dirhodium complexes (**16** & **17**, Figure 8b). The efficiency of the new complexes with these heteroditopic ligands as catalysts for the dihydroalkoxylation reaction was the initial goal of this work. Understanding the nature of electronic communication between the two metal centres and the effect on the reactivity of these metals was the next main target. Cyclic voltammetry was utilised for electrochemical studies in this chapter.

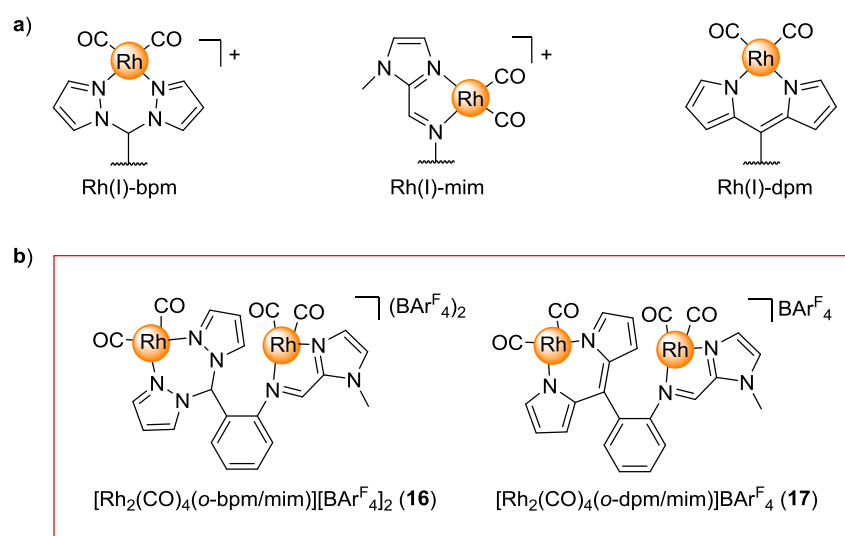


Figure 8a) bpm, mim and dpm ligand motifs bound to Rh(I) centre. **b)** Dirhodium complexes incorporating the bpm, mim and dpm moieties.

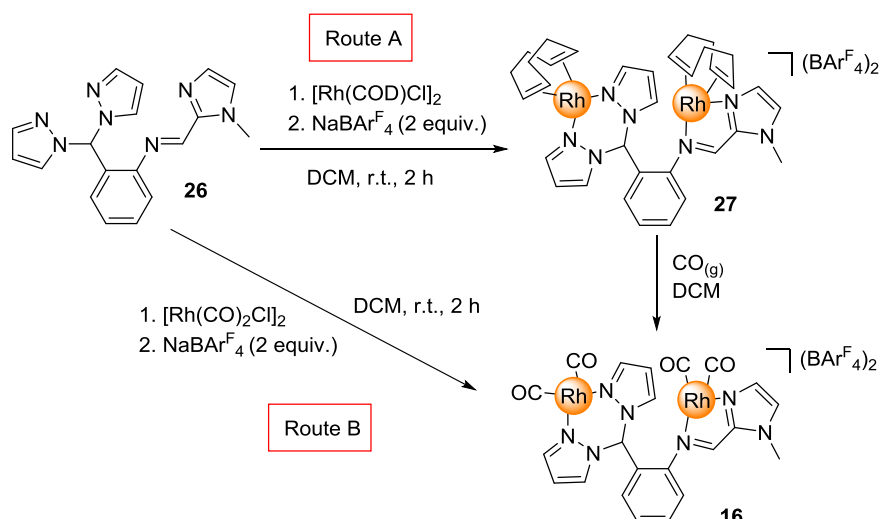
3.1 Synthesis of [Rh₂(CO)₄(o-bpm/mim)][BARF₄]₂ (**16**)

Following on from previous work,³³ in which the ditopic *o*-bpm/mim ligand (**26**) and the dirhodium 1,5-cyclooctadiene (COD) complex [Rh₂(COD)₂(*o*-bpm/mim)][BARF₄]₂ (**27**) (Scheme 7) were synthesised and fully characterised, the corresponding dirhodium carbonyl complex [Rh₂(CO)₄(*o*-bpm/mim)][BARF₄]₂ (**16**) was successfully prepared *via* two different routes.

3.1.1 Route A Towards Complex 16

The first route was *via* the known complex [Rh₂(COD)₂(*o*-bpm/mim)][BARF₄]₂ (**27**).³³ On stirring a degassed DCM solution of the COD complex **27** under a carbon monoxide atmosphere, a colour change from dark red to clear yellow was observed. The dried crude product was triturated with *n*-hexane to afford a maroon solid. The ¹H NMR spectrum of the

complex revealed that COD co-ligands were still bound to some of the Rh centres. To overcome this, the yellow DCM solution of **27** was cannulated into CO-saturated *n*-hexane, from which dicarbonyl complex **16** precipitated as a yellow solid. The free COD remained in the solution phase, thereby preventing complex **16** from reverting back to the COD complex **27**. The resultant precipitate was isolated as a light brown powder in 44% yield.



Scheme 7 Synthesis of $[\text{Rh}_2(\text{CO})_4(o\text{-bpm/mim})][\text{BARF}_4]_2$ (**16**) and $[\text{Rh}_2(\text{COD})_2(o\text{-bpm/mim})][\text{BARF}_4]_2$ (**27**) from ligand **26**.

3.1.2 Route B Towards Complex 16

It was found that complex **16** could also be prepared by using $[\text{Rh}(\text{CO})_2\text{Cl}]_2$ as the rhodium precursor. Ligand **26** was treated with $[\text{Rh}(\text{CO})_2\text{Cl}]_2$ and subsequently NaBARF_4 , the supernatant was filtered off and triturated with hexane to yield **16** as a light brown powder in 48% yield.

Complex **16** was fully characterised using mass spectrometry, elemental analysis, and 1D and 2D NMR spectroscopy.

3.1.3 NMR Characterisation of Complex 16

The ^1H NMR spectrum of **16** exhibited broad resonances between 6 and 9 ppm at 298 K. Upon lowering the temperature to 243 K, these broad resonances resolved into multiple sharp signals (Figure 9a), which suggested that complex **16** undergoes a dynamic structural exchange process at a rate comparable to the NMR timescale at 298 K.

Examination of the number of proton resonances in the spectrum of **16** at 243 K, and their relative integrations, revealed that two sets of resonances appeared to be present. 2D NMR

showed that the two sets of resonances correlate to each other by conformational exchange. This indicates that the NMR spectrum of **16** contains the resonances of two conformers of **16**.

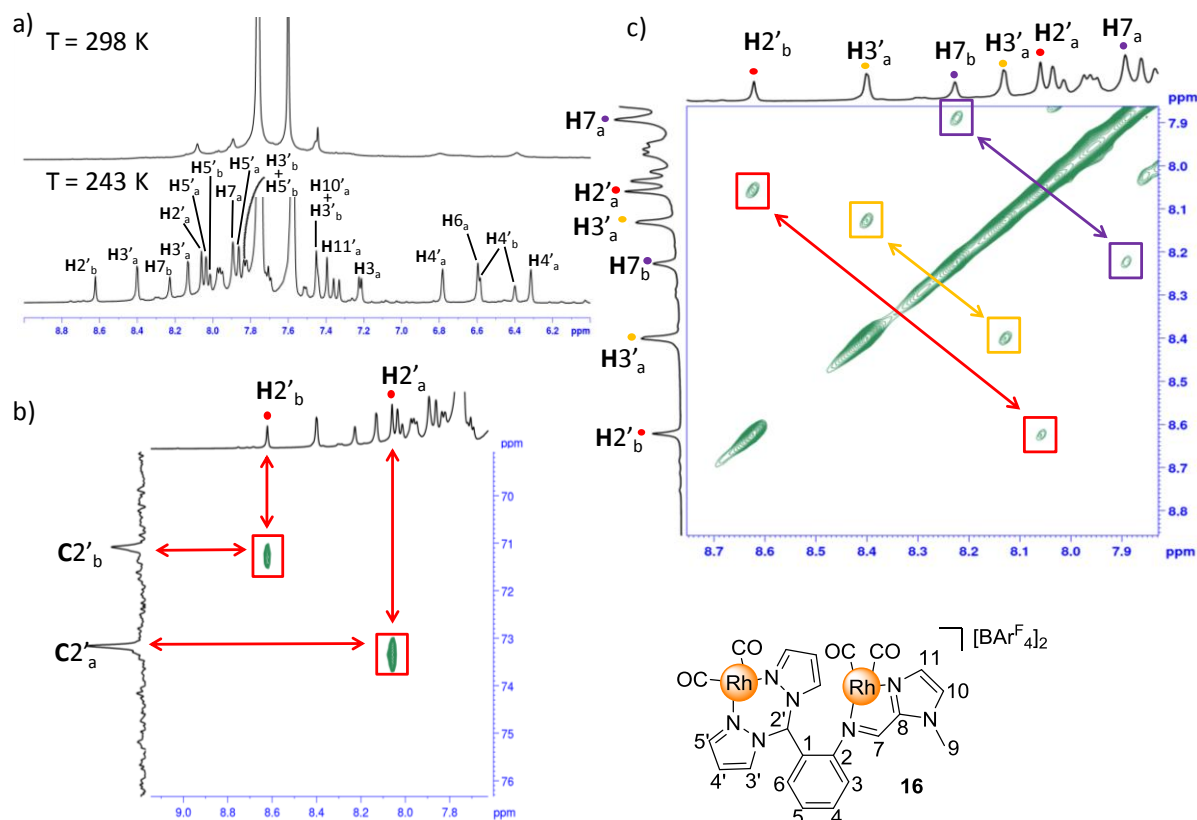


Figure 9a) Stacked VT ^1H NMR spectra of complex **16** taken in CD_2Cl_2 . **b)** HSQC spectrum of complex **16** at 243 K, in the *bis*(pyrazolyl)methane methylene region, showing the correlation of between the carbon-13 and proton resonances at position 2' in complex **16**. **c)** NOESY spectrum of complex **16** at 243 K showing correlation between the $\text{H}2'$ resonances of two different conformers of complex **16** (labelled a & b).

In the 70-80 ppm region of the $^{13}\text{C}\{^1\text{H}\}$ spectrum in the ^1H - ^{13}C HSQC spectrum of **16**, which contains only the ^{13}C resonances due to the *bis*(pyrazolyl)methane carbons of the bpm moieties, two $\text{H}2'$ - $\text{C}2'$ correlations were identified (Figure 9b) which confirmed that there are two conformations in solution (labelled a and b). The ^1H - ^1H NOESY spectrum (Figure 9c) contained an exchange correlation resonance between the two ^1H resonances of $\text{H}2'_a$ and $\text{H}2'_b$, indicating that the two protons are exchanging at 243 K.

It is interesting to note that all cross peaks in the 2D ^1H - ^1H NOESY spectrum were in the same phase as the diagonal. This was likely a result of the relatively slow tumbling of complex **16** and increased viscosity of DMC-d_2 at 243 K, which led to a longer correlation

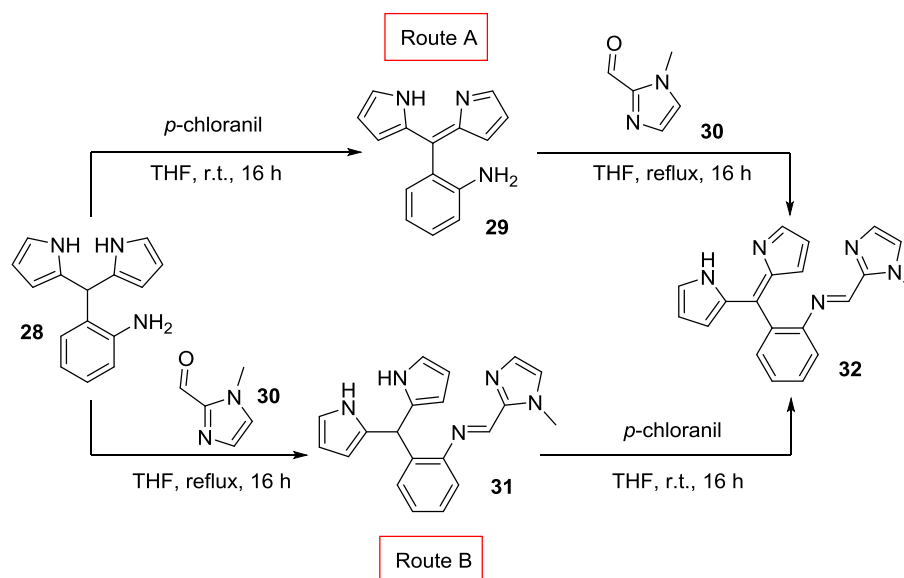
time and favoured zero quantum transitions over double quantum transitions. Thus, a negative nOe enhancement was imparted to the cross peaks which in turn adopted a negative sign, just as those due to conformational exchange as well as the diagonal.

3.2 Synthesis of *o*-dpmH/mim (**32**)

After the success in synthesising $[\text{Rh}_2(\text{CO})_4(o\text{-bpm/mim})][\text{BAr}^{\text{F}}_4]_2$, (**16**), effort was directed towards the preparation of pro-ligand *o*-dpmH/mim (**32**) and the dirhodium(I) complex $[\text{Rh}_2(\text{CO})_4(o\text{-dpm/mim})]\text{BAr}^{\text{F}}_4$ (**17**). Rh(I) complexes of both dpm and mim ligands are effective catalysts for C-X bond formation.^{21b, 22, 28} Each of the rhodacycles in the Rh(I)-dpm and Rh(I)-mim moieties are planar and rigid. The planarity of each monomeric Rh unit of the bimetallic complex **17** should allow an alignment of the Rh centres, with close proximity and well defined intermetallic distances. Thus bimetallic complex **17** incorporating the Rh(I)-dpm and Rh(I)-mim motifs could also display bimetallic cooperativity and efficiently catalyse C-X bond forming reactions and display bimetallic cooperativity.

3.2.1 Route A Towards *o*-dpmH/mim (**32**)

It was demonstrated in previous work that oxidation of *o*-dpmH₃-aniline, **28**, with one equivalent of *p*-chloranil and purification on a silica column afforded **29** in good yield (65%, Scheme 8, Route A).³³ In this work, subsequent condensation of **29** with carbaldehyde **30** was carried out in refluxing toluene. The ¹H NMR spectrum of the crude product showed 80% conversion to **32**, along with other unidentifiable side products. Fewer side reactions were observed when using ⁱPrOH as the solvent, with 70% consumption of the starting materials, and in refluxing THF, a conversion of 58% was achieved without side reactions.



Scheme 8 The preparation of pro-ligand **32** from ligand precursor **28** via two synthetic pathways.

Attempted recrystallisation of the crude product was carried out using boiling toluene. However, this treatment left behind a black solid that was insoluble in both polar and non-polar solvents, and it was speculated that at high temperatures polymerisation and/or the decomposition of the pyrrole containing compound **32** occurs. Subsequent attempts to isolate **32** with two-solvent recrystallisation at room temperature were hampered by the similar solubility of **29** and **32** in *n*-hexane as well as polar solvents. It was also found that **32** did not elute on a silica TLC plate regardless of the eluent polarity. Gravity chromatography using neutral alumina as the stationary phase furnished a mixture of **29** and **32**, which could not be separated by varying the eluent system.

3.2.2 Route B Towards *o*-dpmH/mim (**32**)

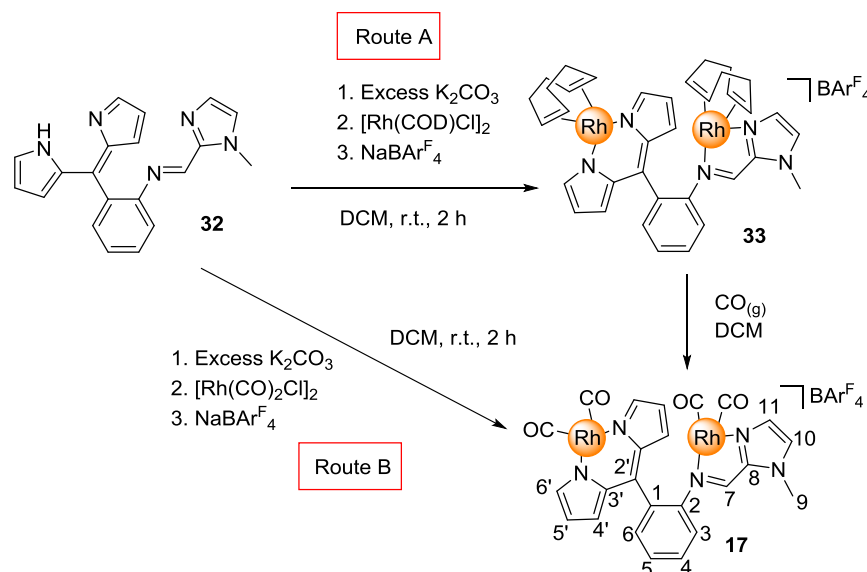
Route B is an alternative route to the preparation of *o*-dpmH/mim (**32**). The condensation of the second imidazole donor **30** with **28** was attempted *prior* to the oxidation of the C_(sp3)-C_(pyrrole) bond. Refluxing **28** with **30** in THF resulted in 90% conversion to **31**, which was chromatographed on silica gel to obtain analytically pure **31** with 66% yield (Scheme 8, Route B). Acid catalysed hydrolysis on the silica column was suppressed by pre-treating the silica gel with Et₃N. Compound **31** was then oxidised by *p*-chloranil in THF to furnish **32**, which was then be separated successfully from tetrachlorohydroquinone by column chromatography using alumina.³⁸

3.3 Synthesis of $[\text{Rh}_2(\text{COD})_2(o\text{-dpm/mim})]\text{BAr}^{\text{F}}_4$ (**33**) and $[\text{Rh}_2(\text{CO})_4(o\text{-dpm/mim})]\text{BAr}^{\text{F}}_4$ (**17**)

In an analogous fashion to the synthesis of **16** above, complex **17** was synthesised *via* the formation of the COD complex **33** and subsequent carbonylation of the complex (Scheme 9, Route A), and also directly using a rhodium carbonyl precursor (Scheme 9, Route B).

In route A, pro-ligand **32** was deprotonated by Et_3N *prior* to complexation with rhodium metal. The resultant $\text{Et}_3\text{N}\cdot\text{HCl}$ salt, could be neither removed completely by precipitation and filtration, nor separated by recrystallisation of complex **33**. As an alternative to using Et_3N , an excess of K_2CO_3 was used as a base, which was filtered off easily along with KHCO_3 and KCl salts. Carbonylation of **33** to afford **17** was attempted by bubbling $\text{CO}_{(\text{g})}$ through a stirred DCM solution of **33**. A ^1H NMR spectrum showed that product **17** contained traces of unreacted **33** when obtained *via* this route.

To obtain analytically pure **17**, $[\text{Rh}(\text{CO})_2\text{Cl}]_2$ was used in Route B as the rhodium precursor and K_2CO_3 as base. Clean complex **17** was prepared directly from **32** as a fine dark purple/red powder *via* this route.



Scheme 9 Synthesis of complex **17** and complex **33** from pro-ligand **32**.

Complex **17** was characterised using 1D and 2D ^1H and ^{13}C NMR spectroscopy, as well as elemental analysis and mass spectrometry. Similar to the spectra for complex **16**, two sets of resonances were observed in the ^1H and ^{13}C NMR spectra of **17** (Figure 10) and these two sets of resonances were attributed to conformational exchange. Upon inspecting the 2D NOESY spectrum, cross peaks due to through space correlation and conformational

exchange could be distinguished by their relative phases. **H4'** was found to correlate to both **H6** and **H7** by polarisation transfer, whereas the cross peaks at (8.49 ppm, 7.97 ppm) and (8.08 ppm, 7.79 ppm) were due to the exchange of pairs of resonances (**H7_a**, **H7_b**) and (**H6'_b**, **H6'_a**) as the two conformers interconvert.

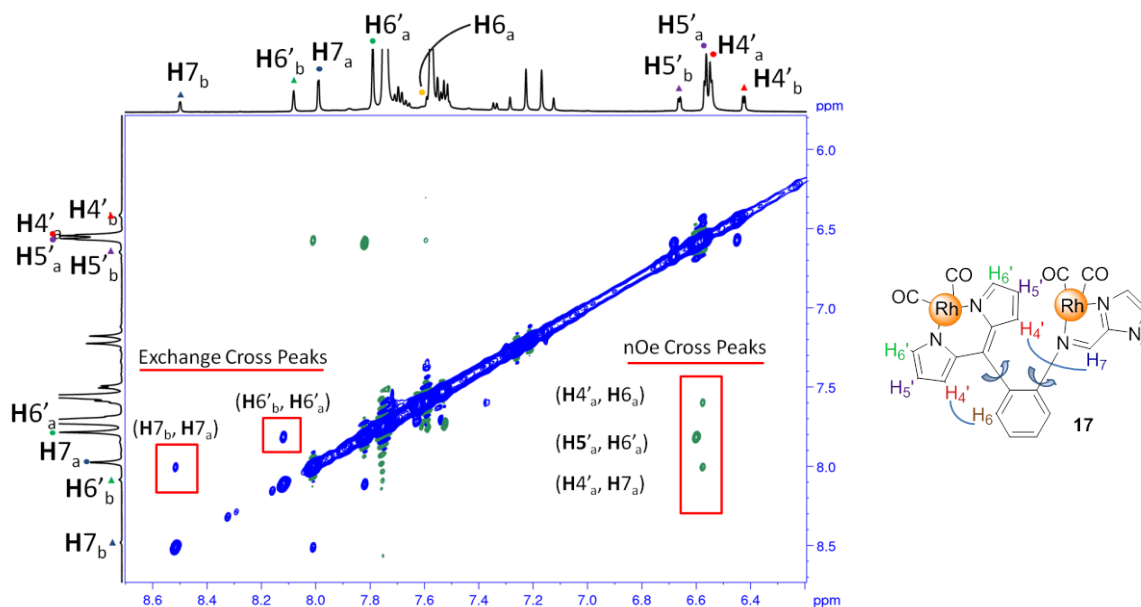


Figure 10 2D NOESY spectrum for complex **17** taken at 298 K in CD₂Cl₂. Both nOe cross peaks (green) and dynamic exchange cross peaks (blue) are present, indicating nOe transfer between closely situated protons as well as conformational exchange of complex **17**.

3.4 Catalysed C-O Bond Formation

After the successful preparation of bimetallic complexes **16** and **17**, the catalytic efficiency of these complexes for the intermolecular hydroalkoxylation and the intramolecular dihydroalkoxylation reactions was investigated, and compared to that of the analogous monometallic complexes **18** (Rh(I)-dpm), **19** (Rh(I)-bpm), and **13a** (Rh(I)-mim). Electrochemical studies of the mono- and bimetallic complexes (**18**, **19** & **13a**; **16** & **17**) were undertaken using cyclic voltammetry (CV) in an attempt to establish their redox potentials, and ultimately correlate this with the performance of the complexes as catalysts and establish whether there is a relationship between the redox behaviour of the complexes and bimetallic cooperativity.

In Chapter 2, the intermolecular hydroalkoxylation of alcohols and terminal alkynes was shown to be efficiently catalysed by complex **18**, which is the monometallic complex of the anionic Phdpm ligand. It was postulated that this reaction benefits from the ability of complex **18** to undergo oxidative addition of the terminal alkyne, and thus access the key

intermediate more easily. In earlier work,³³ complex **18** was also used to catalyse the intramolecular dihydroalkoxylation of alkyne diol **11**, although this occurred in a more sluggish manner than on using the efficient catalysts **19** and **13a**. As such, the bimetallic complexes **17** (which contains the Rh(I)-dpm moiety found in **18**) and **16** (which contains the Rh(I)-bpm moiety found in **19**) have the potential to be efficient catalysts for both the intermolecular hydroalkoxylation of terminal alkynes with alcohols, and for the intramolecular dihydroalkoxylation of alkyne diols. The second Rh centre present in the bimetallic complexes could act as a directing group for the nucleophilic, alcoholic attack on the Rh-alkyne derivative,³⁹ or impart electronic influence upon the neighbouring Rh reaction site through space or *via* the highly conjugated ligand scaffold. Either of these possible modes of interaction between the two rhodium metals in complexes **16** and **17** could result in bimetallic cooperativity in enhancing the catalysed C-O bond forming reactions.

3.4.1 Catalysed Intermolecular Hydroalkoxylation

Bimetallic complexes **16** and **17** with heteroditopic ligands were tested as catalysts for the intermolecular hydroalkoxylation between methanol and phenylacetylene, and the results are summarised in Figure 11.

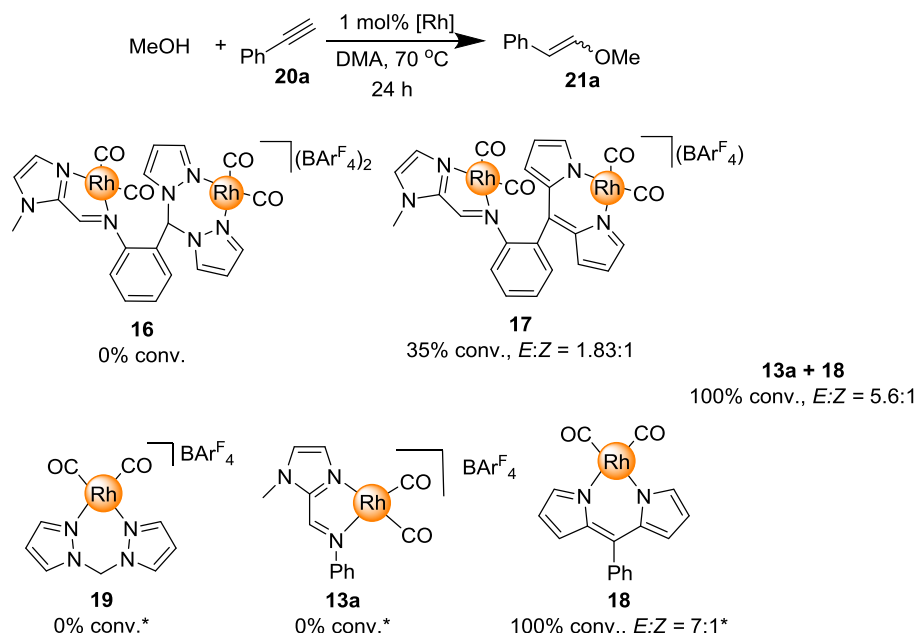


Figure 11 Intermolecular hydroalkoxylation of methanol and phenylacetylene using catalysts **13a**, **18**, **19**, **16** and **17** in DMA (*N,N*-dimethylacetamide), using 1 mol% rhodium loading, at 25°C over 24 h. Conversion was determined after 24 h by comparing the integral ratio of the alkyne proton resonance (*ca.* 3 ppm) and the product alkene resonances (5-7 ppm) using ¹H NMR spectroscopy; *E*/*Z* ratios were determined by comparing the intensity of *E* and *Z* alkene resonances. *Results from previous studies.³³

Complex **16**, containing both the bpm (of **19**) and mim (of **13a**) motifs, was found to be inefficient in catalysing the hydroalkoxylation of phenylacetylene with methanol. No conversion of phenylacetylene to the desired enol ether was observed by ^1H NMR spectroscopy. Similar results were observed using the monometallic complexes **19** and **13a** with the bpm and mim ligands respectively. The incorporation of a second Rh centre in complex **16** did not enhance the reactivity of Rh(I) for catalysing this reaction, as both rhodium metals remained inactive.

On testing the efficiency of the bimetallic complex **17**, which contains both the dpm (of **18**) and the mim (of **13a**) ligands, as a catalyst for the hydroalkoxylation of methanol and phenylacetylene a 35% substrate conversion to the target enol ether products was observed, with an *E:Z* ratio of 1.83:1. Both the substrate conversion and the product selectivity when using the bimetallic complex **17** were found to be intermediate between those achieved using the monometallic complexes **18** and **13a**, suggesting a cooperative but inhibiting effect imposed by the Rh(I)-mim component of the bimetallic catalyst **17**.

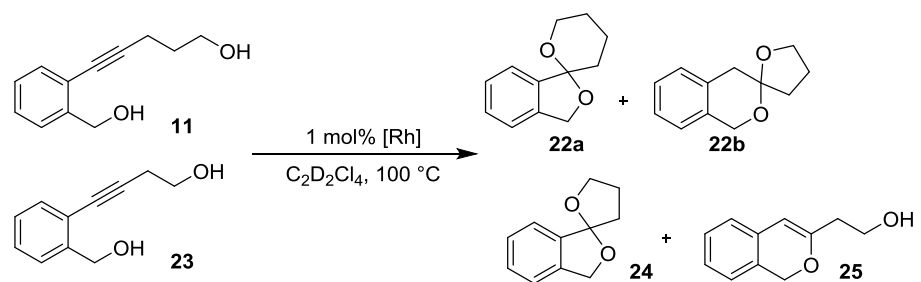
As a control experiment, the intermolecular hydroalkoxylation reaction was also carried out using 0.5 mol% of monometallic complex **18** with the Phdpm ligand, and 0.5 mol% of the monometallic complex **13a** with the Phmim ligand in one pot. A 100% conversion to the desired enol ethers was achieved in 24 h, with an *E:Z* ratio of 5.6:1. The substrate conversion of this experiment was comparable to that achieved using complex **18** alone. The slightly lower selectivity in the mixed-catalyst reaction suggests that complex **13a** may be asserting an influence while the reaction was primarily catalysed by complex **18**, although it was inactive on its own.

3.4.2 Catalysed Intramolecular Dihydroalkoxylation

The direct formation of spiroketals from readily accessible functional groups such as alkynes and alcohols is an attractive synthetic approach, since the traditional preparation involves multiple synthetic steps and harsh conditions.⁴⁰ Therefore, transition metal catalysed spiroketal formation in one pot has been an interest of investigation.^{16a, 21b, 21c, 22, 27b, 41}

The bimetallic complexes **16** and **17** were tested as catalysts for the dihydroalkoxylation of alkyne diols **11** to form the corresponding spiroketals **22a** and **22b**; and **23** to form spiroketal **24** and a cyclic enol ether by-product **25** in one pot, and the results are summarised in Table 3 and Figure 12.

Table 3 Conversion of alkyne diols (**11** & **23**) to regioisomeric spiroketal products (**22a**, **22b** & **24**) and the monocyclised product **25**, using catalysts **16** and **17**, at 1 mol% rhodium loading.



Entry	Substrate	Product	Catalyst ^a	Time (h) ^b	ToF (h ⁻¹) ^c	Ratio ^e
1	11	22a + 22b	16	0.44	900	0.55: 1
2			17	0.39	1833	0.84:1
3 ^{27b}			19	0.22	961	0.7: 1
4 ⁴²			13a	7.3	24	n/a
5 ³³			18	40% conv. in 3 h, ToF n/a		0.52: 1
6	23	24	16	0.57 ^d	1125	1.3: 1
7		+	17	0.56 ^d	963	1.4: 1
8 ^{27b}		25	19	0.09	1121	1.8: 1

^a 0.5 mol% for **16** and **17**, and 1 mol% for **19** and 2 mol% of **18** and **13a**. ^b Time required to reach 98% conversion. ^c Turnover frequency (ToF) is calculated as the amount of product/mole of catalyst/hour at the point of 50% conversion. ^d Time required to reach 97% conversion. ^e Ratio of **22a**: **22b** or **24**: **25** determined by integration of ¹H NMR signal intensities.

Complex **17** catalysed the conversion of **11** to **22a** and **22b** (Table 3, entry 2) with 98% conversion in 0.39 h (ToF 1833 h⁻¹) and a product ratio of 0.84: 1. The time required for **17** to promote quantitative (98%) conversion of **11** was significantly less than that required for either of the monometallic counterparts **13a** and **18** (Table 3, entry 4 & 5; Figure 12a). This indicates that there is a cooperative bimetallic effect present when using complex **17** as a catalyst. Also noteworthy is the similarity in the required time for **16** and **17** to achieve 98% conversion, suggesting the difference in nature of the Rh(I)-dpm and Rh(I)-bpm centres has little bearing on the intramolecular reaction mechanism in this case.

Complex **16** efficiently catalysed the dihydroalkoxylation of alkyne diol **11** to give the spiroketal products **22a** and **22b** (Table 3, entry 1), with 98% conversion achieved in 0.44 h and a turnover frequency (ToF) of 900 h⁻¹. The formation of spiroketal **22a** was less favoured comparing to that of **22b**, with a product ratio of 0.55: 1. The time for bimetallic complex **16**

to reach 98% consumption of substrate was intermediate between the two component monometallic analogues, **19** and **13a** (Figure 12a), requiring twice as long to achieve 98% conversion compared to component complex **19** (Table 3, entry 3), but was more than sixteen times faster than complex **13a** (Table 3, entry 4). This demonstrates the two metals in complex **16** work in a synergistic manner during catalysis, such that one of the rhodium centres may be acting as a cooperative inhibitor.

For the dihydroalkoxylation of alkyne diol **23**, complex **16** with the dpm and mim components efficiently catalyses conversion to a mixture of 5,5-spiroketal product **24** and the monocyclised product **25**, achieving 97% conversion of **23** in 0.57 h with a ToF of 1125 h⁻¹ (Table 3, entry 6; Figure 12b). On comparing the catalytic activity of **16** to that of the monometallic complex **19** for this reaction, it was found that complex **16** took about six times longer to achieve quantitative conversion than **19**. This observation is similar to the case of the dihydroalkoxylation of alkyne diol **11**.

Using complex **17** with dpm and mim components as catalyst for the dihydroalkoxylation of alkyne diol **23** led to a similar outcome to complex **16** for this reaction (Table 3, entry 7; Figure 12b), with 97% substrate conversion achieved in 0.56 h and a ToF of 963 h⁻¹. This suggests that the Rh(I)-bpm motif of complex **16** and the Rh(I)-dpm motif of complex **17** may not have any bearing on the mechanism for this reaction either.

3.5 Electrochemical Studies

The elucidation of reaction mechanisms provides essential information for appropriate catalyst modification and can lead to improved catalytic performance. This section describes the electrochemical studies of monometallic complexes [Rh(CO)₂Phdpm] (**18**), [Rh(CO)₂bpm]BAR^F₄ (**19**), [Rh(CO)₂Phmim]BAR^F₄ (**13a**), and bimetallic complexes [Rh₂(CO)₄(*o*-bpm/mim)][BAR^F₄]₂ (**16**) and [Rh₂(CO)₄(*o*-dpm/mim)][BAR^F₄] (**17**). These results were then used to speculate the mechanism involved for the catalysed hydroalkoxylation reactions of phenylacetylene with methanol, or alkyne diol **11** using complexes **13a**, **18**, **19**, **16** or **17** examined previously.

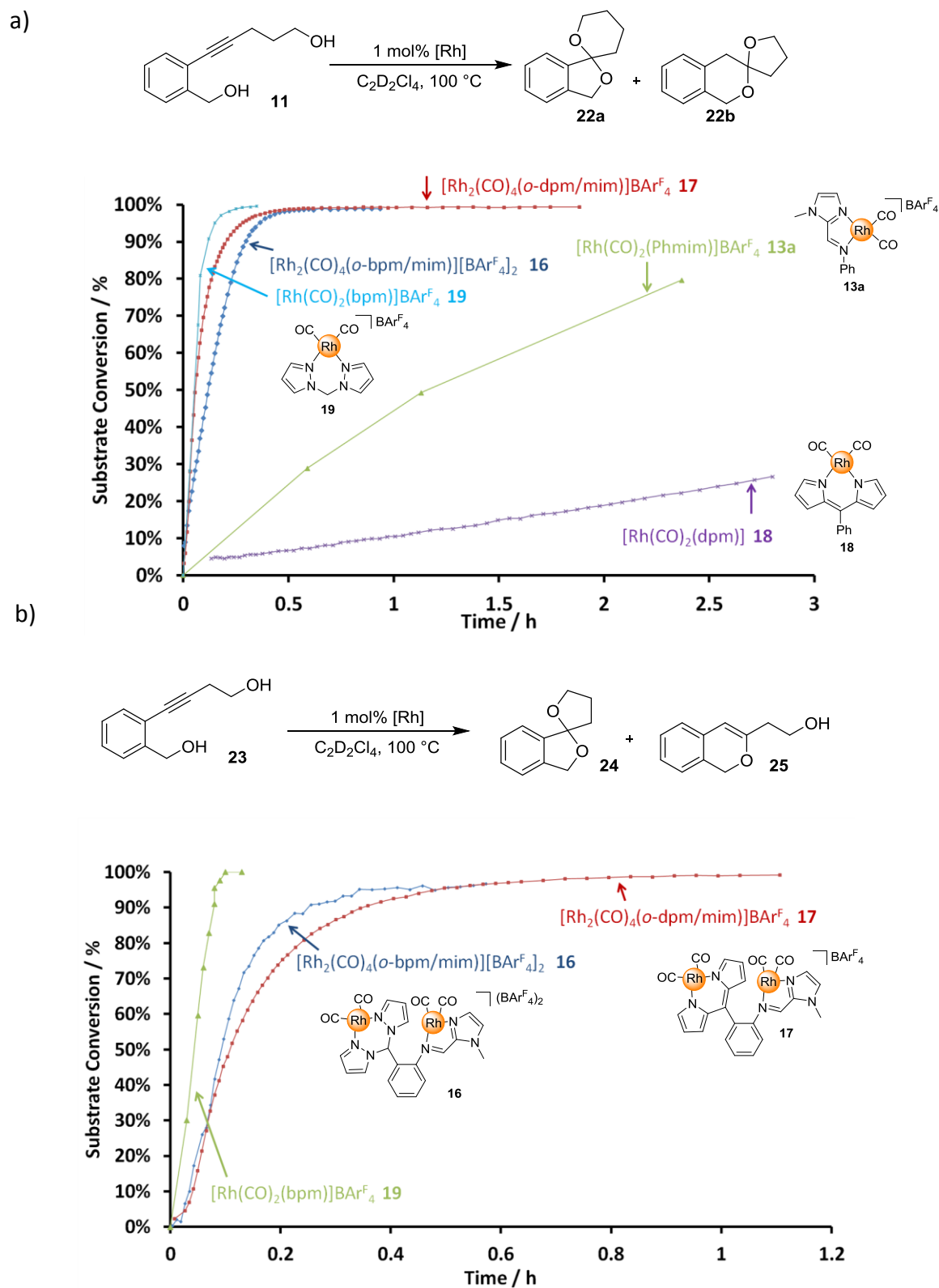


Figure 12a) Reaction profiles of dihydroalkoxylation of 2-(5-hydroxypent-1-ynyl)benzyl alcohol (**11**) to give spiroketals **22a** and **22b** in $\text{C}_2\text{D}_2\text{Cl}_4$ at $100\text{ }^\circ\text{C}$ using individual catalysts, 0.5 mol% $[\text{Rh}_2(\text{CO})_4(o\text{-bpm/mim})][\text{BAr}^{\text{F}}_4]_2$ (**16**), 0.5 mol% $[\text{Rh}_2(\text{CO})_4(o\text{-dpm/mim})]\text{BAr}^{\text{F}}_4$ (**17**), 2 mol% $[\text{Rh}(\text{CO})_2\text{dpm}]$ (**18**), and 1 mol% $[\text{Rh}(\text{CO})_2\text{bpm}]\text{BAr}^{\text{F}}_4$ (**19**). **b)** Reaction profiles of dihydroalkoxylation of 2-(4-hydroxypent-1-ynyl)benzyl alcohol (**23**) to give spiroketal **24** and enol ether **25** in $\text{C}_2\text{D}_2\text{Cl}_4$ at $100\text{ }^\circ\text{C}$ using individual catalysts, 0.5 mol% $[\text{Rh}_2(\text{CO})_4(o\text{-bpm/mim})][\text{BAr}^{\text{F}}_4]_2$ (**16**), 0.5 mol% $[\text{Rh}_2(\text{CO})_4(o\text{-dpm/mim})]\text{BAr}^{\text{F}}_4$ (**17**), and 1 mol% $[\text{Rh}(\text{CO})_2\text{bpm}]\text{BAr}^{\text{F}}_4$ (**19**).

Transition metal (TM) catalysed addition of oxygen nucleophiles to $\text{C}\equiv\text{C}$ bonds is proposed to follow one of two mechanistic pathways (Figure 13).^{29a, 43} The first pathway (Mechanism A, Figure 13) involves the electrophilic activation of the alkyne by π -coordination to the metal centre of the TM complex. The metal centre acts as a Lewis acid and renders the coordinated $\text{C}\equiv\text{C}$ bond prone to nucleophilic attack by the OH moiety. The second pathway (Mechanism B, Figure 13) also proceeds *via* formation of the π complex, which then rearranges to a vinylidene intermediate. The vinylidene may form *via* a direct [1,2]-hydride shift step, or oxidative addition of the terminal C-H bond to the metal centre followed by a [1,3]-hydride shift for d^8 metal systems such as Rh(I) (Section 2.2, Figure 4).³⁵ Hydroalkoxylation reactions of internal alkynes catalysed by Rh(I) or Ir(I) complexes are known to favour Mechanism A, as internal alkynes do not readily undergo oxidative addition in the presence of a metal catalyst.^{16a, 35, 41}

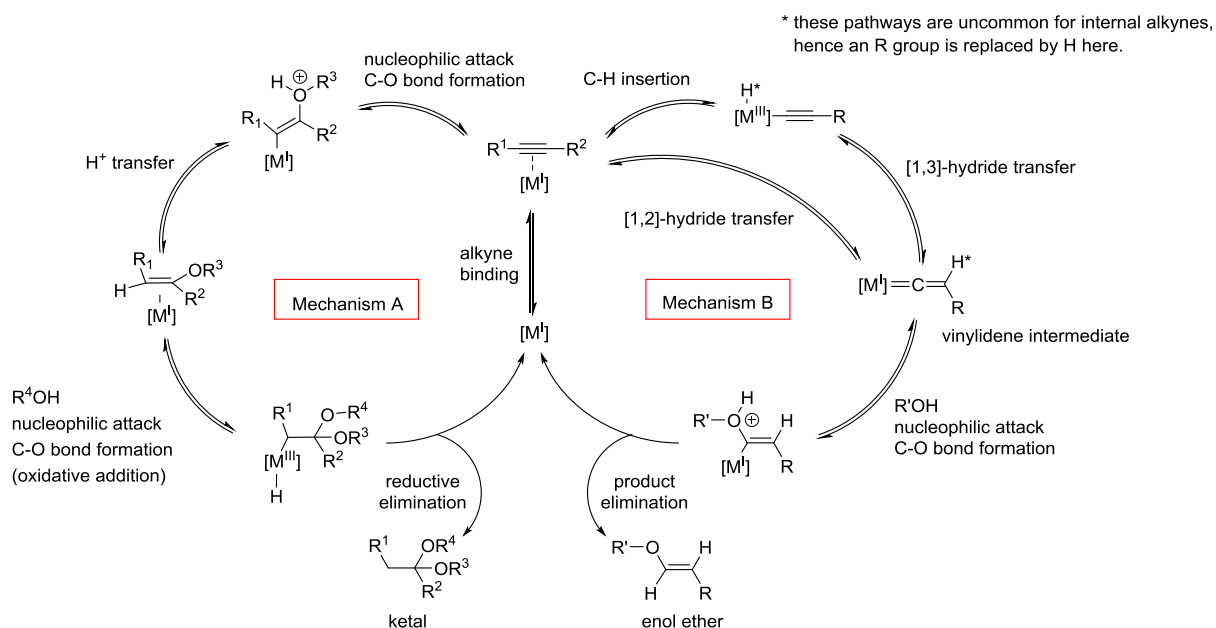


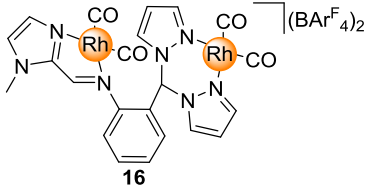
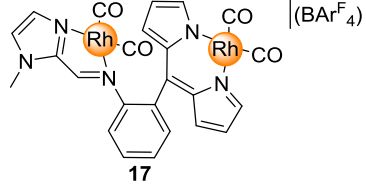
Figure 13 Proposed mechanisms for C-O bond formation by the addition of oxygen nucleophile to $\text{C}\equiv\text{C}$ bond. Mechanism A: direct addition of oxygen nucleophile to the metal-alkyne π -complex. Mechanism B: oxidative C-H insertion, followed by the formation of a vinylidene intermediate and then the attack of oxygen nucleophile.

The redox potentials measured for Rh(I) complexes **13a**, **18**, **19**, **16** and **17** can reflect the ease of which they may undergo oxidative addition. A more large and positive oxidation potential corresponds to a system where higher energies are required to abstract an electron from the metal complex. A very low or largely negative oxidation potential in turn corresponds to a complex that can easily oxidise and may be inclined to form a vinylidene intermediate during the hydroalkoxylation reactions (Mechanism B, Figure 13). The

oxidation potentials may also reflect the donor ability—which is crucial for stabilising high valence metal ions—of the *N,N* bidentate ligands in complexes **13a**, **18**, **19**, **16** and **17**, and that the electron density of the Rh(I) centres and the ease of their oxidation may not be the sole possible cause of the different catalytic efficiencies of complexes **13a**, **18**, **19**, **16** and **17**.

The redox potentials of the bimetallic complexes **16** and **17**, and those of the corresponding component monometallic analogues **18**, **19**, & **13a** were studied using cyclic voltammetry. Full scans of the solvent accessible window are shown in Figure 14 and Figure 15 for complexes **16**, **13a**, and **19**, and for complexes **17**, **13a**, and **18** respectively, and the results are summarised in Table 4. All voltammograms exhibited one irreversible oxidation peak on the forward scan. This does not correspond to a ligand based oxidation (see Appendix B for ligand voltammograms), and can be assigned to the Rh^I/Rh^{III} oxidation by comparison to the cyclic voltammograms reported for other Rh(I) complexes.^{37, 44} On the reverse scan, all complexes (except **19**) also show an irreversible reduction at potentials *ca.* 2 V more negative than the Rh^I/Rh^{III} process. This was attributed to the reduction of a Rh^{III} chemical reaction product derived from the oxidised species in the initial Rh^I/Rh^{III} process (i.e. an ECE process).^{37a}

Table 4 Electrochemical oxidation and reduction data for complexes **16-19** & **13a**. Measurements were undertaken in 0.1 M [Bu₄N][PF₆]/CH₂Cl₂ using a leakless Ag/AgCl reference electrode at 298 K (which comes at -0.625 V vs. Fc/Fc⁺). All potentials were measured at a constant sweep rate of 100 mV/s and are reported relative to the Fc/Fc⁺ couple.

Complex	E_{pa} (Rh) (V)*	E_{pc} (Rh) (V)*	E_{pc} (ligand) (V)
 16	0.98	-1.01	-1.43
 17	1.01	-1.10	-1.77
[Rh(CO) ₂ Phdp _m] (18)	0.96	-0.88	n/a
[Rh(CO) ₂ bpm]BARF ₄ (19)	1.14	n/a	n/a
[Rh(CO) ₂ Phmim]BARF ₄ (13a)	1.05	-1.04	-1.75

* E_{pa} and E_{pc} stand for peak oxidation/anodic potential and peak reduction/cathodic potential respectively.

Figure 14 shows the cyclic voltammograms of bimetallic complex **16**, and the component monometallic complexes **19** & **13a**. Complex **16** exhibits an irreversible oxidation process ($\text{Rh}^{\text{I}}/\text{Rh}^{\text{III}}$) at 0.98 V against Fc/Fc^+ . On the reverse scan, a small reduction peak was observed at -1.01 V and assigned to the reduction of the reacted oxidation product, and a ligand based reduction event at -1.43 V. Similarly, the monometallic complex **13a** exhibited an irreversible $\text{Rh}^{\text{I}}/\text{Rh}^{\text{III}}$ oxidation at 1.05 V, an irreversible $\text{Rh}^{\text{III}}/\text{Rh}^{\text{I}}$ reduction at -1.04 V and a ligand centred reduction at -1.75 V. For complex **19**, the $\text{Rh}^{\text{I}}/\text{Rh}^{\text{III}}$ oxidation occurred at 1.14 V, and no reduction events were observed within the scan window.

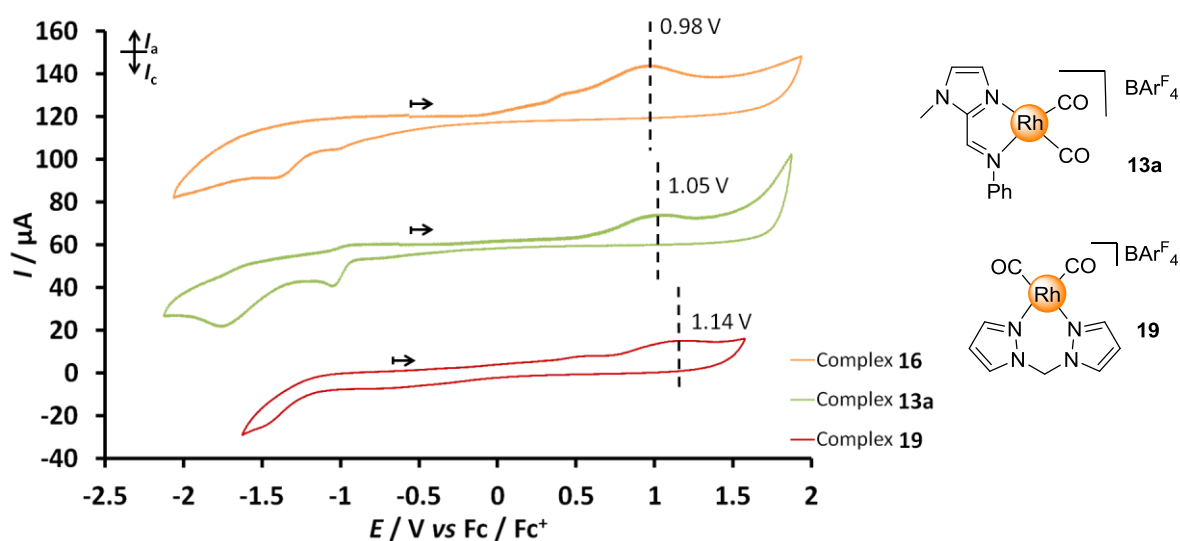


Figure 14 Cyclic voltammograms of complexes **16**, **13a** and **19**. at 100 mV/s. Measurements were conducted in 0.1 M $[\text{Bu}_4\text{N}][\text{PF}_6]/\text{CH}_2\text{Cl}_2$ vs. a leakless Ag/AgCl reference electrode at 298 K. Scans were initiated in the positive direction.

Figure 15 shows the cyclic voltammograms of bimetallic complex **17**, and monometallic counterparts **18** and **13a**. Complex **17** underwent an irreversible oxidation process ($\text{Rh}^{\text{I}}/\text{Rh}^{\text{III}}$) at 1.01 V vs. Fc/Fc^+ , an irreversible reduction process at -1.10 V, and an irreversible ligand centred reduction at -1.77 V. Complex **18** showed an irreversible oxidation peak due to $\text{Rh}^{\text{I}}/\text{Rh}^{\text{III}}$ process at 0.96 V, and an irreversible reduction peak due to the reduction of a $\text{Rh}(\text{III})$ species at -0.88 V.

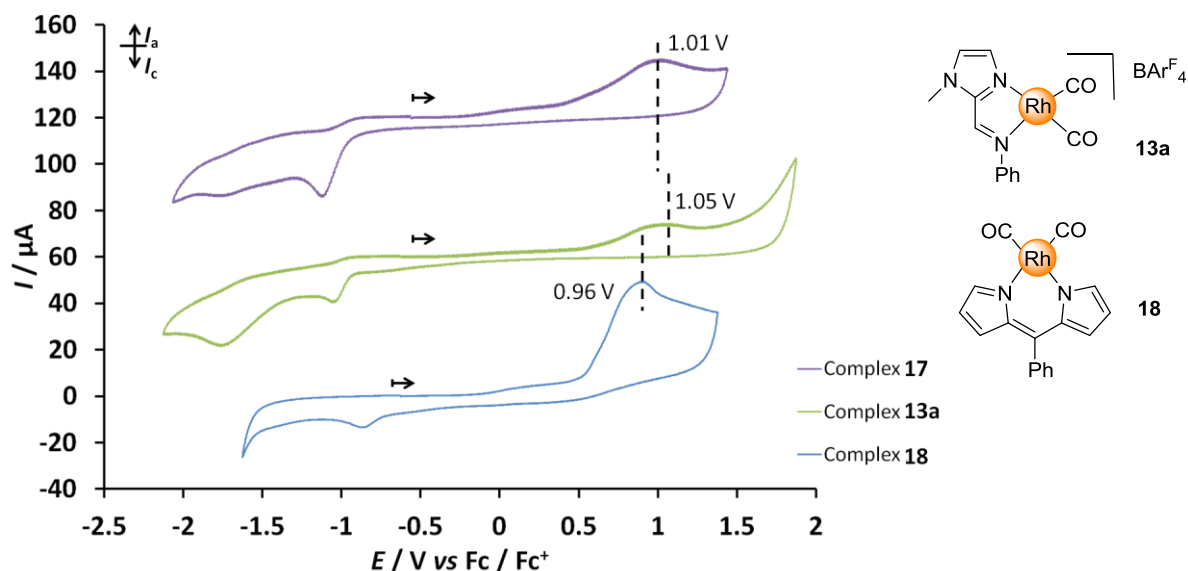


Figure 15 Cyclic voltammograms of complexes **17**, **13a** and **18** at 100 mV/s. Measurements were conducted in 0.1 M $[\text{Bu}_4\text{N}][\text{PF}_6]/\text{CH}_2\text{Cl}_2$ vs. a leakless Ag/AgCl reference electrode at 298 K. Scans were initiated in the positive direction.

3.5.1 Comparison of Bimetallic Complex **16** with Monometallic Complexes **19** and **13a**

The $E_{\text{pa}}(\text{Rh}^{\text{I}}/\text{Rh}^{\text{III}})$ of **16** is 70 mV lower than that of **13a**, and about 160 mV lower than that of complex **19**. The incorporation of a second metal centre to form the bimetallic complex **16** lowered the peak oxidation potential compared to the component complexes **13a** and **19**, however only a single oxidation event is observed for the bimetallic complex, so it is not possible to draw conclusion about electronic coupling between the Rh centres. The oxidation peak of the bimetallic complex **16** is significantly broader than those displayed by the component monometallic counterparts **19** and **13a**. This may result from the overlapping of two oxidation peaks due to the two different monomeric Rh(I) moieties in complex **16**.

To determine if there is any electronic communication between the metal centres, additional experiments are required in addition to electrochemical techniques such as IR and NIR which can also provide information on whether there is any intermetallic communication between the metal centres.

The relative oxidation potentials of **16**, **13a** and **19** do not match the relative catalytic efficiency using these complexes to catalyse the intramolecular hydroalkoxylation reaction of alkyne diol **11**. These metal complexes have catalytic efficiencies in an increasing order of **13a**<**16**<**19**. This suggests that the cooperative rate inhibition observed for complex **16** in this reaction is independent of the oxidation potential of the complex.

The key steps of the possible mechanisms for this reaction (Figure 13) involve direct nucleophilic attack on the metal-alkyne π -complex (Mechanism A), or the formation of a vinylidene complex that requires an increase in oxidation state of the rhodium centre (Mechanism B). The ability of the Rh(I) centre to undergo oxidation in Mechanism B will influence the reaction rate constant (k) of this step. In the event that this oxidative addition step is rate determining for the catalysed hydroalkoxylation the catalytic activities of complexes **16**, **19**, and **13a** would therefore correlate with the respective oxidation potentials (the differences in electron densities and/or donor ability of the ligands reflected in the oxidation potentials). As the trend in $E_{\text{pa}}(\text{Rh}^{\text{I}}/\text{Rh}^{\text{III}})$ for complexes **16**, **13a** and **19** does not match that in their relative catalytic efficiency in the intramolecular dihydroalkoxylation reaction of alkyne diol **11**, the rate limiting steps of this reaction using complexes **16**, **19** and **13a** as catalysts are unlikely to be oxidative addition. This is in line with a previously proposed mechanism (Mechanism A, Figure 13) for the catalysed dihydroalkoxylation of alkynes.^{16a, 41}

The $E_{\text{pa}}(\text{Rh}^{\text{I}}/\text{Rh}^{\text{III}})$ of complexes **16**, **19** and **13a** are 50 – 180 mV higher than that of complex **18** (Table 4), which indicates the $\text{Rh}^{\text{I}}/\text{Rh}^{\text{III}}$ oxidation in these three complexes is more energetically demanding. Should the catalysed intermolecular hydroalkoxylation reaction of phenylacetylene with methanol proceed *via* a rate limiting oxidative addition step (e.g. formation of a vinylidene reaction intermediate), the poor electron density at the respective Rh(I) centres may explain the inactivity of complexes **16**, **19** and **13a** in catalysing this reaction.

3.5.2 Comparison of Bimetallic Complex **17** and Monometallic Complexes **18** and **13a**

The peak anodic potential of bimetallic complex **17** is about 40 mV lower than that of complex **13a**, and about 50 mV higher than that of complex **18**. Only a single oxidation peak was observed for **17** and it cannot be concluded if electronic coupling between the rhodium metals exists in complex **17**.

If the reaction involves a rate limiting oxidative addition step, the catalytic efficiency of **17** is expected to lie between those of **13a** and **18**. This is indeed the case observed for the intermolecular hydroalkoxylation of methanol and phenylacetylene, where complex **13a** was inactive, however the monometallic complex **18** achieved 100% conversion in 24 h, and the bimetallic complex **17** reached 35% conversion in the same time frame (Section 3.4.1, Figure

11). The more positive oxidation potential of the bimetallic complex **17**, relative to that of **18**, correlates with the poor catalytic activity of the former for the catalysed hydroalkoxylation of phenylacetylene with methanol, and therefore suggests that oxidative addition may be rate determining.

The broadness of the oxidation wave of complex **17** is similar to that of **13a**. However the former has a greater peak current intensity than the oxidation wave of **13a**, which may result from two superimposed oxidation peaks due to the two Rh(I) centres in **17**. The peak current intensity is also dependent on the amount of rhodium metals present (1 mM analyte solutions were used for mono- and bimetallic complexes), or the diffusion of the complexes under investigation from the bulk of solution to the electrode surface (i.e. diffusion controlled current) but this requires more in-depth studies with varied scan rates.^{37a, 45} All of the speculated causes of the broad oxidation wave observed for complex **17** are possible because the π -system of the monomeric Rh(I)-dpm and Rh(I)-mim motifs in **17** may both interact with that of the phenylene scaffold, or overlap well with each other owing to their proximity and rigid, planar structure, and allow the rhodium metals to assert a mutual electronic influence. The complexes **17** and **13a** also differ significantly in molecular size, and as a result they may diffuse through the solvent at different rates and influence the respective current intensities observed.

3.5.3 Comparison between Bimetallic Complexes **16** and **17**

Figure 16 shows the offset cyclic voltammograms of bimetallic complexes **16** and **17**. The two complexes have similar $E_{pa}(\text{Rh}^{\text{I}}/\text{Rh}^{\text{III}})$ values, which do not correlate to their catalytic efficiency in the intermolecular hydroalkoxylation reaction. This appears at odds with a catalytic mechanism for the intermolecular hydroalkoxylation of methanol and phenylacetylene (by complexes **18** and **17**) which may involve the formation of a vinylidene intermediate through oxidative addition of phenylacetylene to the rhodium metal. Marcé *et al.* showed that intermediates formed *via* an oxidative addition reaction of cationic Rh(I) complexes are less stable than those produced from neutral Rh(I) complexes. As a result cationic Rh(III) species produced by such oxidative addition process are prone to revert to the initial cationic Rh(I) form.⁴⁶ This could explain the inactivity of bimetallic complex **16** (with bpm and mim motifs) in catalysing the intermolecular hydroalkoxylation of methanol and phenylacetylene, even though it can be oxidised at a similar potential to **17**.

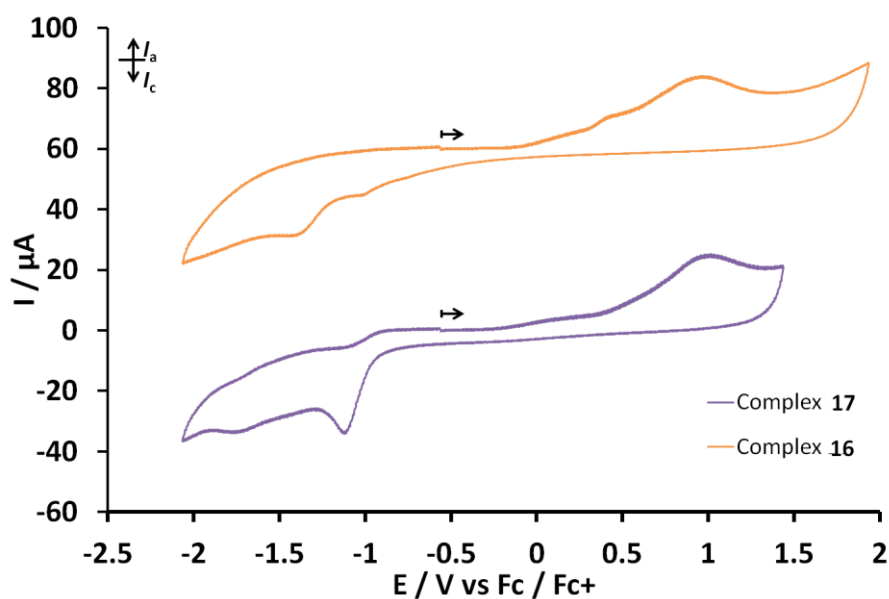


Figure 16 Cyclic voltammograms of complexes **16** and **17** at 100 mV/s. Measurements were conducted in 0.1 M $[\text{Bu}_4\text{N}][\text{PF}_6]/\text{CH}_2\text{Cl}_2$ vs. a leakless Ag/AgCl reference electrode at 298 K. Scans were initiated in the positive direction.

3.5.4 CV Studies on Bimetallic Complex **10**

Figure 17 shows the cyclic voltammograms of $[\text{Rh}_2(\text{CO})_4](\text{L}_{\text{ant}})[\text{BAR}^{\text{F}}_4]_2$ (**10**), the corresponding free ligand **34**, and the precursor $[\text{Rh}(\text{CO})_2\text{Cl}]_2$. Complex **10** was shown to be highly efficient in catalysing the intramolecular dihydroalkoxylation of **11** and **23** in previous studies in the Messerle group.²²

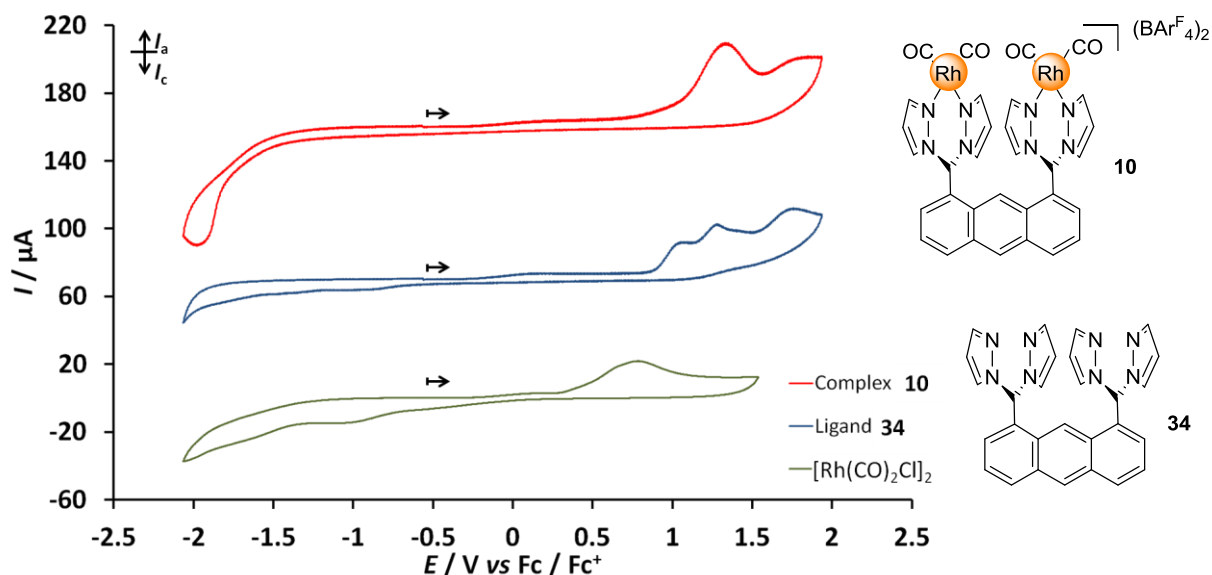


Figure 17 Cyclic voltammograms of complex **10**, ligand **34** and $[\text{Rh}(\text{CO})_2\text{Cl}]_2$ at 100 mV/s. Measurements were conducted in 0.1 M $[\text{Bu}_4\text{N}][\text{PF}_6]/\text{CH}_2\text{Cl}_2$ vs. a leakless Ag/AgCl reference electrode at 298 K. Scans were initiated in the positive direction.

Complex **10** undergoes an irreversible oxidation process at 1.33 V vs. Fc/Fc^+ and an irreversible reduction process at -1.97 V. The free ligand **34** exhibited three oxidation peaks

at 1.05, 1.29 and 1.71 V respectively, and they are all irreversible. $[\text{Rh}(\text{CO})_2\text{Cl}]_2$ displayed an irreversible oxidation peak at 0.78 V.

On comparing the three cyclic voltammograms of **10**, **34** and $[\text{Rh}(\text{CO})_2\text{Cl}]_2$ in Figure 17, the oxidation of complex **10** at 1.34 V more closely resembles that of the ligand, so was assigned to a ligand based process. This is dissimilar to the case for the monometallic analogue **19** which has a metal centred oxidation potential at 1.14 V (*ca.* 190 mV lower than **10**), and the origin of the oxidation event displayed by complex **10** in the scan window is therefore different to those of the other rhodium complexes under investigation in this work.

The origin of these oxidation processes, as well as differences in the oxidation potentials between complexes **10** and **19**, suggest that the rhodium metals in **10** are more electron-deficient. Therefore, electrophilic activation of a $\text{C}\equiv\text{C}$ bond by the rhodium in complex **10** may be more favourable than in **19**, explaining why the catalytic activity of complex **10** surpasses **19**.

3.5.5 Correlation of Electrochemical Studies with Catalysis Results

The redox potentials of bimetallic complexes **16** and **17** were probed using cyclic voltammetry and compared to those of their monometallic analogues **18**, **19**, & **13a**. All observed oxidation peaks were assigned to the $\text{Rh}^{\text{I}}/\text{Rh}^{\text{III}}$ process.

The trend in oxidation potentials of complexes **16**, **13** & **19** does not correlate with the relative performances of these three complexes as catalysts in the intramolecular dihydroalkoxylation reaction, suggesting that the intramolecular dihydroalkoxylation under study does not involve rate-determining oxidation addition steps. The broad current wave exhibited by complex **16** may be caused by two closely situated oxidation peaks due to each of the monomeric $\text{Rh}(\text{I})$ centres. The origin of cooperative inhibition when catalysing the intramolecular hydroalkoxylation displayed by complex **16** could not be elucidated by cyclic voltammetry.

The oxidation potential of **17** was shown to be intermediate between those of complexes **13** and **18**, a similar trend to that observed for their relative catalytic efficiency in the intermolecular hydroalkoxylation of methanol and phenylacetylene. This indicates that the reaction involves a rate limiting oxidative addition step and supports the notion that intermolecular hydroalkoxylation using **17** and **18** as catalysts proceeds *via* the formation of

vinylidene intermediate through oxidative addition of phenylacetylene to the rhodium metals.

The comparable peak oxidation potentials of **16** and **17** suggest both complexes should undergo oxidative addition with similar energy barriers. The differing activity observed for catalysing the intermolecular hydroalkoxylation reaction may therefore be because of the Rh(III) species formed upon oxidative addition of phenylacetylene to the rhodium can only be stabilised by the anionic dpm motif, but not the mim or bpm donors.

3.6 Summary for Chapter 3

This chapter describes the synthesis and characterisation of two novel bimetallic complexes: $[\text{Rh}_2(\text{CO})_4(o\text{-bpm/mim})][\text{BAr}^{\text{F}}_4]_2$ (**16**) and $[\text{Rh}_2(\text{CO})_4(o\text{-dpm/mim})]\text{BAr}^{\text{F}}_4$ (**17**). These two bimetallic complexes were tested as catalysts for the intermolecular hydroalkoxylation of methanol and phenylacetylene, and the intramolecular dihydroalkoxylation reactions of alkyne diol **11** and **23**.

Bimetallic complex **17** displayed significant rate enhancement in catalysing the dihydroalkoxylation of **11** compared to its component monometallic complexes $[\text{Rh}(\text{CO})_2\text{Phmim}]\text{BAr}^{\text{F}}_4$ (**13a**) and $[\text{Rh}(\text{CO})_2\text{Phdpm}]$ (**18**). Complex **17** also displayed cooperative inhibition in the intermolecular hydroalkoxylation of methanol and phenylacetylene.

Bimetallic complex **16** showed cooperative inhibition in the dihydroalkoxylation of alkyne diol **11**, with a reaction rate slower than the monometallic counterpart **19** but quicker than **13a**. Similar to its monometallic analogues **13a** and **19**, bimetallic complex **16** was inactive in promoting the intermolecular hydroalkoxylation of methanol and phenylacetylene.

The redox potentials of bimetallic complexes **16** and **17** were investigated using cyclic voltammetry. The shifts in the peak oxidation potentials observed for bimetallic complexes **16** and **17** comparing to their monometallic counterparts **13a**, **18** and **19** may result from using different ligand systems or the metal, and it is inconclusive whether intermetallic communication is present in these bimetallic complexes. We also cannot rule out that the close proximity of the second metal complex in the bimetallic system may change the reactivity of the complex due to the steric bulk.

The oxidation potentials of complexes **13a**, **17**, and **18** mirror the trend in the efficiency of substrate conversion observed for the intermolecular hydroalkoxylation reaction of methanol and phenylacetylene. Complex **13a** has the most positive oxidation potential and was inactive as a catalyst for the intermolecular hydroalkoxylation of methanol and phenylacetylene. Complex **17** achieved 35% substrate conversion and has an intermediate oxidation potential between those of **13a** and **18**, whereas complex **18** has the least positive oxidation potential and promoted 100% substrate conversion. This suggests that oxidative addition steps may be involved in the reaction mechanism for the intermolecular hydroalkoxylation of alcohols and terminal alkynes catalysed by **13a**, **17** or **18**.

The redox potentials of complexes **16** and **17** do not correlate with their performance as catalysts in the intramolecular dihydroalkoxylation of alkyne diol **11**, suggesting that oxidative addition is unlikely to be involved in the rate limiting step of the reaction mechanism, which is consistent with the previously proposed reaction mechanism, which proceeded *via* electrophilic activation of the alkyne moiety by the metal centre.

4 Conclusions and Future Work

4.1 Conclusions for This Thesis

The first half of this work describes the application of a neutral monorhodium complex $[\text{Rh}(\text{CO})_2\text{Phdpm}]$ (**18**) as catalyst for the intermolecular hydroalkoxylation of alcohols and terminal alkynes. The product enol ethers were obtained in high yield and with high selectivity. Complementary to a reported neutral monorhodium complex bearing *N,O*-donor,³¹ complex **18** formed *E*-substituted enol ethers as the major product. Optimal results were obtained when the reactions were undertaken under inert atmosphere and in dry solvents. The reaction was found to tolerate a range of terminal alkyne substrates bearing different electron-donating and withdrawing groups without compromising the product yield significantly. Internal alkynes were tested as substrates and reactions did not proceed. The redox potentials of monometallic complex **18** (with dpm motif), and another two cationic monometallic complexes **19** (with bpm motif) and **13a** (with mim motif) were probed using cyclic voltammetry. The oxidation peaks observed for complexes **18**, **19**, and **13a** were assigned to the $\text{Rh}^{\text{I}}/\text{Rh}^{\text{III}}$ process. Complex **18** was found to oxidise at a less positive potential than **19** and **13a**. This correlates with the higher efficiency of **18** in catalysing the intermolecular hydroalkoxylation reaction, and the inactivity of **19** and **13a** as catalysts. A reaction mechanism was proposed, which involves oxidative addition of terminal alkyne

substrates to the Rh(I) centre of complex **18**, followed by isomerisation of the hydrido-alkynyl rhodium complex to a vinylidene intermediate, or formation of the vinylidene intermediate directly from the metal-alkyne π -complex by [1,2]-hydride transfer.

The second half of this project describes the synthesis and characterisation of two novel bimetallic complexes **16** and **17** with heteroditopic *N*-donor ligands, their application in catalysing the addition of alcohol nucleophiles across a $C\equiv C$ bond and initial mechanistic studies using cyclic voltammetry. The dirhodium complexes **16** (with a bpm/mim heteroditopic ligand) and **17** (with a dpm/mim heteroditopic ligand) were prepared and characterised using 1D and 2D NMR spectroscopy, mass spectrometry and elemental analysis. The bimetallic complexes **16** and **17** were tested as catalysts for the intermolecular hydroalkoxylation of methanol and phenylacetylene, and for the intramolecular dihydroalkoxylation of alkyne diols **11** and **23**. A significant bimetallic reaction rate enhancement was observed for complex **17** for the intramolecular dihydroalkoxylation of alkyne diol **11**, compared to the rates of catalysis obtained using the component monometallic complexes **18** and **13a**. Cooperative rate inhibition was observed on using complex **17** for the intermolecular hydroalkoxylation reaction and on using complex **16** for the intramolecular dihydroalkoxylation of alkyne diols.

The origin of bimetallic cooperativity observed for complexes **16** and **17**, with heteroditopic *N*-donor ligands, and homobimetallic complex **10**²² was investigated, and mechanistic deductions were made based on the electrochemical studies and the catalysis results (Section 3.4 and 3.5). The redox potentials of the bimetallic complexes **16**, **17** and **10** were recorded using cyclic voltammetry and compared to those of the component monometallic complexes **18** (with Phdpm ligand), **19** (with bpm ligand) and **13a** (with Phmim ligand), however the presence of intermetallic communication between the rhodium could not be concluded in these bimetallic complexes. The trend in the peak oxidation potentials of bimetallic complexes **16**, **17** and monometallic complexes **18**, **19** and **13a** does not correlate with the variation in catalytic efficiency for the intramolecular dihydroalkoxylation of alkyne diol **11** (Table 5), indicating that the intramolecular dihydroalkoxylation of alkyne diol **1** catalysed by complexes **16** and **17** is unlikely to have a rate-limiting oxidative addition step. This finding is consistent with a previously proposed mechanism for rhodium catalysed dihydroalkoxylation of alkyne diols,^{16a, 41} and means that the bimetallic rate enhancement or

inhibition are not a result of electronic communication between the rhodium metals in these bimetallic complexes.

Table 5 Summary of trends observed for mono- and bimetallic complexes as catalysts for C-O bond formation and in electrochemical studies.

Oxidation Potentials	(from least positive) 18 < 16 < 17 < 13a < 19	
Reaction	Intramolecular Dihydroalkoxylation of alkyne diol 11	Intermolecular Hydroalkoxylation of phenylacetylene with MeOH
Catalytic Efficiency	(from least efficient) 18 < 13a < 17 < 16 < 19	(from least efficient) 13a < 17 < 18

On the contrary, the catalytic efficiency for the intermolecular hydroalkoxylation reaction of methanol and phenylacetylene was higher for complexes **13a**, **17** and **18** as the oxidation potentials become less positive. This supports the hypothesis that the intermolecular hydroalkoxylation has a rate limiting oxidative addition step.

The electrochemical oxidation observed for complex **10** in the scan window was attributed to a ligand centred oxidation. It was postulated that the rhodium centres in complex **10** are electron deficient and the complex acts as a stronger Lewis acid for the electrophilic activation of alkyne C≡C bond than the monometallic counterpart **19**, but the validity of this statement should be verified using other spectroscopic techniques and computational studies as well.

4.2 Future Work

Having established that **16** and **17** exhibit a cooperative, bimetallic effect in the intermolecular hydroalkoxylation and intramolecular dihydroalkoxylation, and the role of electronic communications between the two metal centres in this bimetallic cooperativity, a full reaction mechanism elucidation for the intermolecular hydroalkoxylation would be worthy of investigation. Starting from the monometallic systems using complex **18**, **19** and **13a** the reaction intermediates may be isolated or observed *in situ* by reacting complex **18** with an alkyne substrate. Structural information of regarding the intermediates could be obtained using NMR spectroscopy and potentially X-ray crystallography. Labelling studies, such as using CH₃OD, CD₃OH and deuterium-labelled phenylacetylene, can be used to trace

where individual deuterium atoms end up in the product, and infer the interactions between the alcohol and the alkyne substrates. Plausible catalytic cycles could then be further substantiated, and each individual step of the proposed cycles verified with the aid of computational chemistry. Elucidation of the reaction mechanism would be significantly helpful in designing and modifying the bimetallic complexes.

Apart from mechanistic studies, where the interactions between the catalyst and the substrate becomes clear and modification of the catalyst as well as the reaction conditions can be made accordingly, the catalyst can also be improved in terms of the attractiveness to potential industrial applications. Complexes that are readily characterised and found to be efficient homogeneous catalysts (e.g. complex **18** and bimetallic complexes **10**) can be immobilised on solid supports, becoming a “hybrid” of homogeneous and heterogeneous catalysts.⁴⁷ As such, the specificity of single site catalysts can combine with the easy catalyst recovery from the reaction mixture. The reactions catalysed by hybrid catalysts can result in more selective product formation than using conventional heterogeneous catalysts, and have a lower cost from the smaller amount of metal catalysts required in the long run.

5 Experimental

5.1 General Procedure

All manipulations of metal complexes and air-sensitive reagents were carried out using standard Schlenk techniques. Nitrogen gas for Schlenk line operation comes from bulk compressed nitrogen (>99.5%) from Air Liquide and BOC Australia. Bulk compressed carbon monoxide (>99.5%) was obtained from Air Liquide and BOC Australia.

Unless otherwise stated, chemicals were purchased from ChemSupply, Alfa Aesar Inc or Aldrich Chemical Company Inc, and used as received. Rhodium(III) chloride hydrate was purchased from Precious Metals Online P/L and used without further purification. Pyrrole was distilled before use. $[\text{Rh}(\mu\text{-Cl})(\text{COD})]_2$,⁴⁸ 5-phenyldipyrromethane (**18a**)⁴⁹ and 5-phenyldipyrin (**18b**)⁵⁰ were synthesised according to literature procedures. Alkyne diol substrates 2-(5-hydroxypent-1-ynyl)benzyl alcohol **11** and 2-(4-hydroxypent-1-ynyl)benzyl alcohol **23**,⁵¹ bpm ligand **35**,⁵² and $[\text{Rh}(\mu\text{-Cl})(\text{CO})_2]_2$ ⁵³ were kindly donated by Dr. Mark Gatus and Dr. Samantha Binding. The ligand L_{ant} **34** and bimetallic complex $[\text{Rh}_2(\text{CO})_4(\text{L}_{\text{ant}})][\text{Bar}^{\text{F}}_4]_2$ **10**^{27b} were kindly donated by Dr. Joanne Ho. The ligand *o*-bpm/mim **32**, and precursors **26**

and **27** were synthesised previously.³³ The mim ligand **39** and $[\text{Rh}(\text{CO})_2\text{Phmim}]\text{BAr}_4^{\text{F}}$ **13a** were synthesised according to reported procedure.^{21b}

For the purposes of air-sensitive manipulations and preparation of metal complexes, solvents were dispensed from a PuraSolv solvent purification system and stored under nitrogen or argon atmospheres in glass ampoules fitted with Youngs[®] Teflon valves. Solvents for catalysis were deoxygenated by bubbling $\text{N}_2(\text{g})$ through them for 10 minutes.

NMR Spectroscopy

Air sensitive NMR samples were prepared in an argon filled glove box in an NMR tube fitted with a Youngs[®] Teflon valve. Deuterated solvents for NMR purposes were purchased from Cambridge Isotopes and used as received.

^1H NMR spectra were recorded on Bruker DPX300 (fitted with an Autosampler), DPX300, DPX400, DMX400, DMX600, and DRX600 spectrometers, operating at 300.17, 300.30, 399.90, 400.23, 600.13, and 600.18 MHz (^1H), and 75.48, 75.49, 100.55, 100.64, 150.90, and 150.92 MHz (^{13}C) respectively. All spectra were recorded at 298 K unless otherwise stated, and chemical shifts (δ) are quoted in ppm. Coupling constants (J) are quoted in Hz and have uncertainties of ± 0.05 Hz. ^1H and ^{13}C NMR chemical shifts were referenced internally to residual solvent resonances. The following abbreviations are used to report the multiplicity of NMR resonances: s, singlet; d, doublet; t, triplet; q, quartet; m, multiplet. Proton and carbon resonances were assigned using COSY (Correlation Spectroscopy), NOESY (Nuclear Overhauser Effect Spectroscopy), HSQC (^1H - ^{13}C) (Heteronuclear Single Quantum Coherence), and HMBC (^1H - ^{13}C) (Heteronuclear Multiple Bond Coherence) experiments. All NMR data were acquired and processed using TopSpinTM version 3.2 from Bruker NMR software.

Other characterisation techniques

IR spectra were recorded on an Agilent Technologies CARY 630 FTIR spectrometer as neat samples on a mounted diamond crystal. Elemental analysis was carried out at Chemical Analysis Facility, Macquarie University.

Mass spectra were undertaken at the University of New South Wales using Thermo Fisher Scientific LCQ Fleet mass spectrometer. M is defined as the molecular weight of the compound of interest or cationic fragment of the complex in question.

Electrochemistry

Cyclic voltammetry (CV) was performed using an Autolab PGSTAT 302N potentiostat (Eco Chemie, Netherlands) which was interfaced with a computer running Nova 1.11 software. A conventional three-electrode system was employed, in which the glassy carbon working electrodes were purchased from CH Instruments Inc. (TX, USA), the platinum rod counter electrode from Echo Chemie (Netherlands) and the leakless Ag/AgCl reference electrode from eDAQ (Australia). The glassy carbon electrodes were polished sequentially in alumina slurry (distilled water suspension of) 1.0, 0.3, and 0.05 μm on micropolishing cloth (Buehler, IL, USA), rinsing with distilled water between each step, and dried with compressed air before use.

5 μmol of complexes **10**, **13a**, **16-19**, and ligands **31**, **32**, **34-36** were each dissolved in 5 mL of electrolyte (0.1 M $[\text{Bu}_4\text{N}][\text{PF}_6]$ in CH_2Cl_2) to give a 1 mM analyte solution, which was then scanned between +2.5 to -1.5 V at 100 mV/s. Measurements began at 0 V with an anodic sweep unless otherwise stated. The leakless Ag/AgCl reference electrode was calibrated externally to be -0.625 V against the ferrocene/ferrocenium couple in the same supporting electrolyte and solvent.

5.2 Experimental Procedures for Chapter 2

Preparation of Complex $[\text{Rh}(\text{CO})_2\text{Phdp}^{\text{m}}]$ (**18**)

Complex **18** was synthesised following a similar procedure to that reported by Yadav *et al.*^{32, 49-50} Detailed experimental procedure was reported in literature.²⁸

General Procedure for Catalysed Hydroalkoxylation

Substrate and co-solvent screenings were carried out in the Radleys Discovery Technologies Parallel Synthesizer. Alcohol (0.5 mL), co-solvent (0.5 mL), alkyne (0.455 mmol), and catalyst (*ca.* 5.0 μmol , 1.1 mol%) were charged into test tubes with magnetic stirrer bars and placed in the Synthesizer. The reaction chamber was carefully evacuated and filled with nitrogen gas over 5 cycles, and then heated to 70 $^{\circ}\text{C}$ with stirring for 24 h. Upon cooling to r.t., the reaction mixtures were diluted with 1.5 mL with Et_2O , and washed with LiCl solution (0.1 M, 2 \times 2 mL). The organic phase was washed with saturated brine solution (3 mL) and dried over Na_2SO_4 . The organic solvent was removed *in vacuo* and the products were analyzed using ^1H NMR spectroscopy.

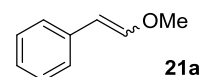
Scaled up reactions were carried out in Schlenk flasks under a nitrogen atmosphere. Reaction mixtures were heated with stirring in a sealed flask at 70 °C for 24 h. Upon cooling to r.t., the mixtures were diluted with Et₂O (20 mL) and washed with LiCl solution (0.1 M, 2 × 30 mL). The organic phases were washed with saturated brine solution (30 mL) and dried over Na₂SO₄, then filtered and concentrated *in vacuo*. The crude products were purified by column chromatography using Et₃N pre-treated silica gel. Eluent and relevant R_f values are reported with the characterisation data below.

Reagent Quantities and Spectroscopic Data for the Catalysed Hydroalkoxylation Reaction Products

The reagent quantities used for catalysis and ¹H NMR data for the products are listed below.

(2-methoxyethenyl)benzene (**21a**)³¹

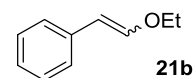
MeOH (5.0 mL, 123 mmol), DMA (*N,N*-dimethylacetamide, 5.0 mL, 54 mmol), phenylacetylene (0.50 mL, 4.6 mmol), catalyst **18** (18.9 mg, 49.7 μmol).



21a, orange oil (582 mg isolated, 4.35 mmol, 95%, *E/Z* = 7/1). ¹H NMR (300.30 MHz, CDCl₃): δ 3.70 (s, 21H, -OCH₃ (*E*-isomer)), 3.79 (s, 3H, -OCH₃ (*Z*-isomer)), 5.24 (d, ³*J*_{H-H} = 6.6, 1H, =CH- (*Z*-isomer)), 5.83 (d, ³*J*_{H-H} = 13.2, 7H, =CH- (*E*-isomer)), 6.15 (d, ³*J*_{H-H} = 6.6, 1H, =CH- (*Z*-isomer)), 7.06 (d, ³*J*_{H-H} = 13.2, 7H, =CH- (*E*-isomer)), 7.10-7.36 (m, 40H, ArH), 7.55-7.62 (m, 2H, ArH) ppm. R_f = 0.3. Eluent 9.5 Hexane: 0.5 DCM v/v.

(2-ethoxyethenyl)benzene (**21b**)³¹

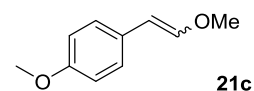
EtOH (5.0 mL, 86 mmol), DMA (5.0 mL, 54 mmol), phenylacetylene (0.50 mL, 4.6 mmol) and catalyst **18** (19.1 mg, 50.3 μmol).



21b, brown oil (527 mg, 3.55 mmol, 78% isolated yield, *E/Z* = 3:1). ¹H NMR (400.23 MHz, CDCl₃): δ 1.31-1.40 (m, 12H, -CH₃ (*E*- and *Z*- isomers)), 3.91 (q, ³*J*_{H-H} = 7.2, 6H, -CH₂- (*E*-isomer)), 3.99 (q, ³*J*_{H-H} = 7.2, -CH₂- (*Z*-isomer)), 5.22 (d, ³*J*_{H-H} = 6.9, 1H, =CH- (*Z*-isomer)), 5.85 (d, ³*J*_{H-H} = 13.1, 3H, =CH- (*E*-isomer)), 6.21 (d, ³*J*_{H-H} = 6.9, 1H, =CH- (*Z*-isomer)), 6.99 (d, ³*J*_{H-H} = 13.1, 3H, =CH- (*E*-isomer)), 7.10-7.16 (m, 4H, ArH), 7.20-7.32 (m, 15H, ArH), 7.57-7.63 (m, 2H, ArH) ppm. R_f = 0.3. Eluent 9.5 Hexane: 0.5 DCM v/v.

1-(2-methoxyethenyl)-4-methoxybenzene (**21c**)³¹

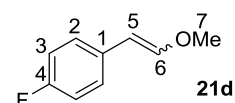
MeOH (2.5 mL, 62 mmol), DMA (2.5 mL, 27 mmol), 4-ethynylanisole (300 mg, 2.27 mmol), and catalyst **18** (9.41 mg, 24.8 μ mol).



21c, orange crystals (339 mg, 2.06 mmol, 90% isolated yield, *E/Z* = 4/1). ^1H NMR (300.30 MHz, CDCl_3) δ 3.66 (s, 12H, $-\text{OCH}_3$ (*E*-isomer)), 3.75 (s, 3H, $-\text{OCH}_3$ (*Z*-isomer)), 3.78-3.79 (m, 15H, $-\text{OCH}_3$ (*E*- and *Z*- isomers)), 5.17 (d, $^3J_{\text{H-H}} = 7.1$, 1H, $=\text{CH-}$ (*Z*-isomer)), 5.78 (d, $^3J_{\text{H-H}} = 13.0$, 4H, $=\text{CH-}$ (*E*-isomer)), 6.05 (d, $^3J_{\text{H-H}} = 7.1$, 1H, $=\text{CH-}$ (*Z*-isomer)), 6.78-6.86 (m, 10H, ArH), 6.92 (d, $^3J_{\text{H-H}} = 13.0$, 4H, $=\text{CH-}$ (*E*-isomer)), 7.12-7.19 (m, 8H, ArH), 7.47-7.54 (m, 2H, ArH) ppm. R_f = 0.6. Eluent 6 Hexane: 4 DCM v/v.

1-(2-methoxyethenyl)-4-fluorobenzene (**21d**)

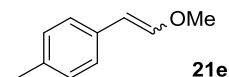
MeOH (1.5 mL, 37 mmol), DMA (1.5 mL, 16 mmol), 4-fluorophenylacetylene (153 μ L, 1.34 mmol) and catalyst **18** (5.54 mg, 14.6 μ mol).



21d, orange oil (170 mg, 1.12 mmol, 84% isolated yield, *E/Z* = 6/1). ^1H NMR (300.30 MHz, CDCl_3) δ 3.70 (s, 18H, H7(*E*-isomer)) 3.80 (s, 3H, H7 (*Z*-isomer)), 5.21 (d, $^3J_{\text{H-H}} = 7.3$, 1H, H5 (*Z*-isomer)), 5.80 (d, $^3J_{\text{H-H}} = 13.2$, 6H, H5 (*E*-isomer)), 6.13 (d, $^3J_{\text{H-H}} = 7.3$, 1H, H6 (*Z*-isomer)), 6.90-7.04 (m, 20H, H2 (*E*- & *Z*-isomer) & H6 (*E*-isomer)), 7.16-7.23 (m, 12H, H3 (*E*-isomer)), 7.51-7.60 (m, 2H, H3 (*Z*-isomer)). ^{13}C NMR (150.92 MHz, CDCl_3) δ 56.68 (s, C7 (*E*-isomer)), 60.81 (s, C7 (*Z*-isomer)), 104.18 (s, C5 (*E*-isomer)), 104.74 (s, C5 (*Z*-isomer)), 115.10 (d, $^2J_{\text{C-F}} = 21.6$, C3 (*Z*-isomer)) 115.59 (d, $^2J_{\text{C-F}} = 21.6$, C3(*Z*-isomer)), 126.57 (d, $^3J_{\text{C-F}} = 8.13$, C2, (*E*-isomer)), 129.81 (d, $^3J_{\text{C-F}} = 7.62$, C2, (*Z*-isomer)), 132.15 (s, C1 (*Z*-isomer)), 132.50 (s, C1 (*E*-isomer)), 147.56 (s, C6 (*Z*-isomer)), 148.74 (s, C6 (*Z*-isomer)), 160.99 (d, $^1J_{\text{C-F}} = 244$, C4 (*Z*-isomer)), 161.30 (d, $^1J_{\text{C-F}} = 245$, C4 (*E*-isomer)) ppm. R_f = 0.8. Eluent 1 Hexane: 1 DCM v/v.

1-(2-methoxyethenyl)-4-methylbenzene (**21e**)³¹

MeOH (2.5 mL, 62 mmol), DMA (2.5 mL, 27 mmol), 4-ethynyltoluene (263 mg, 2.26 mmol) and catalyst **18** (9.21 mg, 24.2 μ mol).

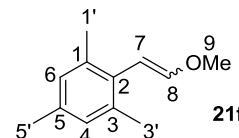


21e, orange oil (247 mg, 1.67 mmol, 74% isolated yield, *E/Z* = 6/1). ^1H NMR (300.30 MHz, CDCl_3) δ 2.31 (s, 21H, ArCH₃ (*E*- & *Z*-isomer)) 3.68 (s, 18H, $-\text{OCH}_3$ (*E*-isomer)), 3.76 (s, 3H, $-\text{OCH}_3$ (*Z*-isomer)), 5.20 (d, $^3J_{\text{H-H}} = 7.0$, 1H, $=\text{CH-}$ (*Z*-isomer)), 5.80 (d, $^3J_{\text{H-H}} = 12.9$, 6H, $=\text{CH-}$ (*E*-isomer)), 6.09 (d, $^3J_{\text{H-H}} = 7.0$, 1H, $=\text{CH-}$ (*Z*-isomer)), 7.01 (d, $^3J_{\text{H-H}} = 12.9$, 6H, $=\text{CH-}$ (*E*-isomer)) ppm.

isomer)), 7.04-7.16 (m, 26H, ArH), 7.43-7.51 (m, 2H, ArH) ppm. R_f = 0.48. Eluent 9 Hexane: 1 DCM v/v.

2-(2-methoxyethenyl)-1,3,5-trimethylbenzene (**21f**)

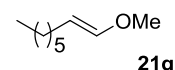
MeOH (1.5 mL, 37 mmol), DMA (1.5 mL, 16 mmol), 2-ethynyl-1,3,5-trimethylbenzene (213 μ L, 1.36 mmol) and catalyst **18** (5.72 mg, 15.1 μ mol).



21f, yellow oil (120 mg, 0.680 mmol, 50% isolated yield, E/Z = 3/1). ^1H NMR (300.30 MHz, CDCl_3) δ 2.20-2.33 (m, 36H, **H1'**, **3'** & **5'** (E - & Z -isomer)), 3.63 (s, 3H, **H9** (Z -isomer)), 3.70 (s, 9H, **H9** (E -isomer)), 5.21 (d, $^3J_{\text{H-H}}$ = 7.2, 1H, **H7** (Z -isomer)), 5.63 (d, $^3J_{\text{H-H}}$ = 13.4, 3H, **H7** (E -isomer)), 6.11 (d, $^3J_{\text{H-H}}$ = 7.2, 1H, **H8** (Z -isomer)), 6.45 (d, $^3J_{\text{H-H}}$ = 13.4, 3H, **H8** (E -isomer)), 6.83-6.96 (m, 8H, **H4** & **6** (E - & Z -isomer)). ^{13}C NMR (100.55 MHz, CDCl_3): δ 20.63 (s, **C1'**, **C3'** (Z -isomer)), 21.01 (s, **C5'** (Z -isomer)), 21.10 (s, **C5'** (E -isomer)), 21.31 (s, **C1'**, **C5'** (Z -isomer)), 56.27 (s, **C9** (E -isomer)), 59.74 (s, **C9** (Z -isomer)), 101.37 (s, **C7** (E -isomer)), 103.72 (s, **C7** (Z -isomer)), 128.05 (s, **C4**, **C6** (Z -isomer)), 128.56 (s, **C4**, **C6** (E -isomer)), 130.87 (s, **C1**, **C3** (E -isomer)), 131.50 (s, **C1**, **C3** (Z -isomer)), 135.57 (s, **C5**, (E -isomer)), 136.02 (s, **C5** (Z -isomer)), 136.65 (s, **C2** (E - & Z - isomer)), 149.57 (s, **C8** (Z -isomer)), 150.72 (s, **C8** (E -isomer)) ppm. R_f = 0.7 (E -isomer), 0.6 (Z -isomer) Eluent neat hexane.

(E)-1-methoxy-1-octene (**21g**)⁵⁴

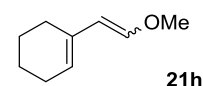
MeOH (5.0 mL, 123 mmol), DMA (5.0 mL, 54 mmol), 1-octyne (0.67 mL, 4.55 mmol) and catalyst **18** (19.2 mg, 5.05 μ mol).



Product not isolated (14% conv., E -isomer only). ^1H NMR (300.30 MHz, CDCl_3) δ 0.85-0.95 (m, $-\text{CH}_3$), 1.20-1.40 (m, $-\text{CH}_2-$), 1.93 (q, $^3J_{\text{H-H}}$ = 6.83, $=\text{CHCH}_2\text{CH}_2-$), 3.52 (s, OCH_3), 4.73 (td, $^3J_{\text{H-H}}$ = 12.6, 7.27, $-\text{CH}_2\text{CH}=\text{CH}-$), 6.27 (d, $^3J_{\text{H-H}}$ = 12.6, $=\text{CHOCH}_3$) ppm.

1-(methoxyethenyl)cyclohexene (**21h**)³¹

MeOH (1.5 mL, 37 mmol), DMA (1.5 mL, 16 mmol), 1-ethynylcyclohexene (160 μ L, 1.36 mmol) and catalyst **18** (5.75 mg, 15.1 μ mol).

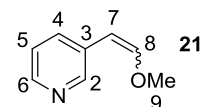


21h, brown oil with small crystals (160 mg, 1.15 mmol, 85% isolated yield, E -isomer only). ^1H NMR (300.17 MHz, CDCl_3) δ 1.57-1.74 (m, 4H, $-\text{CH}_2-$), 2.01-2.19 (m, 4H, $-\text{CH}_2-$), 3.60 (s, 3H, -

OCH₃-), 5.52-5.61 (m, 2H, C₆H₉CH, CH₂CH), 6.53 (d, ³J_{H-H} = 13.3, 1H, =CH-) ppm. R_f = 0.5.
Eluent: neat hexane.

3-methoxyethenylpyridine (**21i**)⁵⁵

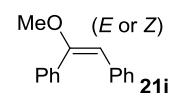
MeOH (1.0 mL, 25 mmol), DMA (1.0 mL, 11 mmol), 3-ethynylpyridine (99 mg, 0.91 mmol) and catalyst **18** (3.7 mg, 9.7 μmol) were used.



21i, brown oil (28% conv., *E/Z* = 1:3; not isolated). ¹H NMR (399.90 MHz, CDCl₃): δ 3.72 (s, 3H, **H9** (*E*-isomer)), 3.82 (s, 9H, **H9** (*Z*-isomer)), 5.20 (d, ³J_{H-H} = 7.6, 3H, **H7** (*Z*-isomer)), 5.76 (d, ³J_{H-H} = 13.1, 1H, **H7** (*E*-isomer)), 6.26 (d, ³J_{H-H} = 7.6, 3H, **H8** (*Z*-isomer)), 7.08 (d, *J* = 13.1, 1H, **H8** (*E*-isomer)), 7.15-7.23 (m, 4H, **H6** (*Z*-isomer & *E*-isomer)), 7.51-7.56 (m, 1H, **H4** (*E*-isomer)), 7.94-8.01 (m, 3H, **H4** (*Z*-isomer)), 8.33-8.39 (m, 4H, **H5** (*Z*-isomer & *E*-isomer)), 8.48 (s, 1H, **H2** (*E*-isomer)), 8.67 (s, 3H, **H2** (*Z*-isomer)) ppm. ¹³C NMR (100.55 MHz, CDCl₃): δ 56.79 (s, **C9** (*E*-isomer)), 61.09 (s, **C9** (*Z*-isomer)), 101.47 (s, **C7** (*E*-isomer)), 102.27 (s, **C7** (*Z*-isomer)), 123.27 (s, **C6** (*Z*-isomer)), 123.53 (s, **C6** (*E*-isomer)), 131.47 (s, **C4** (*E*-isomer)), 131.84 (s, **C3** (*Z*-isomer)), 132.27 (s, **C3** (*E*-isomer)), 135.00 (s, **C4** (*Z*-isomer)), 146.70 (s, **C5** (*Z*-isomer)), 147.01 (s, **C5** (*E*-isomer)), 147.21 (s, **C2** (*E*-isomer)), 149.51 (s, **C2** (*Z*-isomer)), 149.93 (s, **C8** (*Z*-isomer)), 150.27 (s, **C8** (*E*-isomer)) ppm.

1,1'-(1-methoxy-1,2-ethynenediyl)bis-(*E/Z*)-benzene (**21j**)

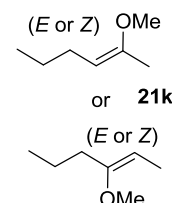
MeOH (0.5 mL, 12.3 mmol), DMA (0.5 mL, 5.4 mmol), diphenylacetylene (82 mg, 0.46 mmol) and catalyst **18** (1.7 mg, 4.8 μmol) were used.



No reaction occurred.

2-methoxy-2-hexene or 3-methoxy-2-hexene (**21k**)

MeOH (1.0 mL, 24.6 mmol), DMA (1.0 mL, 10.8 mmol), 2-hexyne (138 mg, 0.998 mmol) and catalyst **18** (7.0 mg, 0.018 mmol) were used.

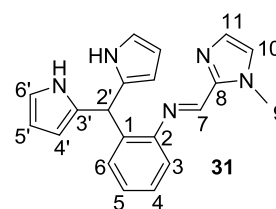


No reaction occurred.

5.3 Experimental Procedures for Chapter 3

Synthesis of o-dpmH3/mim (**31**)

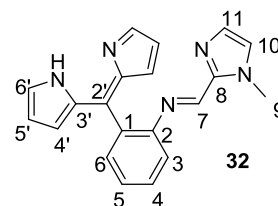
Activated 3 Å molecular sieves (ca. 3.5g), 2-(di(1*H*-pyrrol-2-yl)methyl)aniline (**28**, 500 mg, 2.11 mmol) and 1-methyl-2-



imidazolecarboxaldehyde (**30**, 232 mg, 2.11 mmol) were added to dry THF (20 mL). The mixture was refluxed with stirring under nitrogen overnight. After cooling to r.t., the reaction mixture was filtered through a celite pad and the filtrate was concentrated *in vacuo*. The crude product was purified by column chromatography (SiO₂ pre-treated with Et₃N. Eluent 3 EtOAc: 1 Hexane v/v. R_f for **31**: 0.3) to yield the product **31** as an off-white solid (466 mg, 1.34 mmol, 66%). ESI-MS (ESI+ MeOH), m/z (% assignment): 330.05 (65%, [M + H]⁺) amu. ¹H NMR (399.90 MHz, CDCl₃): δ 3.90 (s, 3H, **H9**), 5.89 (m, 2H, **H4'**), 5.97 (s, 1H, **H2'**), 6.12 (m, 2H, **H5'**), 6.64 (m, 2H, **H6'**), 6.98 (d, 1H, **H10**), 7.06 (d, ³J_{H-H} = 7.75, 1H, **H3**), 7.17-7.24 (m, 3H, **H11**, **H5**, **H6**), 7.30 (m, 1H, **H4**), 8.21 (br s, 2H, 2 x **NH**), 8.40 (s, 1H, **H7**) ppm. ¹³C{¹H}s NMR (100.55 MHz, CDCl₃): δ 35.53 (**C9**), 39.00 (**C2'**), 107.18 (**C4'**), 108.51 (**C5'**), 116.97 (**C6'**), 117.87 (**C3**), 125.74 (**C10**), 127.17 (**C5**), 128.48 (**C4**), 129.42 (**C6**), 130.36 (**C11**), 132.59 (**C3'**), 136.70 (**C11**), 143.67 (**C8**), 149.23 (**C2**), 151.11 (**C7**) ppm. Elemental Anal. found: C, 69.77; H, 6.09; N, 20.36%; calculated for C₂₀H₁₉N₅·H₂O: C, 69.14; H, 6.09; N, 20.16%

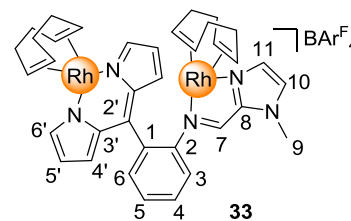
Synthesis of o-dpmH/mim (**32**)

Activated 3 Å molecular sieves (*ca.* 3.5g), *o*-dpmH₃/mim (**31**, 100 mg, 0.304 mmol) and *p*-chloranil (75 mg, 0.305 mmol) were added to dry THF (20 mL) and the reaction mixture was stirred overnight



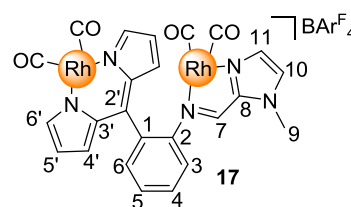
under a nitrogen atmosphere. The mixture was filtered through a celite pad and the solvent was removed from the filtrate under reduced pressure. The residue was re-dissolved in a minimum amount of DCM, and passed through a neutral alumina plug (*ca.* 5-7 cm long, 3 cm diameter). The yellow band was collected. The solvent was removed *in vacuo* to yield a sticky yellow solid (79.1 mg, 24.2 mmol, 80%). ¹H NMR showed that the product contained *ca.* 5% hydrolysed products (**29** and **30**) and was used in preparation of complexes **17** and **33** without further purification. ESI-MS (ESI+ MeOH), m/z (% assignment): 350.42 (100, [M + Na]⁺), 328.50 (24%, [M + H]⁺) amu. ¹H NMR (600.18 MHz, CD₂Cl₂): δ 3.45 (s, 3H, **H9**), 6.33 (m, 2H, **H5'**), 6.46 (m, 2H, **H4'**), 6.87 (m, 1H, **H10**), 7.06 (s, 1H, **H11**), 7.28 (d, ³J_{H-H} = 8.1, 1H, **H3**), 7.34 (t, ³J_{H-H} = 7.1, 1H, **H5**), 7.43 (d, ³J_{H-H} = 7.3, 1H, **H6**), 7.54 (t, ³J_{H-H} = 8.1, 1H, **H4**), 7.57 (s, 2H, **H6'**), 8.46 (s, 1H, **H7**) ppm. ¹³C{¹H} NMR (150.92 MHz, CD₂Cl₂): δ 35.37 (**C9**), 117.08 (**C3**), 117.86 (**C5'**), 125.91 (**C5**), 126.10 (**C10**), 128.72 (**C4'**), 130.00 (**C11**), 130.32 (**C4**), 131.52 (**C6**), 132.86 (**C1**), 140.37 (**C2'**), 141.66 (**C3'**), 143.59 (**C8**), 143.66 (**C6'**), 150.50 (**C2**), 150.95 (**C7**) ppm.

Synthesis of $[\text{Rh}_2(\text{COD})_2(o\text{-dpm/mim})]\text{BAR}^{\text{F}}_4$ (**33**)



Bitopic proligand *o*-dpmH/mim (**32**, 38.1 mg, 0.117 mmol) and K_2CO_3 (1.00 g, 7.24 mmol) were added to dry DCM (20 mL) and the suspension was stirred for 1 h. $[\text{Rh}(\text{COD})\text{Cl}]_2$ (57.5 mg, 0.117 mmol) was then added to the mixture and was stirred for an additional 1 h. $\text{NaBAR}^{\text{F}}_4$ (104 mg, 0.117 mmol) was added to the red solution, resulting in a dark red mixture which was again stirred for 1 h. The mixture was filtered through glass fibre filter paper and the filtrate was concentrated to *ca.* 5 mL and *n*-hexane was added dropwise to the solution with vigorous stirring until the a maroon oil is formed. The supernatant was filtered off and the product was dried *in vacuo* to yield a dark red solid (47.6 mg, 29.5 μmol , 25%). ESI-MS (ESI+ MeOH), m/z (% assignment): 748.17 (100, $[\text{M} - \text{BAR}^{\text{F}}_4]^+$) amu. ^1H NMR (600.18 MHz, CD_2Cl_2 , 253 K): δ 1.83 (m, 4H, COD $-\text{CH}_2-$), 2.01 (m, 4H, COD $-\text{CH}_2-$), 2.32 (m, 4H, COD $-\text{CH}_2-$), 2.54 (m, 4H, COD $-\text{CH}_2-$), 3.56 (s, 3H, **H9**), 4.29 (m, 4H, COD $=\text{CH}-$), 4.54 (m, 4H, COD $=\text{CH}-$), 6.42 (m, 4H, **H4'/5'/6'**), 6.75 (m, 1H, **H11**), 7.09 (d, $^3J_{\text{H-H}} = 7.81$, 1H, **H3**), 7.14 (m, 2H, **H4'/5'/6'**), 7.15 (m, 1H, **H10**), 7.41-7.49 (m, 2H, **H5**, **H6**), 7.53 (t, $^3J_{3-3} = 7.62$, 1H, **H4**), 7.56 (br s, 4H, $\text{BAR}^{\text{F}}_4^-$ **H_{para}**), 7.72 (m, 8H, $\text{BAR}^{\text{F}}_4^-$ **H_{ortho}**), 7.95 (m, 1H, **H7**) ppm. $^{13}\text{C}\{^1\text{H}\}$ NMR (150.92 MHz, CD_2Cl_2 , 253 K): δ 30.64 (COD $-\text{CH}_2-$), 35.56 (**C9**), 78.90 (d, $^1J_{\text{C-Rh}} = 11.9$, COD $=\text{CH}-$), 80.02 (d, $^1J_{\text{C-Rh}} = 11.9$, COD $=\text{CH}-$), 117.87 ($\text{BAR}^{\text{F}}_4^-$ **C_{para}**), 118.96 (**C4'/5'/6'**), 121.39 (**C3**), 124.96 (q, $^1J_{\text{C-F}} = 271.1$, $\text{BAR}^{\text{F}}_4^-$ **-CF₃**), 127.14 (**C10**), 127.82 (**C5**), 129.05 (**C11**), 129.23 (q, $^2J_{\text{C-F}} = 39.4$, $\text{BAR}^{\text{F}}_4^-$ **C_{meta}**), 129.89 (**C4**), 131.34 (**C1**), 131.67 (**C4'/5'/6'**), 132.02 (**C6**), 135.22 ($\text{BAR}^{\text{F}}_4^-$ **-C_{ortho}**), 137.77 (**C3'**), 142.07 (**C2'**), 145.63 (**C2**), 147.28 (**C8**), 150.00 (**C4'/5'/6'**), 155.56 (**C7**), 162.12 (q, $^1J_{\text{C-B}} = 49.3$, $\text{BAR}^{\text{F}}_4^-$ **C_{ipso}**) ppm. Elemental Anal. found: C, 50.62; H, 3.18; N, 4.13%; calculated for $\text{C}_{68}\text{H}_{52}\text{BF}_{24}\text{N}_5\text{Rh}_2$: C, 50.67; H, 3.25; N, 4.35%

Synthesis of $[\text{Rh}_2(\text{CO})_4(o\text{-dpm/mim})]\text{BAR}^{\text{F}}_4$ (**17**)

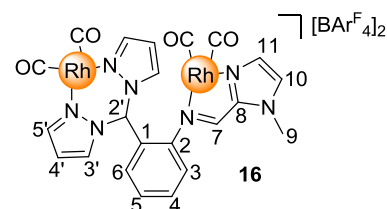


Proligand *o*-dpmH/mim (**32**, 38.9 mg, 0.119 mmol) and K_2CO_3 (1.00 g, 7.24 mmol) were added to dry DCM (20 mL) and the suspension was stirred for 1 h. $[\text{Rh}(\mu\text{-Cl})(\text{CO})_2]_2$ (47.0 mg, 0.121 mmol) was added and the mixture was stirred for an additional 1 h. $\text{NaBAR}^{\text{F}}_4$ (107 mg, 0.120 mmol) was subsequently added and the reaction mixture was stirred for another hour. The mixture was filtered through glass fibre filter paper and the filtrate was concentrated to *ca.* 5 mL. The product was recrystallised by slow addition of *n*-hexane with vigorous stirring (57.3 mg, 38.0 μmol , 32%). ESI-MS (ESI+ MeOH), m/z (% assignment): 615.83 (100, $[\text{M} - \text{BAR}^{\text{F}}_4]^-$

CO]⁺) amu. Selected FTIR (solid, ν_{CO}): 2012.41 (s), 2043.96 (s), 2075.51 (s), 2101.85 (s) cm⁻¹. ¹H NMR (600.13 MHz, CD₂Cl₂, 253 K): δ 3.59 (s, 3H, **H9**), 6.54 (m, 2H, **H4'**), 6.57 (m, 2H, **H5'**), 7.18 (s, 1H, **H11**), 7.25 (s, 1H, **H10**), 7.48-7.60 (m, 7H, **H3**, **H5**, **H6**, **BARF₄⁻ H_{para}**), 7.71 (t, ³*J*_{H-H} = 8.02 1H, **H4**), 7.75 (br s, 8H, **BARF₄⁻ H_{ortho}**), 7.80 (s, 2H, **H6'**), 8.00 (m, 1H, **H7**) ¹³C{¹H} NMR (150.90 MHz, CD₂Cl₂, 253 K): δ 35.69 (**C9**), 117.55 (**BARF₄⁻ -C_{para}**), 120.47 (**C5'**), 121.55 (**C3**), 124.53 (q, ¹*J*_{C-F} = 272.7, **BARF₄⁻ -CF₃**), 128.19 (**C10**), 128.75 (q, ²*J*_{C-F} = 32.7e, **BARF₄⁻ C_{meta}**), 129.05 (**C5**), 129.33 (**C1**), 130.90 (**C4**), 131.25 (**C4'**), 131.67 (**C6**), 133.05 (**C11**), 134.71 (**BARF₄⁻ -C_{ortho}**), 136.52 (**C3'**), 140.87 (**C2'**), 146.67 (**C8**), 147.51 (**C2**), 154.58 (**C7**), 156.85 (**C6'**), 161.73 (q, ¹*J*_{C-B} = 49.3, **BARF₄⁻ C_{ipso}**), 181.78 (d, ¹*J*_{C-Rh} = 71.8, **CO**), 186.02 (d, ¹*J*_{C-Rh} = 68.0, **CO**) ppm. Elemental Anal. found: C, 44.56; H, 1.78; N, 4.74%; calculated for C₅₆H₂₈BF₂₄N₅Rh₂: C, 44.62; H, 1.87; N, 4.25%

Synthesis of [Rh₂(CO)₄(*o*-bpm/mim)][BARF₄]₂ (**16**)

Ligand *o*-bpm/mim (**26**, 16.1 mg, 48.6 μ mol) and [Rh(μ -Cl)(CO)₂]₂ (18.9 mg, 48.6 μ mol) were added to dry DCM (20 mL) and the solution was stirred for 1 h. NaBARF₄ (86.9



mg, 97.3 μ mol) was then added and the mixture was stirred for another hour. The mixture was filtered through glass fibre filter paper and the filtrate concentrated to *ca.* 5 mL. The product was recrystallised by slow addition of *n*hexane with vigorous stirring until a light brown precipitate forms, then triturated with *n*hexane (2 \times 20 mL) to afford a light brown powder (55.5 mg, 23.3 μ mol, 48%) ESI-MS (ESI+ MeOH), *m/z* (% assignment): 434.00 (42, [M – 2BARF₄ – Rh – 4CO]⁺), 462.08 (100, [M – 2BARF₄ – Rh – 3CO]⁺), 593 (30, [M – 2BARF₄ – 2CO]⁺) amu. Selected FTIR (solid, ν_{CO}): 2053.41 (s), 2110.75 (s) cm⁻¹. ¹H NMR (600.13 MHz, CD₂Cl₂): δ 3.93 (s, 3H, **H9**), 6.59 (m, 1H, **H6**), 6.31 (m, 1H, **H4'**), 6.59 (m, 1H, **H6**), 6.78 (s, 1H, **H4'**), 7.22 (m, 1H, **H3**), 7.39 (s, 1H, **H11**), 7.45 (s, 1H, **H10**), 7.53-7.65 (br s, 9H, **H5**, **BARF₄⁻ H_{para}**), 7.67-7.81 (m, 17H, **H4**, **BARF₄⁻ H_{ortho}**), 7.86 (s, 1H, **H3'**), 7.89 (s, 1H, **H7**), 8.03 (s, 1H, **H5'**), 8.06 (s, 1H, **H2'**), 8.13 (s, 1H, **H5'**), 8.40 (s, 1H, **H3'**) ppm. ¹³C{¹H} NMR (150.90 MHz, CD₂Cl₂): δ 36.52 (**C9**), 73.25 (**C2'**), 108.74 (**C4'**), 110.33 (**C4'**), 117.67 (**BARF₄⁻ -C_{para}**), 123.82 (**C3**), 124.52 (q, ¹*J*_{C-F} = 273.9, **BARF₄⁻ -CF₃**), 124.57 (**C1**), 128.76 (q, ²*J*_{C-F} = 32.7, **BARF₄⁻ C_{meta}**), 128.96 (**C6**), 130.31 (**C10**), 131.14 (**C5**), 134.43 (**C4**), 134.73 (**BARF₄⁻ -C_{ortho}**), 134.96 (**C11**), 136.02 (**C3'**), 136.32 (**C3'**), 145.83 (**C8**), 147.09 (**C2**), 147.71 (**C5'**), 148.85 (**C5'**), 155.06 (**C7**), 161.77 (q, ¹*J*_{C-B} = 48.2, **BARF₄⁻ C_{ipso}**), 179.50-182.00 (m, **CO**) ppm. Elemental Anal. found: C, 43.24; H, 1.52; N, 3.43%; calculated for C₈₆H₄₁B₂F₄₈N₇O₄Rh₂·0.3C₆H₁₄: C, 43.91; H, 1.90; N, 4.08%

General Procedure for Catalysed C-O Bond Forming Reactions

The catalysed dihydroalkoxylation reaction of 2-(5-hydroxypent-1-ynyl)benzyl alcohol (**11**) and 2-(4-hydroxypent-1-ynyl)benzyl alcohol (**23**) were performed on a small scale in NMR tubes fitted with a concentric Teflon Young's valve. The complex and the substrate were weighed into the NMR tube, and the solvent was added under an inert atmosphere glovebox. The catalysed reactions were conducted at elevated temperatures either in the NMR spectrometer or in an oil bath if prolonged heating was required. The temperature in the NMR magnet was calibrated using a digital thermometer connected to a K-type thermocouple (NiCr-Ni, mineral insulated), immersed in neat ethylene glycol. The products were identified and confirmed by comparing the NMR data with ^1H NMR data reported previously in the literature.⁴¹

The rate of conversion was determined by integration of the product resonances relative to the substrate resonances in the ^1H NMR spectra acquired at regular intervals. Quantitative conversion (>98%) was taken to be the time where no remaining resonances due to substrate were evident in the NMR spectrum. The turnover frequency (ToF) was calculated as the number of moles of product(s) produced per mole of catalyst used per hour and was calculated at the point of 50% conversion of substrate to product, unless otherwise stated. All results for the catalysed reactions, including outcomes of integration, concentration and reaction times are reported in full in the Appendices. Relative quantities of catalyst and substrate are presented here.

Catalysed Hydroalkoxylation of Methanol and Phenylacetylene using complexes **16**, **17** and a mixture of **18/13a**.

Table 6 Quantities of catalyst and phenylacetylene used.

Entry	Catalyst	Quant. Of Phenylacetylene		Quant. Of Catalyst	
1	16	50 μL	0.46 mmol	5.85 mg	2.46 μmol
2	17	50 μL	0.46 mmol	3.65 mg	2.42 μmol
3	18	50 μL	0.46 mmol	0.94 mg	2.5 μmol
	13a			3.11 mg	2.58 μmol

Catalysed Dihydroalkoxylation of Alkyne Diol, 2-(5-hydroxypent-1-ynyl)benzyl alcohol (**11**) using complexes **16** and **17**.

Table 7 Quantities of catalyst and 2-(5-hydroxypent-1-ynyl)benzyl alcohol (**11**) used.

Catalyst	Run	Quant. Of Diol		Quant. Of Catalyst	
16	1	38.9 mg	205 μmol	2.39 mg	1.01 μmol
	2	38.9 mg	205 μmol	2.36 mg	0.994 μmol
17	1	40.4 mg	213 μmol	1.55 mg	1.03 μmol
	2	39.9 mg	210 μmol	1.53 mg	1.02 μmol

Catalysed Dihydroalkoxylation of Alkyne Diol, 2-(4-hydroxypent-1-ynyl)benzyl alcohol (23**) using complexes **16** and **17**.**

Table 8 Quantities of catalyst and 2-(4-hydroxypent-1-ynyl)benzyl alcohol (**23**) used.

Catalyst	Run	Quant. Of Diol		Quant. Of Catalyst	
16	1	36.7 mg	208 μmol	2.37 mg	1.00 μmol
	2	36.1 mg	205 μmol	2.38 mg	1.01 μmol
17	1	35.1 mg	199 μmol	1.43 mg	0.949 μmol
	2	36.0 mg	204 μmol	1.45 mg	0.949 μmol

6 References

- (1) Van Santen, R. A.; Van Leeuwen, P. W. N. M.; Moulijn, J. A.; Averill, B. A.; Editors, *Catalysis: an Integrated Approach, Second, Revised and Enlarged Edition*. [In: *Stud. Surf. Sci. Catal.*, 1999; 123]. Elsevier: 1999; p 1-68.
- (2) (a) Hagen, J., *Industrial Catalysis: A Practical Approach*. Wiley: Weinheim, 1999; p 1-14; (b) Bhaduri, S.; Mukesh, D., *Homogeneous Catalysis: Mechanisms and Industrial Applications*. Wiley: New York, 2000; p 1-11.
- (3) IUPAC. Compendium of Chemical Terminology, 2nd ed. (the "Gold Book"). Compiled by A. D. McNaught and A. Wilkinson. Blackwell Scientific Publications, Oxford (1997). XML on-line corrected version: <http://goldbook.iupac.org> (2006-) created by M. Nic, J. Jirat, B. Kosata; updates compiled by A. Jenkins. ISBN 0-9678550-9-8. doi:10.1351/goldbook.
- (4) Housecroft, C. E.; Sharpe, A. G., *Inorganic Chemistry*. Pearson: UK, 2012; p 786-798.
- (5) van Leeuwen, P. W. N. M., *Homogeneous Catalysis: Understanding the Art*. Springer: Netherlands, 2004; p 1-28.
- (6) (a) Li, C.-J.; Trost, B. M., *Proc. Natl. Acad. Sci. U. S. A.* **2008**, *105*, 13197-13202; (b) Zanardi, A.; Corberan, R.; Mata, J. A.; Peris, E., *Organometallics* **2008**, *27*, 3570-3576; (c) Trost, B. M., *Science* **1991**, *254*, 1471-7.
- (7) Alberico, E.; Nielsen, M., *Chem. Commun.* **2015**, *51*, 6714-6725.
- (8) (a) Sheldon, R. A.; Arends, I.; Hanefeld, U., *Environmental Chemistry - Industrial Application: Catalysis*. Wiley-VCH: Weinheim, Germany, 2007; p 49, 91, 133, 223; (b) Dondoni, A.; Massi, A., *Angew. Chem., Int. Ed.* **2008**, *47*, 4638-4660; (c) Taylor, M. S.; Jacobsen, E. N., *Angew. Chem., Int. Ed.* **2006**, *45*, 1520-1543; (d) Bertelsen, S.; Jorgensen, K. A., *Chem. Soc. Rev.* **2009**, *38*, 2178-2189; (e) Park, J.; Hong, S., *Chem. Soc. Rev.* **2012**, *41*, 6931-6943.
- (9) Herrmann, W. A.; Cornils, B., *Angew. Chem., Int. Ed. Engl.* **1997**, *36*, 1049-1067.
- (10) Blaser, H.-U.; Indolese, A.; Schnyder, A., *Curr. Sci.* **2000**, *78*, 1336-1344.
- (11) Busacca, C. A.; Fandrick, D. R.; Song, J. J.; Senanayake, C. H., *Adv. Synth. Catal.* **2011**, *353*, 1825-1864.
- (12) Omae, I., *Applications of Organometallic compounds*. Wiley: UK, 1998; p 1-6.
- (13) (a) O'Reilly, M. E.; Veige, A. S., *Chem. Soc. Rev.* **2014**, *43*, 6325-6369; (b) Matthews, R. C.; Howell, D. K.; Peng, W.-J.; Train, S. G.; Treleaven, W. D.; Stanley, G. G., *Angew. Chem., Int. Ed.* **1996**, *35*, 2253-2256.
- (14) (a) Balamurugan, M.; Vadivelu, P.; Palaniandavar, M., *Dalton Trans.* **2014**, *43*, 14653-14668; (b) Balamurugan, M.; Mayilmurugan, R.; Suresh, E.; Palaniandavar, M., *Dalton Trans.* **2011**, *40*, 9413-9424.
- (15) (a) Larionov, E.; Nakanishi, M.; Katayev, D.; Besnard, C.; Kuendig, E. P., *Chem. Sci.* **2013**, *4*, 1995-2005; (b) Katayev, D.; Nakanishi, M.; Buergi, T.; Kuendig, E. P., *Chem. Sci.* **2012**, *3*, 1422-1425; (c) Jia, Y.-X.; Katayev, D.; Bernardinelli, G.; Seidel, T. M.; Kuendig, E. P., *Chem. - Eur. J.* **2010**, *16*, 6300-6309.
- (16) (a) Fjermestad, T.; Ho, J. H. H.; MacGregor, S. A.; Messerle, B. A.; Tuna, D., *Organometallics* **2011**, *30*, 618-626; (b) Miller, K. J.; Kitagawa, T. T.; Abu-Omar, M. M., *Organometallics* **2001**, *20*, 4403-4412.
- (17) (a) Mulyana, Y.; Alley, K. G.; Davies, K. M.; Abrahams, B. F.; Moubaraki, B.; Murray, K. S.; Boskovic, C., *Dalton Trans.* **2014**, *43*, 2499-2511; (b) Alley, K. G.; Poneti, G.; Robinson, P. S. D.; Nafady, A.; Moubaraki, B.; Aitken, J. B.; Drew, S. C.; Ritchie, C.; Abrahams, B. F.; Hocking, R. K.; Murray, K. S.; Bond, A. M.; Harris, H. H.; Sorace, L.; Boskovic, C., *J. Am. Chem. Soc.* **2013**, *135*, 8304-8323.

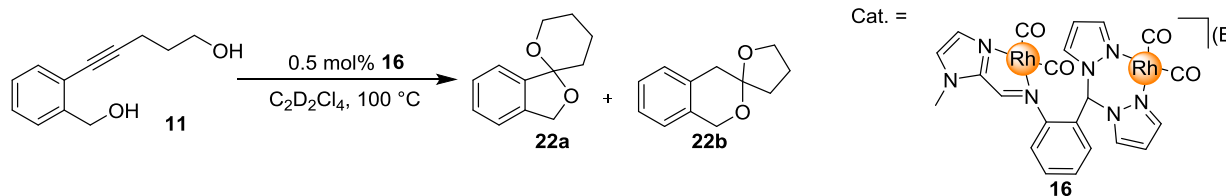
- (18) (a) Kuriyama, S.; Arashiba, K.; Nakajima, K.; Tanaka, H.; Yoshizawa, K.; Nishibayashi, Y., *Chem. Sci.* **2015**, *6*, 3940-3951; (b) Aguirre-Etcheverry, P.; O'Hare, D., *Chem. Rev.* **2010**, *110*, 4839-4864.
- (19) Lee, J. M.; Na, Y.; Han, H.; Chang, S., *Chem. Soc. Rev.* **2004**, *33*, 302-312.
- (20) (a) Perron, F.; Albizzati, K. F., *Chem. Rev.* **1989**, *89*, 1617-61; (b) Hall, N., *Science* **1994**, *266*, 32-4.
- (21) (a) Broussard, M. E.; Juma, B.; Train, S. G.; Peng, W. J.; Laneman, S. A.; Stanley, G. G., *Science* **1993**, *260*, 1784-8; (b) Choy, S. W. S.; Page, M. J.; Bhadbhade, M.; Messerle, B. A., *Organometallics* **2013**, *32*, 4726-4729; (c) Timerbulatova, M. G.; Gatus, M. R. D.; Vuong, K. Q.; Bhadbhade, M.; Algarra, A. G.; MacGregor, S. A.; Messerle, B. A., *Organometallics* **2013**, *32*, 5071-5081; (d) Matsunaga, S.; Shibasaki, M., *Chem. Commun.* **2014**, *50*, 1044-1057; (e) Shibasaki, M.; Kanai, M.; Matsunaga, S.; Kumagai, N., *Top. Organomet. Chem.* **2011**, *37*, 1-30; (f) Li, H.; Marks, T. J., *Proc. Natl. Acad. Sci. U. S. A.* **2006**, *103*, 15295-15302; (g) Delferro, M.; Marks, T. J., *Chem. Rev.* **2011**, *111*, 2450-2485.
- (22) Ho, J. H. H.; Choy, S. W. S.; MacGregor, S. A.; Messerle, B. A., *Organometallics* **2011**, *30*, 5978-5984.
- (23) Jones, S. C.; Hascall, T.; Barlow, S.; O'Hare, D., *J. Am. Chem. Soc.* **2002**, *124*, 11610-11611.
- (24) Van Den Beuken, E. K.; Feringa, B. L., *Tetrahedron* **1998**, *54*, 12985-13011.
- (25) Sabater, S.; Mata, J. A.; Peris, E., *Organometallics* **2012**, *31*, 6450-6456.
- (26) Gonell, S.; Peris, E., *ACS Catal.* **2014**, *4*, 2811-2817.
- (27) (a) Man, B. Y. W.; Bhadbhade, M.; Messerle, B. A., *New J. Chem.* **2011**, *35*, 1730-1739; (b) Ho, J. H. H.; Hodgson, R.; Wagler, J.; Messerle, B. A., *Dalton Trans.* **2010**, *39*, 4062-4069.
- (28) Lam, R. H.; Walker, D. B.; Tucker, M. H.; Gatus, M. R. D.; Bhadbhade, M.; Messerle, B. A., *Organometallics* **2015**, *34*, 4312-4317.
- (29) (a) Alonso, F.; Beletskaya, I. P.; Yus, M., *Chem. Rev.* **2004**, *104*, 3079-3159; (b) Mueller, T. E.; Hultsch, K. C.; Yus, M.; Foubelo, F.; Tada, M., *Chem. Rev.* **2008**, *108*, 3795-3892.
- (30) (a) Effenberger, F., *Angew. Chem., Int. Ed.* **1969**, *8*, 295-312; (b) Donohoe, T. J.; Fishlock, L. P.; Lacy, A. R.; Procopiou, P. A., *Org. Lett.* **2007**, *9*, 953-956; (c) de los Santos, J. M.; Ignacio, R.; Es Sbai, Z.; Aparicio, D.; Palacios, F., *J. Org. Chem.* **2014**, *79*, 7607-7615; (d) Gao, S.; Chen, J.-R.; Hu, X.-Q.; Cheng, H.-G.; Lu, L.-Q.; Xiao, W.-J., *Adv. Synth. Catal.* **2013**, *355*, 3539-3544; (e) Roche, C.; Delair, P.; Greene, A. E., *Org. Lett.* **2003**, *5*, 1741-1744; (f) Shirakawa, S.; Lombardi, P. J.; Leighton, J. L., *J. Am. Chem. Soc.* **2005**, *127*, 9974-9975; (g) Puglisi, A.; Lee, A.-L.; Schrock, R. R.; Hoveyda, A. H., *Org. Lett.* **2006**, *8*, 1871-1874; (h) Pedzisa, L.; Vaughn, I. W.; Pongdee, R., *Tetrahedron Lett.* **2008**, *49*, 4142-4144.
- (31) Kondo, M.; Kochi, T.; Kakiuchi, F., *J. Am. Chem. Soc.* **2011**, *133*, 32-34.
- (32) Yadav, M.; Kumar, P.; Pandey, D. S., *Polyhedron* **2010**, *29*, 791-800.
- (33) Lam, R. H. Honours Thesis. UNSW, 2014.
- (34) Dang, Y.; Qu, S.; Wang, Z.-X.; Wang, X., *Organometallics* **2013**, *32*, 2804-2813.
- (35) (a) Otsuka, M.; Tsuchida, N.; Ikeda, Y.; Kimura, Y.; Mutoh, Y.; Ishii, Y.; Takano, K., *J. Am. Chem. Soc.* **2012**, *134*, 17746-17756; (b) Otsuka, M.; Tsuchida, N.; Ikeda, Y.; Lambert, N.; Nakamura, R.; Mutoh, Y.; Ishii, Y.; Takano, K., *Organometallics* **2015**, *34*, 3934-3943.
- (36) Cowley, M. J.; Lynam, J. M.; Slattey, J. M., *Dalton Trans.* **2008**, 4552-4554.
- (37) (a) Ferreira, H.; Conradie, M. M.; Conradie, J., *Electrochim. Acta* **2013**, *113*, 519-526; (b) Conradie, J.; Swarts, J. C., *Dalton Trans.* **2011**, *40*, 5844-5851; (c) Erasmus, J. J. C.; Conradie, J., *Electrochim. Acta* **2011**, *56*, 9287-9294; (d) Kuhn, A.; von Eschwege, K. G.; Conradie, J., *Electrochim. Acta* **2011**, *56*, 6211-6218.
- (38) Kadish, K. M.; Smith, K. M.; Guillard, R.; Editors, *The Porphyrin Handbook: Volume 18 / Multiporphyrins, Multiphthalocyanines, and Arrays*. Academic press: San Diego, 2003; p 315-316.

- (39) Timerbulatova, M. G. PhD Thesis. UNSW, 2013.
- (40) (a) Doubsky, J.; Streinz, L.; Saman, D.; Zednik, J.; Koutek, B., *Org. Lett.* **2004**, *6*, 4909-4911; (b) Bai, R.; Cichacz, Z. A.; Herald, C. L.; Pettit, G. R.; Hamel, E., *Mol. Pharmacol.* **1993**, *44*, 757-66; (c) Ghosh, S. K.; Hsung, R. P.; Liu, J., *J. Am. Chem. Soc.* **2005**, *127*, 8260-8261.
- (41) Messerle, B. A.; Vuong, K. Q., *Organometallics* **2007**, *26*, 3031-3040.
- (42) Choy, S. W. S. Honours Thesis. UNSW, 2010.
- (43) (a) Evano, G.; Gaumont, A.-C.; Alayrac, C.; Wrona, I. E.; Giguere, J. R.; Delacroix, O.; Bayle, A.; Jouvin, K.; Theunissen, C.; Gatignol, J.; Silvanus, A. C., *Tetrahedron* **2014**, *70*, 1529-1616; (b) Goodwin, J. A.; Aponick, A., *Chem. Commun.* **2015**, *51*, 8730-8741; (c) Low, P. J.; Bock, S., *Electrochim. Acta* **2013**, *110*, 681-692; (d) Jiménez-Tenorio, M.; Puerta, M. C.; Valerga, P.; Ortuño, M. A.; Ujaque, G.; Lledós, A., *Inorg. Chem.* **2013**, *52*, 8919-8932; (e) Pickup, O. J. S.; Khazal, I.; Smith, E. J.; Whitwood, A. C.; Lynam, J. M.; Bolaky, K.; King, T. C.; Rawe, B. W.; Fey, N., *Organometallics* **2014**, *33*, 1751-1761; (f) Breit, B.; Gellrich, U.; Li, T.; Lynam, J. M.; Milner, L. M.; Pridmore, N. E.; Slattery, J. M.; Whitwood, A. C., *Dalton Trans.* **2014**, *43*, 11277-11285; (g) Lynam, J. M., *Chem. - Eur. J.* **2010**, *16*, 8238-8247.
- (44) (a) Conradie, J., *Electrochim. Acta* **2013**, *110*, 718-725; (b) Erasmus, J. J. C.; Conradie, J., *Dalton Trans.* **2013**, *42*, 8655-8666; (c) Conradie, J., *Inorg. Chim. Acta* **2012**, *392*, 30-37; (d) Conradie, J.; Swarts, J. C., *Dalton Trans.* **2011**, *40*, 5844-5851; (e) Conradie, J.; Cameron, T. S.; Aquino, M. A. S.; Lamprecht, G. J.; Swarts, J. C., *Inorg. Chim. Acta* **2005**, *358*, 2530-2542; (f) Lamprecht, D.; Lamprecht, G. J., *Inorg. Chim. Acta* **2000**, *309*, 72-76.
- (45) Bard, A.; Faulkner, L. R., *Electrochemical Methods: Fundamentals and Applications*. 2nd ed.; Wiley: New York, 2001; p 137-155.
- (46) Marcé, P.; Godard, C.; Feliz, M.; Yáñez, X.; Bo, C.; Castellón, S., *Organometallics* **2009**, *28*, 2976-2985.
- (47) Tregubov, A. A.; Vuong, K. Q.; Luais, E.; Gooding, J. J.; Messerle, B. A., *J. Am. Chem. Soc.* **2013**, *135*, 16429-16437.
- (48) Choudhury, J.; Podder, S.; Roy, S., *J. Am. Chem. Soc.* **2005**, *127*, 6162-6163.
- (49) Laha, J. K.; Dhanalekshmi, S.; Taniguchi, M.; Ambroise, A.; Lindsey, J. S., *Org. Process Res. Dev.* **2003**, *7*, 799-812.
- (50) Yu, L.; Muthukumaran, K.; Sazanovich, I. V.; Kirmaier, C.; Hindin, E.; Diers, J. R.; Boyle, P. D.; Bocian, D. F.; Holten, D.; Lindsey, J. S., *Inorg. Chem.* **2003**, *42*, 6629-6647.
- (51) (a) Li, X.; Chianese, A. R.; Vogel, T.; Crabtree, R. H., *Org. Lett.* **2005**, *7*, 5437-5440; (b) Fugami, K.; Hagiwara, N.; Okeda, T.; Kosugi, M., *Chem. Lett.* **1998**, 81-82.
- (52) Julia, S.; Del Mazo, J. M.; Avila, L.; Elguero, J., *Org. Prep. Proced. Int.* **1984**, *16*, 299-307.
- (53) McCleverty, J. A.; Wilkinson, G., *Inorg. Synth.* **1990**, *28*, 84-6.
- (54) Waldraff, C.; Bernet, B.; Vasella, A., *Helv. Chim. Acta* **1997**, *80*, 1882-1900.
- (55) Sakamoto, T.; Kondo, Y.; Shiraiwa, M.; Yamanaka, H., *Synthesis* **1984**, 245 - 247.

Appendix A: Catalysis Data (Chapter 3)

A1 Catalysed Dihydroalkoxylation of 2-(5-(hydroxymethyl)phenyl)pent-4-yn-1-ol (**11**)

Entry 1, Table 3; Figure 12a

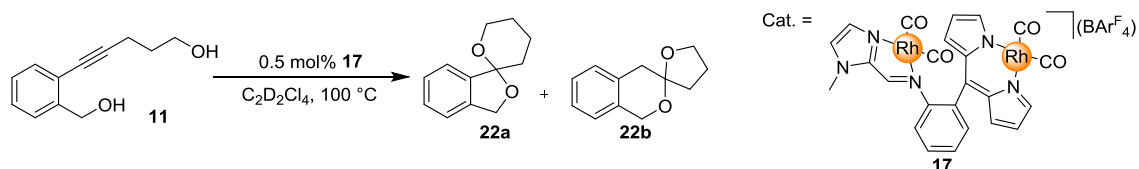


Time (s)	Time (h)	Conv. to 22a	Conv. to 22b	Total Conv.
10	0.003	3%	4%	8%
37	0.010	3%	4%	9%
65	0.018	5%	6%	13%
93	0.026	7%	7%	17%
120	0.033	8%	8%	20%
148	0.041	9%	10%	23%
176	0.049	10%	11%	26%
204	0.057	11%	13%	28%
231	0.064	12%	15%	31%
259	0.072	13%	16%	34%
286	0.079	14%	18%	37%
314	0.087	15%	20%	39%
347	0.096	16%	22%	42%
379	0.105	17%	25%	45%
412	0.114	19%	26%	49%
445	0.124	20%	29%	52%
478	0.133	21%	31%	55%
511	0.142	22%	33%	57%
543	0.151	22%	35%	60%
576	0.160	23%	37%	63%
609	0.169	24%	39%	65%

642	0.178	25%	40%	68%
674	0.187	26%	42%	70%
707	0.196	27%	43%	72%
760	0.211	27%	46%	76%
813	0.226	28%	48%	79%
865	0.240	29%	50%	82%
918	0.255	29%	52%	84%
971	0.270	30%	53%	87%
1024	0.284	31%	54%	89%
1076	0.299	31%	55%	90%
1130	0.314	31%	56%	92%
1182	0.328	31%	57%	93%
1235	0.343	30%	58%	94%
1318	0.366	30%	59%	95%
1401	0.389	30%	60%	96%
1484	0.412	30%	60%	97%
1567	0.435	30%	61%	98%
1649	0.458	29%	62%	98%
1732	0.481	29%	62%	98%
1814	0.504	29%	62%	98%
1897	0.527	28%	63%	99%
1980	0.550	28%	62%	99%
2063	0.573	27%	63%	99%
2145	0.596	27%	63%	99%
2228	0.619	28%	62%	99%
2371	0.659	26%	64%	99%
2514	0.698	27%	62%	99%
2656	0.738	25%	64%	99%
2799	0.778	25%	64%	99%

2942	0.817	25%	64%	99%
3085	0.857	25%	65%	99%
3228	0.897	26%	64%	99%
3370	0.936	25%	64%	99%

Entry 2, Table 3; Figure 12a



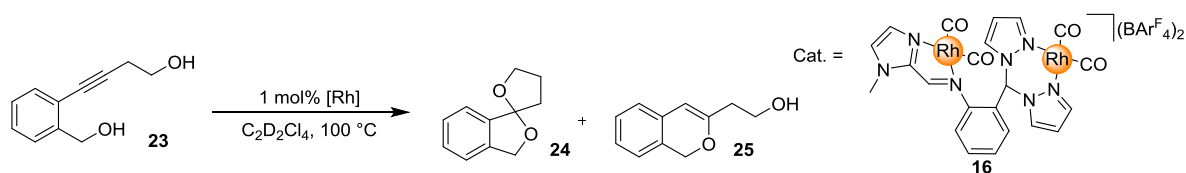
Time (s)	Time (h)	Conv. to 22a	Conv. to 22b	Total Conv.
10	0.003	1%	2%	3%
37	0.010	2%	2%	6%
65	0.018	5%	2%	12%
93	0.026	8%	3%	20%
121	0.034	12%	4%	28%
148	0.041	15%	5%	36%
176	0.049	18%	5%	43%
203	0.056	21%	6%	49%
231	0.064	22%	7%	54%
259	0.072	25%	7%	59%
286	0.079	26%	8%	63%
314	0.087	28%	8%	66%
347	0.096	29%	9%	70%
379	0.105	30%	10%	73%
412	0.114	31%	11%	75%
444	0.123	32%	11%	78%
477	0.133	33%	12%	80%
510	0.142	33%	13%	82%
543	0.151	34%	14%	83%

576	0.160	35%	15%	85%
609	0.169	36%	16%	86%
641	0.178	36%	17%	87%
674	0.187	36%	18%	88%
706	0.196	36%	19%	89%
759	0.211	37%	21%	91%
812	0.226	38%	23%	92%
864	0.240	38%	25%	93%
917	0.255	38%	27%	94%
970	0.269	39%	28%	95%
1022	0.284	39%	30%	95%
1075	0.299	39%	32%	96%
1128	0.313	39%	34%	96%
1180	0.328	39%	36%	97%
1233	0.343	39%	38%	97%
1315	0.365	40%	40%	97%
1398	0.388	40%	42%	98%
1481	0.411	40%	44%	98%
1564	0.434	40%	46%	98%
1646	0.457	40%	48%	99%
1729	0.480	40%	50%	99%
1812	0.503	41%	51%	99%
1894	0.526	41%	52%	99%
1977	0.549	40%	53%	99%
2060	0.572	41%	54%	99%
2142	0.595	40%	55%	99%
2225	0.618	40%	55%	99%
2368	0.658	41%	56%	99%
2510	0.697	40%	57%	99%

2653	0.737	41%	57%	99%
2796	0.777	41%	57%	99%
2938	0.816	41%	56%	99%
3081	0.856	40%	58%	99%
3224	0.896	40%	58%	99%
3366	0.935	41%	57%	99%
3509	0.975	41%	57%	99%
3652	1.014	40%	58%	99%
3914	1.087	40%	58%	99%
4177	1.160	40%	58%	99%
4440	1.233	41%	57%	99%
4703	1.306	40%	58%	99%
4965	1.379	40%	58%	99%
5228	1.452	41%	57%	99%
5491	1.525	41%	57%	99%
5754	1.598	40%	58%	99%
6017	1.671	40%	58%	99%
6279	1.744	41%	58%	99%
6782	1.884	40%	58%	99%

A2 Catalysed Dihydroalkoxylation of 2-(4-hydroxypent-1-ynyl)benzyl alcohol (23)

Entry 6, Table 3; Figure 12b



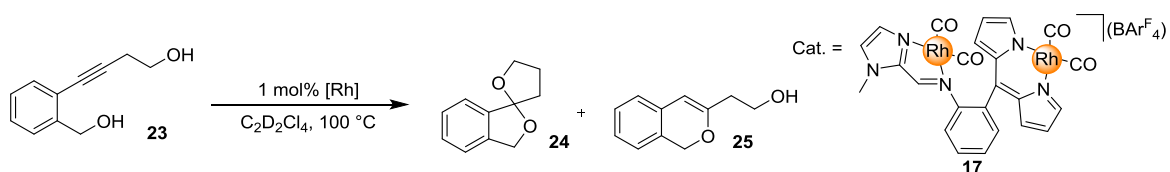
Time (s)	Time (h)	Conv. to 24	Conv. to 25	Total Conv.
13	0.004	0%	0%	0%
42	0.012	1%	1%	2%
69	0.019	0%	2%	2%

97	0.027	3%	4%	7%
125	0.035	4%	6%	10%
153	0.043	9%	8%	17%
208	0.058	15%	11%	26%
235	0.065	15%	13%	28%
263	0.073	18%	16%	34%
290	0.081	23%	19%	42%
318	0.088	26%	22%	47%
350	0.097	28%	25%	53%
383	0.106	32%	27%	59%
416	0.116	35%	29%	64%
448	0.124	36%	31%	67%
481	0.134	40%	32%	72%
513	0.143	40%	33%	73%
546	0.152	43%	34%	77%
578	0.161	44%	35%	79%
611	0.170	46%	35%	81%
643	0.179	46%	36%	82%
676	0.188	45%	38%	83%
709	0.197	48%	37%	85%
761	0.211	48%	38%	86%
814	0.226	50%	39%	88%
866	0.241	48%	40%	88%
919	0.255	51%	40%	91%
972	0.270	50%	40%	91%
1024	0.284	50%	42%	92%
1077	0.299	51%	41%	92%
1130	0.314	51%	42%	93%
1183	0.329	51%	42%	93%

1235	0.343	53%	42%	95%
1318	0.366	53%	42%	95%
1400	0.389	53%	42%	95%
1483	0.412	53%	43%	96%
1566	0.435	53%	42%	95%
1648	0.458	54%	42%	96%
1731	0.481	53%	42%	95%
1814	0.504	54%	42%	96%
1896	0.527	54%	42%	96%
1979	0.550	55%	42%	96%
2062	0.573	55%	41%	97%

App

Entry 7, Table 3; Figure 12b



Time (s)	Time (h)	Conv. to 24	Conv. to 25	Total Conv.
27	0.008	2%	2%	4%
96	0.027	3%	3%	6%
124	0.034	4%	4%	8%
152	0.042	6%	6%	12%
179	0.050	9%	8%	17%
207	0.058	13%	10%	23%
235	0.065	17%	11%	28%
262	0.073	21%	13%	34%
290	0.081	24%	14%	38%
318	0.088	27%	15%	42%
345	0.096	29%	17%	46%
373	0.104	30%	18%	49%

405	0.113	33%	20%	52%
438	0.122	35%	20%	56%
471	0.131	37%	22%	59%
504	0.140	39%	23%	62%
537	0.149	41%	23%	64%
570	0.158	42%	24%	67%
602	0.167	44%	25%	69%
636	0.177	45%	26%	71%
669	0.186	46%	26%	73%
702	0.195	47%	27%	74%
734	0.204	48%	27%	76%
767	0.213	49%	28%	77%
819	0.228	50%	29%	79%
872	0.242	52%	29%	81%
924	0.257	53%	30%	83%
977	0.271	54%	31%	84%
1030	0.286	55%	31%	85%
1082	0.301	55%	31%	87%
1135	0.315	56%	32%	88%
1187	0.330	57%	32%	89%
1240	0.344	58%	32%	90%
1292	0.359	59%	32%	91%
1375	0.382	59%	33%	92%
1458	0.405	60%	33%	93%
1540	0.428	59%	34%	93%
1624	0.451	61%	34%	94%
1709	0.475	61%	34%	95%
1791	0.498	62%	34%	96%
1874	0.521	62%	34%	96%

1957	0.544	62%	34%	96%
2044	0.568	62%	35%	97%
2126	0.591	63%	34%	97%
2209	0.614	63%	34%	97%
2293	0.637	63%	34%	97%
2436	0.677	63%	34%	98%
2578	0.716	63%	35%	98%
2721	0.756	63%	35%	98%
2864	0.796	63%	35%	99%
3007	0.835	64%	35%	99%
3150	0.875	64%	35%	99%
3293	0.915	64%	35%	99%
3435	0.954	64%	35%	99%
3578	0.994	64%	35%	99%
3721	1.034	64%	35%	99%
3983	1.106	65%	35%	99%
9882	2.745	67%	32%	99%

Appendix B: Stacked Cyclic Voltammograms of Complexes 13a, 19 and 16, the Corresponding Free Ligands and $[\text{Rh}(\text{CO})_2\text{Cl}]_2$

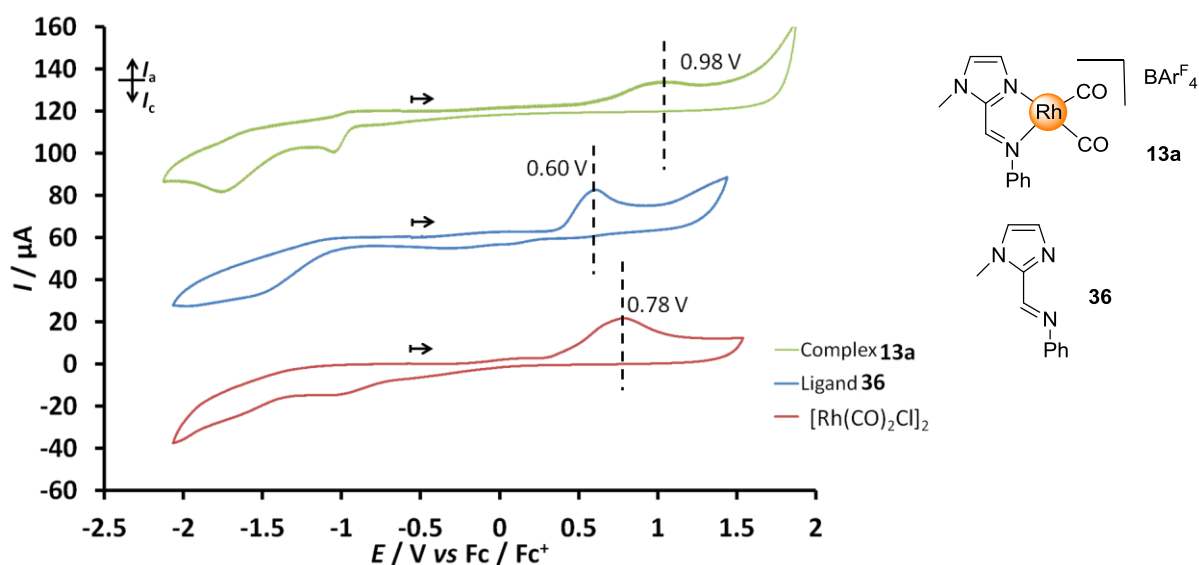


Figure 18 Cyclic voltammograms of complex **13a**, ligand **36** and $[\text{Rh}(\text{CO})_2\text{Cl}]_2$ at 100 mV/s. Measurements were conducted in 0.1 M $[\text{Bu}_4\text{N}][\text{PF}_6]/\text{CH}_2\text{Cl}_2$ vs. a leakless Ag/AgCl reference electrode at 298 K. Scans were initiated in the positive direction.

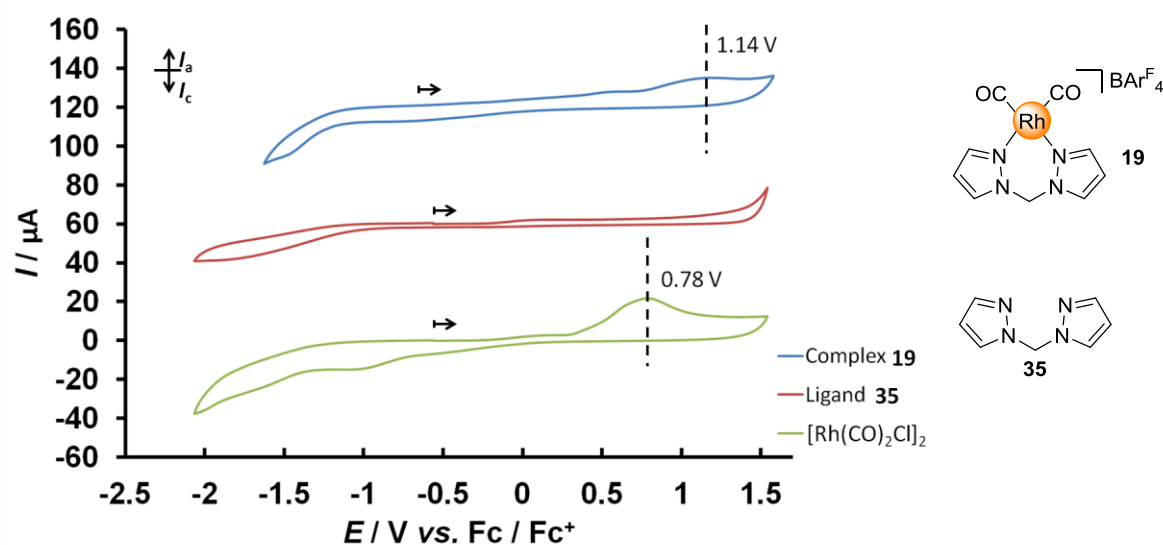


Figure 19 Cyclic voltammograms of complex **19**, ligand **35** and $[\text{Rh}(\text{CO})_2\text{Cl}]_2$ at 100 mV/s. Measurements were conducted in 0.1 M $[\text{Bu}_4\text{N}][\text{PF}_6]/\text{CH}_2\text{Cl}_2$ vs. a leakless Ag/AgCl reference electrode at 298 K. Scans were initiated in the positive direction.

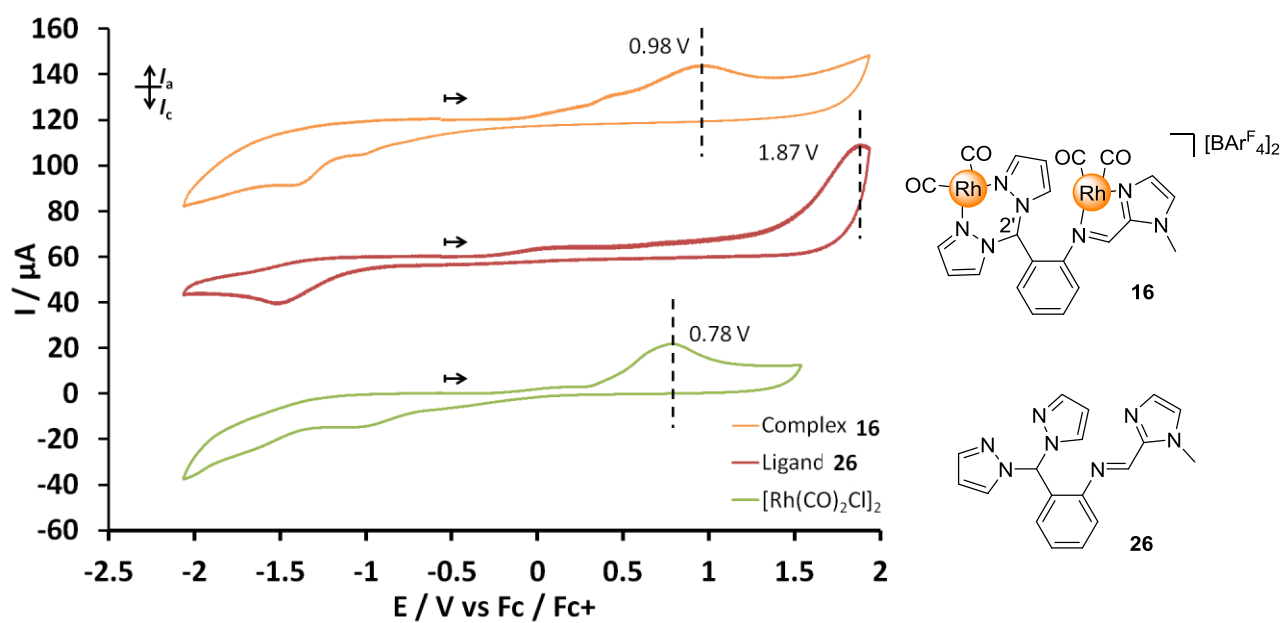


Figure 20 Cyclic voltammograms of complex **16**, ligand **26** and $[\text{Rh}(\text{CO})_2\text{Cl}]_2$ at 100 mV/s. Measurements were conducted in 0.1 M $[\text{Bu}_4\text{N}][\text{PF}_6]/\text{CH}_2\text{Cl}_2$ vs. a leakless Ag/AgCl reference electrode at 298 K. Scans were initiated in the positive direction.

Appendix C: List of Numbered Compounds

